



Interaction of a Three-Dimensional Roughness Element with a Laminar Boundary Layer

P. S. Klebanoff, W. G. Cleveland, Jr.,
and
K. D. Tidstrom
U. S. Department of Commerce
National Bureau of Standards
Gaithersburg, Maryland 20899

March 1987

Final Report for Period June 1, 1982 – January 31, 1987

Approved for public release; distribution unlimited.

**TECHNICAL REPORTS
FILE COPY**

PROPERTY OF U.S. AIR FORCE
AEDC TECHNICAL LIBRARY

**ARNOLD ENGINEERING DEVELOPMENT CENTER
ARNOLD AIR FORCE STATION, TENNESSEE
AIR FORCE SYSTEMS COMMAND
UNITED STATES AIR FORCE**

NOTICES

When U. S. Government drawings, specifications, or other data are used for any purpose other than a definitely related Government procurement operation, the Government thereby incurs no responsibility nor any obligation whatsoever, and the fact that the Government may have formulated, furnished, or in any way supplied the said drawings, specifications, or other data, is not to be regarded by implication or otherwise, or in any manner licensing the holder or any other person or corporation, or conveying any rights or permission to manufacture, use, or sell any patented invention that may in any way be related thereto.

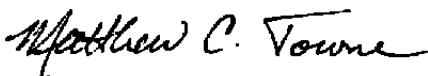
Qualified users may obtain copies of this report from the Defense Technical Information Center.

References to named commercial products in this report are not to be considered in any sense as an endorsement of the product by the United States Air Force or the Government.

This report has been reviewed by the Office of Public Affairs (PA) and is releasable to the National Technical Information Service (NTIS). At NTIS, it will be available to the general public, including foreign nations.

APPROVAL STATEMENT

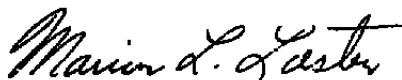
This report has been reviewed and approved.



MATTHEW C. TOWNE, Capt, USAF
Facility Technology Division
Directorate of Technology
Deputy for Operations

Approved for publication:

FOR THE COMMANDER



MARION L. LASTER
Director of Technology
Deputy for Operations

UNCLASSIFIED

SECURITY CLASSIFICATION OF THIS PAGE

REPORT DOCUMENTATION PAGE

1a. REPORT SECURITY CLASSIFICATION UNCLASSIFIED		1b. RESTRICTIVE MARKINGS	
2a. SECURITY CLASSIFICATION AUTHORITY		3. DISTRIBUTION/AVAILABILITY OF REPORT Approved for public release; distribution is unlimited.	
2b. DECLASSIFICATION/DOWNGRADING SCHEDULE			
4. PERFORMING ORGANIZATION REPORT NUMBER(S) AEDC-TR-87-7		5. MONITORING ORGANIZATION REPORT NUMBER(S)	
6a. NAME OF PERFORMING ORGANIZATION U. S. Department of Commerce	6b. OFFICE SYMBOL (If applicable) DO	7a. NAME OF MONITORING ORGANIZATION	
6c. ADDRESS (City, State and ZIP Code) National Bureau of Standards Gaithersburg, Maryland 20899		7b. ADDRESS (City, State and ZIP Code)	
8a. NAME OF FUNDING/SPONSORING ORGANIZATION Arnold Engineering Development Center	8b. OFFICE SYMBOL (If applicable) DO	9. PROCUREMENT INSTRUMENT IDENTIFICATION NUMBER F40600-82-F0001	
8c. ADDRESS (City, State and ZIP Code) Air Force Systems Command Arnold Air Force Station, TN 37389-5000		10. SOURCE OF FUNDING NOS.	
11. TITLE (Include Security Classification) SEE REVERSE OF THIS PAGE		PROGRAM ELEMENT NO 65807F	PROJECT NO 65807F
12. PERSONAL AUTHOR(S) Klebanoff, P. S., Cleveland, W. G., Jr., and Tidstrom, K. D., U. S. Dept. of Commerce		TASK NO	WORK UNIT NO.
13a. TYPE OF REPORT Final	13b. TIME COVERED FROM 6/1/82 TO 1/31/87	14. DATE OF REPORT (Yr., Mo., Day) March 1987	15. PAGE COUNT 120
16. SUPPLEMENTARY NOTATION Available in Defense Technical Information Center (DTIC).			
17. COSATI CODES		18. SUBJECT TERMS (Continue on reverse if necessary and identify by block number)	
FIELD	GROUP	SUB. GR.	
20	04	boundary layer transition	
01	03	turbulent flow	
		hemispherical roughness elements	
19. ABSTRACT (Continue on reverse if necessary and identify by block number) An experimental investigation is described that is directed toward extending the technical database and furthering our understanding of boundary layer transition induced by three-dimensional roughness elements. The investigation was carried out in an "unsteady" wind tunnel, principally with hemispherical roughness elements, in a well characterized zero-pressure gradient laminar boundary layer on a flat plate. Attention was directed toward the following aspects of the behavior of a three-dimensional roughness element: (1) the critical Reynolds number of transition and the effect of aspect ratio thereon, (2) eddy generation in steady and unsteady flows, (3) is the fundamental process stability governed, and (4) the evolutionary change in mean velocity and intensity of the velocity fluctuation associated with the transition to fully developed turbulent flow.			
20. DISTRIBUTION/AVAILABILITY OF ABSTRACT UNCLASSIFIED/UNLIMITED <input type="checkbox"/> SAME AS RPT <input checked="" type="checkbox"/> DTIC USERS <input type="checkbox"/>		21. ABSTRACT SECURITY CLASSIFICATION UNCLASSIFIED	
22a. NAME OF RESPONSIBLE INDIVIDUAL W. O. Cole		22b. TELEPHONE NUMBER (Include Area Code) (615) 454-7813	22c. OFFICE SYMBOL DOS

UNCLASSIFIED

SECURITY CLASSIFICATION OF THIS PAGE

11. TITLE

Interaction of a Three-Dimensional Roughness Element with a Laminar Boundary Layer

UNCLASSIFIED

SECURITY CLASSIFICATION OF THIS PAGE

PREFACE

This work was done by the National Bureau of Standards, U. S. Department of Commerce, Gaithersburg, Maryland, under contract F40600-82-F-0001 for the Directorate of Technology (DOT), Arnold Engineering Development Center (AEDC), Air Force Systems Command, Arnold Air Force Station, Tennessee. The primary Air Force Project Manager for this effort was Captain Matthew C. Towne, AEDC/DOT. The work reported covers the period from June 1, 1982 to January 31, 1987, and the manuscript was submitted for publication March 12, 1987.

CONTENTS

	<u>Page</u>
1. INTRODUCTION	7
2. EXPERIMENTAL ARRANGEMENT AND PROCEDURE	9
2.1 The Flow Facility	9
2.2 The Flat Plate and Traversing Arrangement.....	11
2.3 The Laminar Boundary Layer	13
2.4 Procedure	16
3. RESULTS AND DISCUSSION	18
3.1 Critical Reynolds Number	18
3.2 Eddy Shedding - Steady Flow	21
3.3 Eddy Shedding - Unsteady Flow	28
3.4 Instability and Induced Transition	37
4. SUMMARY AND CONCLUSIONS	48
5. ACKNOWLEDGMENT	50
REFERENCES	51

ILLUSTRATIONS

<u>Figure</u>	<u>Page</u>
1. Schematic Drawing of Unsteady Flow Facility	57
2. Turbulence Intensity Upstream of Flat Plate	58
3. Distribution of Freestream Velocity Along Flat Plate	59
4. Photographs of the Overall Experimental Arrangement	60
5. Close-Up View of Experimental Arrangement	61
6. Transverse Contamination Along Flat Plate	62
7. Mean-Velocity Profiles Without Roughness	63
8. Intensity of u-Fluctuation Without Roughness	64
9. Spectrum of u-Fluctuation in Boundary layer Without Roughness	65
10. Spectrum of u-Fluctuation in the Freestream	66
11. Spectrum of the output of an Accelerometer Attached to the Fan Housing	67
12. Variation of Reynolds Number of Transition with Roughness Reynolds Number for Hemispherical Roughness Elements	68
13. Variation of Reynolds Number of Transition with Roughness Reynolds Number for a Cylindrical Roughness Element	69
14. Oscillograms of u-Fluctuation Downstream of a Hemispherical Roughness Element Illustrating Variation in Frequency with Freestream Velocity; $k = 1.7 \text{ mm}$, $x_k = 91.4 \text{ cm}$, $\bar{x} = 2.54 \text{ cm}$, $\bar{z} = 0.0 \text{ cm}$	70
15. Oscillograms of Simultaneous u-Fluctuations Downstream of a Hemispherical Roughness Element Illustrating Phase in y-Direction; $k = 1.7 \text{ mm}$, $x_k = 91.4 \text{ cm}$, $\bar{z} = 0.0 \text{ cm}$	71
16. Oscillograms of Simultaneous u-Fluctuation Downstream of a Hemispherical Roughness Element Illustrating Phase in z-Direction; $k = 1.7 \text{ mm}$, $x_k = 1.27 \text{ cm}$, $\bar{x} = 1.27 \text{ cm}$, $y = 3.18 \text{ mm}$..	72
17. Variation of Eddy Shedding Frequency with Freestream Velocity for Hemispherical Roughness Elements of Different Size and Position	73

<u>Figure</u>	<u>Page</u>
18. Scaling of Data of Figure 17 with k/x_k and v	74
19. Strouhal Behavior for Hemispherical Roughness Elements with Boundary Layer Scaling	75
20. Variation of k/δ^*k with Roughness Reynolds Number for Hemispherical Roughness Elements of Different Size and Position	76
21. Strouhal Behavior for Hemispherical Roughness Elements with Geometric Scaling	77
22. Comparison of Variation of Eddy Shedding Frequency with Freestream Velocity for a Hemispherical and a Cylindrical Roughness Element	78
23. Comparison of Strouhal Behavior for a Hemispherical and a Cylindrical Roughness Element	79
24. Comparison of Strouhal Behavior for Hemispherical Roughness Elements Observed in the Present Study with the Observations of Strouhal Behavior in Reference 21	80
25. Comparison of Strouhal Behavior for a Cylindrical Roughness Element Observed in the Present Study with the Observations of Strouhal Behavior in Reference 18	81
26. Phase and Amplitude Response of the Laminar Boundary Layer Without Roughness to a Freestream Oscillation; $U_1 = 6.8$ m/s, $x = 94$ cm, $n = 1.0$ Hz	82
27. Comparison of Mean-Velocity Profiles for Steady and Unsteady Flow With and Without a Roughness Element	83
28. Strip-Chart Recordings of Simultaneous u -Fluctuations in an Oscillatory Freestream, and in the Boundary Layer Downstream of a Hemispherical Roughness Element; $k = 1.7$ mm, $x_k = 91.4$ cm, $\bar{x} = 2.54$ cm, $y = 3.18$ mm, $\bar{z} = 0.0$ cm	84
29. Strip-Chart Recordings of Simultaneous u -Fluctuations in a Oscillatory Freestream, and in the Boundary Layer Downstream of a Hemispherical Roughness Element; $k = 1.7$ mm, $x_k = 91.4$ cm, $\bar{x} = 2.54$ cm, $y = 3.18$ mm, $\bar{z} = 0.0$ cm	86
30. Strip-Chart Recordings of Simultaneous u -Fluctuations in an Oscillatory FreeStream, and in the Boundary Layer Downstream of a Hemispherical Roughness Element; $k = 1.7$ mm, $x_k = 91.4$ cm, $\bar{x} = 30.5$ cm, $y = 0.61$ mm, $\bar{z} = 0.0$ cm	88
31. Strip-Chart Recordings of Simultaneous u -Fluctuations in an Oscillatory Freestream, and in the Boundary Layer Downstream of a Hemispherical Roughness Element; $k = 1.7$ mm, $x_k = 91.4$ cm, $\bar{x} = 30.5$ cm, $y = 0.61$ mm, $\bar{z} = 0.0$ cm	89
32. Strip-Chart Recordings of Simultaneous u -Fluctuations in an Oscillatory Freestream, and in the Boundary layer Downstream of a Hemispherical Roughness Element; $k = 1.7$ mm, $x_k = 91.4$ cm, $\bar{x} = 30.5$ cm, $y = 6.35$ mm, $\bar{z} = 0.0$ cm	90
33. Strip-Chart Recordings of Simultaneous u -Fluctuations in an Oscillatory Freestream, and in the Boundary Layer Downstream of a Hemispherical Roughness Element; $k = 1.7$ mm, $x_k = 91.4$ cm, $\bar{x} = 30.5$ cm, $y = 6.35$ mm, $\bar{z} = 0.0$ cm	91
34. Strip-Chart Recordings of Simultaneous u -Fluctuations in an Oscillatory FreeStream, and in the Boundary Layer Downstream of a Hemispherical Roughness Element; $k = 1.7$ mm, $x_k = 91.4$ cm, $\bar{x} = 61.0$ cm, $y = 0.61$ mm, $\bar{z} = 0.0$ cm	92

FigurePage

35. Strip-Chart Recordings of Simultaneous u-Fluctuations in an Oscillatory Freestream, and in the Boundary Layer Downstream of a Hemispherical Roughness Element; $k = 1.7$ mm, $x_k = 91.4$ cm, $\bar{x} = 61.0$ cm, $y = 0.61$ mm, $\bar{z} = 0.0$ cm	93
36. Strip-Chart Recordings of Simultaneous u-Fluctuations in an Oscillatory Freestream, and in the Boundary Layer Downstream of a Hemispherical Roughness Element; $k = 1.7$ mm, $x_k = 91.4$ cm, $\bar{x} = 61.0$ cm, $y = 6.35$ mm, $\bar{z} = 0.0$ cm	94
37. Strip-Chart Recordings of Simultaneous u-Fluctuations in an Oscillatory Freestream, and in the Boundary Layer Downstream of a Hemispherical Roughness Element; $k = 1.7$ mm, $x_k = 91.4$ cm, $\bar{x} = 61.0$ cm, $y = 6.35$ mm, $\bar{z} = 0.0$ cm	95
38. Comparison of the Duration of Eddy Shedding with the Duration of Resulting Turbulent "Spot"	96
39. Spanwise Distributions of Mean Velocity at Various Postions from the Surface for Varying Unit Reynolds Number; $k = 1.7$ mm, $x_k = 91.4$ cm, $\bar{x} = 2.54$ cm	97
40. Spanwise Distributions of the Intensity of u-Fluctuation at Various Positions from the Surface for Varying Unit Reynolds Number; $k = 1.7$ mm, $x_k = 91.4$ cm, $\bar{x} = 2.54$ cm	98
41. Mean-Velocity Distributions for Varying Unit Reynolds Number; $k = 1.7$ mm, $x_k = 91.4$ cm, $\bar{z} = 0.0$ cm	99
42. Intensity of u-Fluctuation for Varying Unit Reynolds Number; $k = 1.7$ mm, $x_k = 91.4$ cm, $\bar{z} = 0.0$ cm	106
43. Comparison of Mean-Velocity Profiles at 1.27 cm Downstream of a Hemispherical Roughness Element with the Mean-Velocity Profiles; $k = 1.7$ mm, $x_k = 91.4$ cm, $\bar{z} = 0.0$ cm	113
44. Comparison of Mean-Velocity Profiles Downstream of a Hemispherical Roughness Element with the Mean-Velocity Profile Without Roughness; $k = 1.7$ mm, $x_k = 91.4$ cm, $\bar{z} = 0.0$ cm ..	114
45. Comparison of Mean-Velocity Profiles Downstream of a Hemispherical Roughness Element with the Mean-Velocity Profile for a "Fully-Developed" Turbulent Boundary Layer; $k = 1.7$ mm, $x_k = 91.4$ cm, $\bar{z} = 0.0$ cm	115
46. Comparison of Intensity of u-Fluctuation Downstream of a Hemispherical Roughness Element with the Intensity of u-Fluctuation for a "Fully-Developed" Turbulent Boundary Layer; $k = 1.7$ mm, $x_k = 91.4$ cm, $\bar{z} = 0.0$ cm, $U_1/v = 6.81 \times 10^5$ (m ⁻¹)	116

1. Introduction

The transition from laminar to turbulent flow in boundary layers has been a subject of active research for many years. The intense interest in this subject stems not only from its intrinsic importance to an understanding of boundary-layer behavior but also from important technological considerations associated with many aerodynamic and hydrodynamic flows, and the need to predict essential design criteria and to exert some measure of control over the state of the boundary layer. Considerable progress has been made in revealing the fundamentals and evolutionary nature of the instability and transition processes that are involved, and excellent summaries of the progress made to date can be found in references 1-5. However, despite the progress that has been made, the inherent complexities of the problem have prevented the prediction of transitional behavior with a degree of accuracy required for practical applications. This situation results from the fact that there are many factors which affect the transition process and much more needs to be known about the nature of the interaction of such factors as freestream turbulence, surface roughness, surface curvature, surface temperature, pressure gradients, Mach number, noise and vibration on the transition process, either singly or in combination. All of the aforementioned factors have been investigated to some degree with surface roughness receiving the most attention. This emphasis on surface roughness stems not only from the obvious interest in maximizing the extent of laminar flow, but also from the converse, in that it is often desirable, for example, in wind tunnel tests to "artificially" trip the boundary layer to make it turbulent. In this regard it is desirable to "trip" the boundary layer as efficiently as possible, i.e., with as small a roughness as possible, not only to avoid contributing to the form drag but to avoid "distortion" of the resulting turbulent boundary layer (reference 6), and the effect on test data resulting

from such "distortion." Although much work has been carried out on roughness induced transition, too little attention has been given to characterizing the state of the resulting boundary layer.

The experimental activity dealing with the effect of roughness on boundary layer transition at both incompressible and compressible flow speeds spans a period of approximately forty years, and may be considered to consist of two approaches: one in which the activity concerns itself with the location of transition and its dependence on parameters characterizing the boundary layer and roughness, and the other concerned with details of the flow behavior and its relation to instability processes and the mechanism of transition. Using the former approach, considerable data was obtained for both two-dimensional and three-dimensional roughness elements in which correlations of Reynolds numbers of transition with roughness size and position and boundary layer thickness were obtained. Excellent accounts of this approach with appropriate bibliographies have been given by Smith and Clutter (reference 7) and Tani (reference 8). Although the parametric approach has provided the basic data base which is used for present day criteria involving the effect of roughness, it has not clarified the basic processes.

In general, the effect of roughness is to induce earlier transition. However, it has been demonstrated that the behavior of a three-dimensional roughness element (references 8, 9) is markedly different than that for two-dimensional roughness elements. It is not as effective as a two-dimensional roughness in inducing transition, and its behavior is much more critical. Transition moves forward gradually with increasing velocity for a two-dimensional roughness, whereas for a three-dimensional roughness transition moves rapidly toward the roughness with a relatively small increase in velocity after a critical velocity has been reached. It is generally recognized that in

order to materially advance the state-of-the-art and our understanding of the basic mechanisms involved in this behavior, the approach of investigating the steady and fluctuating flow fields in detail is required. This more basic approach has been used with some success in connection with two-dimensional roughness elements, and it has been shown (reference 10) that the basic mechanism by which a two-dimensional roughness element induces earlier transition to turbulent flow is by the destabilizing influence of the flow in the immediate downstream vicinity of the roughness. The flow downstream of isolated three-dimensional roughness elements has received considerable attention (references 11-21). However, much of this work utilized flow visualization techniques and the resulting insight into the flow processes is primarily qualitative in nature. Detailed measurements of the flow downstream of a three-dimensional roughness are limited and as yet no clear explanation of its behavior in inducing transition, similar to that for two-dimensional roughness, exists. Nevertheless, it is felt that the behavior should in some manner be stability governed. It was with the objective of providing information on this aspect, to considerably extend the data base, and characterize the state of the boundary layer, if only for a single roughness element, that the present investigation was undertaken.

2. Experimental Arrangement and Procedure

2.1 The Flow Facility

The investigation was conducted in the National Bureau of Standards Unsteady Flow Facility shown schematically in figure 1. The facility is of the closed-return type with a square test section, 1.37 m in cross-section and 4.88 m in length. It is powered by a 100 h.p. constant speed motor and single stage axial fan equipped with shutters for varying the flowrate. The tunnel can

be operated either in a steady mode as a conventional wind tunnel, or in an unsteady mode for generating oscillatory flows with varying frequency and amplitude. Both modes of operation were used in the present investigation.

The unsteady operation of the wind tunnel is accomplished by using a system of rotating shutters and a secondary or bypass test section. The secondary test section is solely for the purpose of providing a nearly constant volume flowrate through the fan. This is achieved by balancing the mean flow between the two sections with the trim shutters and by alternatively directing part of the flow between the two sections by rotating the shutters in each section 90° out-of-phase. Guide vanes are installed at each corner, and the solid lines at the guide vane positions shown in the figures serve to indicate the beginning and ending of the partitioning of the flow in the wind tunnel circuit. A screen from position C and another from position D, as indicated, and extending to the leading edge, AB, of the dividing partition, assist in diverting the flow into the two ducts as required by the rotating shutters. Each bank of shutters consists of nine counter-rotating shutters, any one of which may be positioned at a fixed angle between 0° and 90° . By varying the number of rotating shutters, the angle of the fixed shutters, and the flowrate through the fan, both the mean velocity and the velocity amplitude in the working test section can be controlled. The rotational speed of the shutters determines the frequency which ranges from 0.1 Hz to 25 Hz.

The lower duct, resulting from the partitioning of the flow, is the primary duct. It contains the working test section and conforms to conventional wind tunnel design. The contraction ratio is 5.3, and the settling chamber contains a honeycomb and screens for flow conditioning, i.e., for obtaining a spatially uniform mean flow, and a reduced freestream turbulence in the test section. The maximum velocity that can be attained in the test section when operating in a

conventional steady mode, with the upper duct closed, is 27 m/s. The centerline turbulence intensity, i.e., the ratio of the rms value of the axial component of the velocity fluctuations, u'_0 , to U_0 , a reference mean velocity, and its variation with U_0 at 0.5 m upstream from the boundary layer plate is shown in figure 2. Despite the complexity of the wind tunnel configuration, the turbulence intensity, above 12 m/s, is about 0.06 percent and is characteristic of turbulence levels of conventional low turbulence wind tunnels. Below 12 m/s, and over the speed range covered with the roughness element the turbulence intensity increases with decreasing velocity to about 0.15 percent at 5 m/s.

2.2 The Flat Plate and Traversing Arrangement

The investigation was carried out using a boundary layer on an aluminum plate, 3.66 m long, 1.22 m wide and 9.5 mm thick which had a leading edge in the form of a half-wedge with a 5° angle on the non-working side of the plate. The leading edge itself is rounded with a radius of approximately 0.4 mm. The plate is mounted vertically and centrally with the leading edge at a distance 1.0 m downstream of the entrance to the test section. A false wall made of plexiglass mounted on the tunnel wall opposite the working side of the plate permitted the adjustment of the pressure gradient within moderate limits and was used to compensate for the boundary layer growth and establish a zero pressure gradient along the plate. A positive angle of attack was obtained by some blocking of the air passage on the working side of the plate with screens of 16-mesh and wire diameter 0.28 mm. Since the blocking screens had to be placed farther downstream than any usable portion of the plate, the passage was extended 0.86 m by joining the trailing edge of the plate with a section of plywood. This extension also prevented a sharp change in pressure along the plate that would

otherwise occur once the carriage for the traversing equipment passed the downstream end of the plate. The positive angle of attack, with the stagnation point on the working side of the plate, provided a smooth flow condition at the leading edge, with a resulting favorable pressure gradient over the first 2 feet of surface. The distribution of mean velocity, U_1 , in the free-stream outside the boundary layer, with distance from the leading edge, x , obtained by adjusting the false wall, is shown in figure 3. It is seen that beyond the first two feet of surface a reasonable zero pressure gradient condition has been obtained.

A view of the experimental arrangement from upstream of the plate and looking downstream is shown in figure 4. As can be seen, the surface is highly polished to a mirror-like finish. Also shown in the figure is an overall view of the arrangement for traversing the boundary layer. Close-up views of the roughness element, hot-wire probe and traversing mechanism used to traverse either in a spanwise direction or in a direction normal to the plate surface are shown in figures 5a and 5b. The traverse is mounted to a streamlined strut which can ride along the plate on two rails attached at the top and bottom of the plate for traversing in a downstream direction. The measuring probe, which extends 25 cm upstream from the point of support to avoid interference effects, is driven by a micrometer screw of 0.5 mm pitch. Additional probes can be attached at fixed locations, as for example, the Pitot-static tube in figure 5a, for measuring the free-stream velocity during boundary layer surveys. The initial distance of the probe from the surface is obtained by making use of the mirror-like finish, and using a prism to reflect the probe and its image onto a calibrated reticule of a microscope.

2.3 The Laminar Boundary Layer

It was necessary before proceeding with the study of the behavior of a roughness element to determine the extent and character of the laminar boundary layer that was established on the plate. The extent of the laminar boundary layer "window" is shown in figure 6. The figure shows the well-known phenomenon of transverse contamination of turbulent flow originating at the top and bottom corners of the plate at the leading edge. The transverse contamination angle, as measured from the rail support for the strut is about 10° , in good agreement with existing data for such behavior. Figure 7 shows the mean velocity distributions across the boundary layer at the centerline of the plate at two free-stream speeds, and for two downstream positions. The two downstream positions were chosen so as to cover a considerable extent of the laminar boundary layer "window." The distributions are plotted nondimensionally for comparison with the Blasius distribution for a zero-pressure gradient boundary layer, where U is the x-component of the local mean velocity in the boundary layer, y is the distance from the surface, and ν is the kinematic viscosity. It may be that the tendency of the velocity profiles to be slightly steeper in shape than the Blasius reflects the effect of the favorable pressure gradient over the forward part of the plate, and/or a virtual origin other than at the leading edge, but the effect, if any, is sufficiently small, and within the experimental uncertainty the boundary layer may be considered to be of the Blasius type. Consequently, in characterizing the flow or flow parameters at the roughness element, with the roughness element present, the Blasius distribution is used. Although this assumption neglects the distortion in the immediate vicinity upstream of the roughness, and at the roughness, the Blasius length scale, $\eta = (\nu x/U_1)^{1/2}$, is a realizable length scale, and provides consistency with other investigations. Measurements of the disturbance level in the boundary layer

without roughness within the laminar boundary layer "window" are shown in figure 8. Distributions across the boundary layer of the rms value of the longitudinal component of the velocity fluctuation, u' , are shown relative to its value in the freestream, u'_f , for the same x-positions and for about the same freestream velocities as for figure 7. The nature of the distributions is such that one can infer that, to a considerable degree, the disturbance level is a consequence of variations of boundary layer thickness in space and time associated with free-stream turbulence effects as proposed in reference 22 and not as a result of a Tollmien-Schlichting type of instability. The maximum in the disturbance level, at about 0.5 the boundary layer thickness, which in Blasius coordinates is at 2.5, and the relatively large low frequency content of the disturbance, i.e., below the Tollmien-Schlichting range of instability, are consistent with this conclusion. This behavior is illustrated in figure 9 which shows the spectral content relative to the range of Tollmien-Schlichting frequencies for the highest boundary layer Reynolds number of figure 8, i.e., at $U_f = 12.1$ m/s and $x = 213.4$ cm, for which the boundary layer Reynolds number based on displacement thickness, R_{δ^*} , was 2070. The spectral distribution was obtained in the region of the maximum in u'/u'_f at $\eta = 2.45$, and the Roman numerals I and II noted on the figure indicate the frequencies corresponding to Branches I and II of the stability diagram for a Blasius flow. The nominal band-width of the spectral analyzer is proportional to the band-pass, and for the 100 Hz band-pass it is 0.3 Hz. In addition, the nominal low-frequency cut-off of the analyzer is 0.4 Hz. Consequently, no particular significance should be attached to the fall-off in spectral intensity that is shown in the range from 0.0 to 1.0 Hz. The peak in the spectral intensity at 20 Hz, in view of its proximity to Branch I, should not be interpreted as being due to a Tollmien-Schlichting instability. It is a consequence of a vibration induced by the fan motor, and is accentuated

by the velocity gradient in the boundary layer. Attempts to eliminate the 20 Hz vibration by soft-mounting, damping, etc. were not successful. Although it was minimized to the extent shown, it was not possible to eliminate it inasmuch as the 20 Hz vibration from the fan motor was transmitted to the flat plate and wind tunnel walls as evidenced by accelerometer measurements. The free-stream disturbance level, u'_1/U_1 , along the plate is about a factor of 1.9 ± 10 percent larger than the corresponding disturbance level, u'_0/U_0 , upstream of the plate. This increase in disturbance level along the plate, although it has never been thoroughly evaluated, has been observed in previous investigations. However, it is not unexpected, and may be attributed to potential fluctuations arising from the turbulent boundary layers on the walls of the tunnel. The magnitude of the effect may therefore differ from one flow configuration to another. In addition there may be very low frequency potential fluctuations, i.e., below 2 Hz, in the free-stream arising from an intermittent separation in the wind tunnel circuit. It is believed that this behavior may be responsible for much of the increase in disturbance intensity at the lower velocities shown in figure 2. Another contributing component to the free-stream disturbance level is the free-stream turbulence, i.e., turbulent vorticity fluctuations, which were the type of disturbances considered in reference 22.

It is evident that sound and vibration are factors that may affect the state of the boundary layer and are important considerations particularly in investigations pertaining to flow instability. In order to assess this aspect the spectrum of the u -fluctuation was measured in the free stream at $x = 221$ cm, $y = 3.49$ cm and $U_1 = 8.1$ m/s. The spectrum in terms of the relative rms amplitude is shown in figure 10. No particular significance should be attached to the relative amplitudes. The position at which the spectrum was measured was arbitrarily selected, and the amplitude of the various frequencies may vary with

position in the test section. The purpose is to illustrate the spectral peaks present in the free-stream turbulence that may serve as a source of input disturbances for any flow instability. The source of the spectral peaks is attributed to the wind tunnel fan. The peak at 20 Hz, as alluded to previously, corresponds to the fan motor rpm. The peaks at 180 Hz and the higher harmonics of 180 Hz are a consequence of the passage frequency of a 9-bladed fan. A more direct evaluation is given by figure 11 which shows the spectrum of the output of an accelerometer attached to the fan housing. It is seen that the peaks correlate well with the peaks observed in the spectrum of the free-stream turbulence. Microphone spectra taken in the room near the test section also corroborated that the spectral peaks were a consequence of sound and vibration.

It is noted, as is reflected in figure 8, that there is an anomaly in the increase in u'/u_1 from $x = 91.4$ cm to $x = 213.4$ cm for the lower free-stream velocity as compared to that at the higher free-stream velocity. There is no ready explanation for this behavior. One may speculate that in addition to the complex interactions referred to above, the situation is further complicated by the transverse contamination, and that the effect of free-stream turbulence on the boundary layer may also depend on the thickness of the layer relative to the scale of the turbulence. Be that as it may, the state of the layer is such as to not prevent, nor unduly complicate, an adequate study of the effect of roughness.

2.4 Procedure

The roughness elements were, for the most part, hemispherical with nominal diameters, d , of 3.18 and 6.36 mm. They were individually studied and were attached, using rubber cement, to the surface on the centerline ($z = 0$) at varying distances from the leading edge, x_k , which were well within the laminar boundary layer "window". The actual roughness height, k , due to the method of

attachment and the tolerance in the nominal values, could differ from the nominal value and was measured in each case with a dial indicator. A cylindrical element with $d = 3.18$ mm, $k/d = 1.0$, and positioned at $x_k = 91.4$ cm, with its axis in the y-direction was also used.

In documenting the behavior of a single roughness element a number of different aspects required attention. One was the variation of the Reynolds number of transition, Re_t , with roughness Reynolds number, Re_k , defined by $U_1 x_t / \nu$ and $U_k k / \nu$ respectively where x_t is the distance from the leading edge of the plate to the beginning of transition to turbulent flow in the boundary layer, and U_k is the mean velocity that would exist in the boundary layer at the height of the roughness without the roughness present. Another aspect is the parametric behavior of the frequency, f , of eddies generated by the roughness. Attention was also given to the nature of the boundary layer distributions of mean velocity and intensity of disturbances at various distances downstream from the roughness, \bar{x} , as well as to the effect of an oscillatory flow on eddy shedding and roughness induced transition. In regard to the latter two aspects, the behavior of only one size of roughness at one roughness position was investigated, i.e., $d = 3.18$ mm, $k = 1.7$ mm and $x_k = 91.4$ cm.

The distributions of U and u' , at \bar{x} ranging from 1.27 cm to 30.5 cm, were measured on the centerline and in the spanwise direction for various unit Reynolds numbers, U_1 / ν , using conventional constant temperature hot-wire anemometry. During the boundary layer surveys, a given unit Reynolds number was constant to within \pm two percent. Platinum wires 1.27 μ m in diameter and 0.25 mm in length were used, and no correction for wire length, nor for the nonlinear response of the hot-wire was deemed necessary. The length of the wire was selected as being adequate for the size of the roughness under study from comparative measurements of the mean velocity in the immediate downstream

vicinity of the roughness with different wire lengths. Equipment customarily used in association with hot-wire anemometry for processing data such as a real-time spectral analyzer with an on-line x-y plotter, film recordings from an oscilloscope, and strip-chart recordings also proved useful.

3. Results and Discussion

3.1 Critical Reynolds Number

The existence of a critical roughness Reynolds number for correlating the Reynolds number of transition for three-dimensional roughness elements was first prepared by Schiller (reference 23). It was predicated on the analogy to the critical Reynolds number for an obstacle in uniform flow at which the downstream flow becomes altered by vortex shedding. Although considerable data on the critical roughness Reynolds number for three-dimensional elements exists in the literature for a variety of geometrical shapes such as spheres, cones, and cylinders (references 7,9,11,13,24), no comparable data exists for hemispherical roughness.

The critical behavior of three-dimensional hemispherical roughness elements in inducing earlier transition to turbulent flow, as observed in the present study, is illustrated in figure 12. The measurements shown were made for two different sizes of roughness mounted at different positions from the leading edge. The position, x_t , was determined by placing a hot-wire probe close to the surface along the centerline at different locations, \bar{x} , and slowly increasing U_1 until turbulent bursts first occurred. The results clearly demonstrate the critical behavior of the transition process induced by the roughness in that transition moves rapidly upstream toward the roughness element with a relatively small increase in velocity after a critical velocity has been reached. The limiting case of $x_t = x_k$ is shown by the solid line, and the critical Re_k is

determined, as in reference 13, by the extrapolated intersection with the limiting curve indicated by the dashed line. The increase in Re_k at the lower values of Re_t , indicating that the transition is not moving forward as rapidly, is generally observed to be the case when x_t is less than 30.5 cm from the roughness element. This behavior is apparently a consequence of the finite distance required for the transition to turbulence associated with the stability of the flow. It illustrates that considerable care should be given to the state of the "tripped" boundary layer, particularly when using "trips" in wind tunnel testing, in order to ascertain the degree to which the boundary layer is free of "distortion". This question is addressed further for a given size of roughness in Section 3.4.

It should be noted that Re_k is constant with a value of about 325 for the various conditions shown in figure 12. This is at variance with the results of reference 13 for cylindrical roughness elements for which the critical value of Re_k was found to vary from 600 to 1000 and increasing with decreasing Re_t . However, in reference 13, x_t was defined as the position where the turbulent "bursts" had an intermittency factor of 50 percent, and the aspect ratio, k/d , of the cylindrical elements was 1.0 compared to a value of 0.5 for hemispherical elements. Smith and Clutter (reference 7) with the data of references 9, 11 and 24, coupled to their own data for cylindrical elements with ratios of k/d which ranged from 0.046 to 0.48, concluded that the critical Re_k increased with k/d . However, the scatter in the data exceeded 100 percent. In view of the differences among the various experiments, not only in regard to the type of roughness but to such factors as the nature of the free-stream turbulence, pressure gradient, and as to how the critical roughness Reynolds number was determined, it was deemed advisable to assess the effect of k/d , if only in a limited way, in the present investigation in which the same experimental

"environment" is provided. The result obtained for a cylindrical element with a k/d of 1.0, and $k = 3.18$ mm at an $x_k = 91.4$ cm is shown in Figure 13. The critical Re_k has a value of 450 and is higher than that obtained with a hemispherical element of comparable k . However, the values of 325 and 450 are on the extreme low side of the range of data for the same k/d examined by Smith and Clutter. In addition to the effect of k/d it is reasonable to expect from a stability point of view that roughness shape may play a role but the data in the literature is rather limited and inconclusive on this point. Klanfer and Owen (reference 25) reanalyzed the data of reference 11 for conical elements with a k/d of 0.87 and suggested a critical value of 440 for Re_k . Klebanoff et al (reference 9) for spherical elements in a lateral row with various spacings obtained an average value for the critical Re_k of 577, whereas Hall (reference 17), for isolated spherical elements, obtained critical values of Re_k ranging from 585 to 655. Smith and Clutter (reference 7), on the other hand, for a spanwise row of circular discs with k/d ranging from 0.046 to 0.48 obtained values ranging from 100 to 500. In the latter case, the critical Re_k was that for which the Reynolds number of transition had decreased to 95 percent of the value without roughness. The average of the critical Re_k they obtained for when transition was considered as having moved to the roughness was 600. The lowest value of the critical Re_k , for a three-dimensional type of roughness, was that obtained by Hama (reference 26) who used a spanwise row of flat equilateral triangular patches, 1 mm thick, with their vertex pointing upstream and touching at their base, and obtained a value of 45. It is evident that there is a need for more controlled and well defined experiments in order to satisfactorily resolve the trend of the critical roughness Reynolds number with roughness size and shape for single roughness elements. An improved insight into this behavior

may well provide the basis for an improved experimental approach to the study of, and the interpreting of, the behavior of distributed roughness.

3.2 Eddy Shedding - Steady Flow

It has been known for some time (references 11, 12, 14-21) that associated with the behavior of three-dimensional roughness elements there are periodic disturbances generated in the immediate downstream vicinity of the roughness. The view stemming primarily from the flow visualization studies is that these periodic disturbances reflect the presence of an eddy shedding mechanism that involves the generation of three-dimensional vortices having a "hairpin" or "arch" shape.

The presence of the periodic disturbances was readily detected by hot-wire anemometry in the present investigation. They are illustrated by oscillograms of the u -fluctuation shown in figure 14. The oscillograms were obtained downstream of a hemispherical element for the conditions, $k = 1.7$ mm, $\bar{x} = 2.54$ cm, and $\bar{z} = 0.0$ cm, where $\bar{z} = z - z_k$, and z_k is the spanwise position of the roughness. The sweep speed of 5 ms is noted on each oscillogram. Time increases from left to right, and a decreasing velocity is in a downward direction. It is seen from figure 14 that the frequency increases with U_1 . The distance from the surface at which the oscillograms were obtained was, in general, increased with increasing U_1 , reflecting the behavior of the region of periodicity to extend further from the surface with increasing U_1 and \bar{x} . This behavior is consistent with the flow visualization studies in which the increasing extent of the "hairpin" eddies with their "heads" moving out from the surface, with increasing U_1 and \bar{x} was observed.

Wynanski and Petersen (reference 27) showed that the presence of vortical structures and their behavior inferred from flow visualization studies may not

always be of dynamical significance. Such structures in free-shear flows could be viewed as a manifestation of Rayleigh instability and that an amalgamation of "tagged" particles evidenced by streaklines does not necessarily coincide with a redistribution of vorticity. Hama in an earlier paper (reference 28) had obtained a similar result. He showed that the rolling up of a streakline in a mixing layer which had one fluid at rest could result from a superposed neutral wave, and therefore could not necessarily be viewed as a positive indication of the presence of vortices. However, references 27 and 28 do not necessarily negate the presence of vortices. The question of wave or vortex may be viewed as alternate approaches to the same phenomenon. Nevertheless, it is desirable to identify the physical entity actually involved since each view can provide a different mechanism for the final onset of turbulence.

It is evident that the oscillograms of figure 14 do not distinguish between wave and vortex. In order to make this distinction, the oscillograms shown in figures 15 and 16 were obtained for the same roughness element and roughness position as for figure 14. In figures 15 and 16, as for figure 14, time increases from left to right, and a decreasing velocity is in a downward direction. However, the sweep speed was 2 ms rather than 5 ms. The oscillograms of figure 15 are of simultaneous signals from two hot-wires separated in the y direction at $\bar{x} = 1.27$ and 2.54 cm. The top trace in each oscillogram is the signal from the hot-wire that is furthest from the surface. The important features are the phase reversal with distance from the surface, which is clearly evident with increasing U_1 , and the characteristic "spike" appearance of the fluctuation. The latter permitted the use of one hot-wire for detecting the existence of a phase reversal with varying \bar{z} . The resulting oscillograms obtained with $U_1 = 11.8$ m/s, and at $\bar{x} = 1.27$ cm, $y = 3.18$ mm are shown in figure 16. It is seen that phase reversals occur at $+\bar{z}$ and $-\bar{z}$ with a spacing which is

less than the diameter of the roughness. It is unlikely that a three-dimensional wave motion could provide the appropriate phase reversals and "spike" appearance. It is therefore concluded, in accord with the flow visualization studies, that the observed periodicity when exhibiting the appropriate phase reversals is indicative of an eddy shedding frequency. In figure 15, with $U_1 = 7.0$ and 7.2 m/s at $\bar{x} = 1.27$ and 2.54 cm, respectively, it is seen that there is no discernible phase reversal, although there is clear evidence of a periodic fluctuation at the inner y position. At U_1 equal to 8.2 and 8.3 m/s and $\bar{x} = 1.27$ and 2.54 cm, respectively, the phase reversal is barely discernible indicating a less intense vortex than at the higher velocities. The critical velocity, U_c , corresponding to the critical roughness Reynolds number of 325 is 8.1 m/s. The oscillograms in figure 14 also demonstrate the existence of periodicity at $U_1 < U_c$. It would thus appear that there is a rapid change from wave to vortex with increasing U_1 , and by inference, similar behavior with \bar{x} at a given $U_1 \geq U_c$. The latter implies an initial wave motion of relatively short wave length with the change from wave to vortex occurring within a distance less than $7.5 k$.

The dependence of the frequency on U_1 was determined for the hemispherical elements, and the cylindrical element under essentially the same conditions, i.e., roughness size and position, as for the determination of the critical roughness Reynolds number. The results obtained with the hemispherical elements are shown in figure 17. The data for $x_k/k = 359$ and 393 were, within the experimental accuracy, considered to be at the same x_k/k . The straight lines are a least-squares fit to the data. The maximum and minimum deviations about an average value of 940 Hz shown for an $x_k/k = 538$ were obtained from the twelve oscillograms of figure 16. Their magnitude should not be regarded as being applicable to any of the other measurements which were made at $\bar{x} = 2.54$ cm,

$\bar{z} = 0.0$ cm, and at each U_1 were obtained from only one or two oscillograms of the type shown in figure 14. The deviations shown, however, do illustrate the variability of the eddy shedding process and the lack of control over the frequency, in contrast, for example, to the control over the frequency when using a vibrating ribbon. In this connection, it is of interest to note that the more appreciable scatter occurs at frequencies which reflect the effect of the free-stream disturbances shown in figure 10, i.e., 180 Hz and its harmonics. The effect of free-stream disturbances in biasing the maximum amplified frequency is not unexpected for a stability governed phenomenon, and stresses the importance of the experimental environment.

The dependence of the eddy shedding frequency on U_1^2 and x_k/k , as shown in figure 17, suggests that the Strouhal behavior can be nondimensionally characterized with U_k as the characteristic velocity, and δ_k^* as the characteristic length, with a resulting linear relation for f , such that

$$f \propto C \frac{U_1^2}{v} \cdot \frac{k}{x_k} \quad (1)$$

and

$$\frac{f \delta_k^*}{U_k} = 5.2C \quad (2)$$

The frequency measurements are shown in figures 18 and 19 as suggested by (1) and (2). The Strouhal number obtained from the least-squares fit to the data in figure 18, in accordance with (2), is 0.29, and is compared in figure 19 with the actual values of $f \delta_k^* / U_k$. Implicit in (2) is the assumption that U_k varies linearly with U_1 which for a Blasius flow is reasonably valid for values of

$k/\delta_k^* \leq 1.0$. The range of k/δ_k^* covered in the measurements is shown in figure 20 and it is seen that for Re_k greater than 700, the use of (2) would tend to underestimate the Strouhal number. However, the effect of k/δ_k^* is not large, being on the order of 10 percent for the largest value of k/δ_k^* . Although (2) appears to mask, particularly at the lower Reynolds numbers, a small dependence on Reynolds number, it is within the experimental uncertainty, a reasonable representation of the Strouhal behavior of hemispherical elements. In any event, it indicates that δ_k^* is a more appropriate characteristic length for the Strouhal number for single roughness elements in a laminar boundary layer than a length, such as k , which has generally been used in characterizing Strouhal behavior. The latter, in contrast, and as illustrated in figure 21, exhibits a very strong dependence on Reynolds number.

The shedding frequencies, and the resulting Strouhal number obtained with the cylindrical element, albeit for only one size and position, are compared with the results obtained for the corresponding hemispherical element, i.e., the same k , and x_k , in figures 22 and 23, respectively. Both sets of measurements were made at $\bar{x} = 2.54$ cm. It is seen that the shedding frequency for the cylindrical element is also linearly dependent on U_1^2 . However, the frequency is lower than that for a hemispherical element at the same Re_k and k/δ_k^* . The Strouhal number is correspondingly lower, and exhibits a greater dependence on Re_k at the lower Reynolds numbers, i.e., for $Re_k < 800$. This difference in shedding frequency of the hemispherical and cylindrical elements is consistent with the greater stability of the cylindrical roughness in inducing earlier transition. It is reasonable to infer that it is due to the difference in stability of the mean velocity profiles established by the elements in their immediate downstream vicinity. This behavior of the profiles may not only be reflected in the greater variation of $f\delta_k^*/U_k$ with Re_k for the cylindrical

element, but also in the variation of the critical Re_k referred to previously in Section 3.1.

Data in the literature pertaining to the parametric behavior of the eddy shedding frequencies is minimal and limited to references 18 and 21. Reference 18 provides data on the Strouhal behavior for spherical and cylindrical elements with the latter having their axis in the spanwise direction rather than in the y-direction as in the present study. Reference 21, however, did study the Strouhal behavior of hemispherical elements. Both of these investigations, in contrast to the present study, were conducted in water channels, and in neither investigation are the results presented in a form sufficiently explicit to permit comparison with the present study on a basis other than that shown in figure 21. Be that as it may, the Strouhal behavior for hemispherical elements, as illustrated in figure 21, is compared in figure 24 with the Strouhal behavior as presented in reference 21. The nomenclature of reference 21 is such that S , R , x_R , and Re_R correspond to fk/U_k , k , x_k , and Re_k , respectively. The present measurements are significantly higher than those of reference 21 over the range of Re_k . Acarlar and Smith observe that the large scatter in their results for $Re_k > 1000$ is not due to experimental uncertainties but infer from the occurrence of multiple peak power spectra that there is an actual instability in the shedding behavior. Apart from the deviations in shedding frequency previously mentioned, this unstable behavior was not observed in the present study. The reason for the differences between the present study and that of reference 21 is not readily apparent, other than to comment that in the present study the frequencies were obtained from oscillograms, whereas in reference 21 the shedding frequency was determined from power spectra. It is perhaps worth commenting that the occurrence of multiple peak power spectra is not a sufficient condition for unstable behavior. It is not surprising that power spectra of asymmetric

and modulated signals, for example, as shown in figures 14, 15 and 16 would exhibit multiple peaks that vary not only with U_1 but with y and \bar{x} .

The variation of the Strouhal number, fk/U_k , with Re_k for the cylindrical element with $k/d = 1.0$ is compared in figure 25 with data faired from reference 18. The data selected from reference 18 are for a spherical element, and a cylindrical element with an aspect ratio of 1.0. The cylindrical element of the present study exhibits, within the experimental uncertainty, about the same Strouhal numbers for a comparable range of Reynolds number as does the spherical element. However, both have values that are almost half of those for the cylinder of reference 18. Inasmuch as a two-dimensional roughness element has been found to be more effective than a three-dimensional roughness element in inducing transition, it is perhaps not surprising that the cylinder with its axis in the spanwise direction would exhibit greater instability, if such is to be inferred from the greater Strouhal number, than one with its axis normal to the surface. The effect of aspect ratio, i.e., length to diameter ratio, on the Reynolds number of transition for cylindrical elements mounted on the surface with their axis in the spanwise direction was examined by Norman (reference 19). The Reynolds number of transition, as observed at a fixed distance downstream from the element, was found to decrease with increasing aspect ratio, over a range of aspect ratios from 1 to 8, and at an aspect ratio of 8 the Reynolds number of transition was actually lower than for a two-dimensional element. Furuya and Miyata (reference 18), on the other hand, investigated the effect of aspect ratio on Strouhal numbers for cylindrical elements with their axis in the spanwise direction. They found, over a range of aspect ratios from 1 to 6 that the Strouhal numbers decreased with increasing aspect ratio. The forementioned results from references 18 and 19 lead to the inference of decreasing Strouhal numbers with decreasing critical roughness Reynolds numbers for cylindrical

elements with their axis in the spanwise direction. This trend of Strouhal number with critical roughness Reynolds number is opposite in direction from that observed in the comparison of the behavior of hemispherical elements, and a cylindrical element in the present study. The issue is complicated by the evidence (reference 10) that two-dimensional roughness elements in inducing earlier transition do not exhibit the critical behavior involving the shedding of discrete vortices. Roughness shape, as well as aspect ratio, appear to play a role, and it may well be that the Strouhal number is not a sufficient criterion for indicating the degree of instability. It is apparent that these aspects warrant further study. Their resolution is amenable to experiment, and would go a long way toward providing a better understanding of the mechanism by which discrete roughness elements induce earlier transition to turbulent flow.

3.3 Eddy Shedding - Unsteady Flow

One would readily infer from the discussion in Section 3.2 that the "hairpin" eddies are intrinsic to the transition process induced by a three-dimensional roughness element. However, the view existing in the literature (references 14, 19, 20, 29, 30) is that such eddies are not related, or at best are only indirectly related, to the transition process. It was therefore deemed desirable to attempt to clarify the role they do play. To this end, the effect of an oscillatory free-stream was investigated. The free-stream velocity, U_1 , was oscillated sinusoidally with a small amplitude, ΔU_1 , about some mean value, \bar{U}_1 , and at a sufficiently low frequency, n , for a quasi-steady assumption to be valid. That is,

$$U_1(t) = \bar{U}_1 (1 + A \sin \omega t) \quad (3)$$

where $A = \Delta U_1 / \bar{U}_1$, and $\omega = 2\pi n$. Of particular interest is the effect of the variation of \bar{U}_1 relative to U_c .

The response of the laminar boundary layer without roughness to the free-stream oscillation is illustrated in figure 26. Figure 26 shows the distributions across the boundary layer of the oscillating velocity component, ΔU , and the phase of the oscillation, ϕ . A positive angle represents an advance in phase relative to the free-stream oscillation. The measurements were made at $x = 94$ cm with $\bar{U}_1 = 6.8$ m/s and $n = 1.0$ Hz. The resulting frequency parameter, x_ω , given by $x\omega/\bar{U}_1$, was 0.87, and A was 0.12. The trends exhibited by the distributions are similar to previous results (reference 31). The mean velocity distribution for the unsteady boundary layer without roughness is compared with its steady flow counterpart in figure 27. Also shown in figure 27 is a comparison of the mean velocity profiles for steady and unsteady flow downstream of a hemispherical roughness element. In the latter case, the measurements were made on the centerline at 2.54 cm downstream of a hemispherical element which had a nominal diameter of 3.18 mm, an effective height of 1.7 mm and was positioned at $x_k = 91.4$ cm. The free-stream velocities were slightly above critical being 8.3 and 8.2 m/s for the steady and unsteady flow respectively. The oscillating frequency was 1 Hz with $A = 0.13$. It can be concluded from the agreement of the disturbances for steady and unsteady flow that the oscillation behaves linearly. In addition, it is of interest to note that the mean velocity distribution at $\bar{x} = 14.9 k$, at about the critical speed, is insensitive to the time dependence of the eddy generating process associated with the unsteady flow.

The effect of an oscillating free-stream on the eddy shedding process was studied with the hemispherical element positioned at $x_k = 91.4$ cm with a $k = 1.7$

mm. Simultaneous signals of u in the boundary layer and of U_1 in the free-stream with free-stream oscillation frequencies of 1 and 2 Hz, at various \bar{U}_1 and associated ΔU_1 , were monitored by strip-chart recording at $\bar{z} = 0.0$ cm and $\bar{x} = 2.54, 30.5, \text{ and } 71.0$ cm. Figures 28-37 show the recordings that were obtained. The upper trace in each recording is the free-stream oscillating velocity, and the lower trace is the u -fluctuation in the boundary layer. Time increases from left to right, and a decreasing velocity is in a downward direction. Figures 28 and 29 show the recordings at $\bar{x} = 2.54$ cm for oscillation frequencies of 1 and 2 Hz respectively. The position in the boundary layer was at $y = 3.18$ mm. The eddy shedding is characterized by intense fluctuations in the direction of lower velocity superposed on the primary oscillation. This type of signal is consistent with the passage of "hairpin" eddies with "legs" that are rotating as indicated in Section 3.2. It should be noted that the asymmetry of eddy shedding relative to the free-stream oscillation as shown in figures 28 and 29 is not a real effect. It should not be interpreted, for example, as arising from a difference in the stability of an accelerating flow vis a vis a decelerating flow. It arises from an inadvertent low-frequency cut-off of 2 Hz in the hot-wire electronics for both probes which introduced a 60 degree and a 40 degree phase advance relative to the phase of the eddies for oscillation frequencies of 1 and 2 Hz respectively. In addition, the low-amplitude ripple of 20 Hz in the boundary layer signal is a consequence of the vibration induced by the fan motor which was previously referred to in Section 2.3 and which manifests itself because of the velocity gradient in the boundary layer. In any event, these extraneous effects do not mitigate the essential features of the effect of unsteady flow on the behavior of the roughness.

It is seen from figure 28 that for a steady flow at $U_1 = 8.5$ m/s ($Re_k = 337$) that eddies are shed continuously. When the flow is oscillated at a value

of \bar{U}_1 which coupled to the associated ΔU_1 is below some value of U_1 then no eddies are observed as in the recording for $\bar{U}_1 = 5.8$ m/s with $\Delta U_1 = 0.64$ m/s. However, eddies, although of relatively lower intensity, are observed over part of the cycle in the recording for $\bar{U}_1 = 6.9$ m/s and $\Delta U_1 = 0.84$ m/s. As \bar{U}_1 is further increased, the duration, ΔT , of the eddies increases, and at $\bar{U}_1 = 9.7$ m/s with $\Delta U_1 = 1.38$ m/s eddies are shed continuously over the cycle. A recording with a much faster chart speed, for the latter condition, is also shown in order to more clearly illustrate the nature of the fluctuations in the recording and their similarity to the fluctuations for the steady flow condition. If an appropriate allowance is made for the aforementioned phase advance, the variation of the amplitude and frequency of the fluctuation with U_1 is consistent with quasi-steady behavior. The recordings in figure 29 show results similar to figure 28. The smaller amplitude at the various \bar{U}_1 with $n = 2$ Hz, as compared to $n = 1$ Hz, is a consequence of the time constant of the Unsteady Wind Tunnel. However, it is evident that except for the effect the amplitude may have on ΔT the behavior scales with the frequency n .

It appears from the recordings in figures 28 and 29 that the onset of the "hairpin" eddies is associated with a critical value, U_{1c} , of the oscillatory free-stream. It can be readily shown from equation (3) that

$$\Delta T = \frac{1}{\omega} \left[\pi - 2 \sin^{-1} \left(\frac{U_{1c} - \bar{U}_1}{\Delta U_1} \right) \right] \quad (4)$$

and

$$U_{1c} = \Delta U_1 \sin \left[\left(\frac{\pi}{\omega} - \Delta T \right) \frac{\omega}{2} \right] + \bar{U}_1 \quad (5)$$

It is seen from equation (4) that the scaling of ΔT with frequency n is to be expected and that the effect of amplitude is to change the slope of the variations of ΔT with \bar{U}_1 about $\Delta T = 0.5$. It is of interest to compare the values of U_{1c} with the critical velocity, U_c , corresponding to the critical roughness Reynolds number of transition observed in Section 3.1. The values of U_{1c} obtained from equation (5) for the various recordings in figures 28 and 29, using the measured values of ΔT , averaged over a number of cycles, are summarized in Table I.

Table I

\bar{U}_1 (m/s)	ΔU_1 (m/s)	n (Hz)	ΔT (s)	U_{1c} (m/s)
6.9	0.84	1.0	0.19	7.6
7.6	0.98	1.0	0.36	8.0
8.7	1.20	1.0	0.68	8.1
7.1	0.58	2.0	0.09	7.6
7.6	0.64	2.0	0.19	7.9
8.7	0.78	2.0	0.39	8.1

No attempt was made to establish with specificity the conditions for $\Delta T = 1$, and consequently the associated value of U_{1c} is not included in the table. The consideration of a critical value of velocity, U_{1c} , from the recordings in figures 28 and 29 is not inconsistent with the discussion in Section 3.2, i.e., the presence of periodic disturbances at values of $U_1 < U_c$ and that there is a continuous transition from wave to vortex with increasing U_1 . It is not inconsistent because of the inference from figures 28 and 29 that disturbances which may exist for $U_1 < U_{1c}$, are restricted in their extent from the surface to $y < 3.18$ mm. Concomitantly, at a given \bar{U}_1 and ΔU_1 , U_{1c} is not a uniquely critical velocity. It may vary with \bar{x} and y , depending on the topology of the

vortical structures. Nevertheless, the correspondence of the values of U_{1c} and $U_c = 8.3$ m/s ($Re_k = 325$) is consistent with the conclusion that the eddy generation is a necessary condition for the induced transition. The difference in the value of $U_c = 8.3$ m/s from the previously stated value of 8.1 m/s used in connection with the discussion of figures 14 and 15 arises from the variation in v .

The question as to the intrinsic importance of the eddies to the transition process and the turbulence structure is addressed further by the strip-chart recordings shown in figures 30-37. These were obtained over a range of \bar{U}_1 and ΔU_1 comparable to those in figures 28 and 29. The various positions in the boundary layer and frequencies of the oscillating free stream velocity for which the recordings were obtained are summarized in Table II.

Table II

Figure No.	\bar{x} (cm)	y (mm)	n (Hz)
30	30.5	0.61	1.0
31	30.5	0.61	2.0
32	30.5	6.35	1.0
33	30.5	6.35	2.0
34	61.0	0.61	1.0
35	61.0	0.61	2.0
36	61.0	6.35	1.0
37	61.0	6.35	2.0

As for figures 28 and 29, time increases from left to right, and a decreasing velocity is in a downward direction. The recordings reveal a number of interesting features. It is seen that the eddies which are clearly observable at $\bar{x} = 2.54$ cm have, by $\bar{x} = 30.5$ cm, induced or evolved into a turbulent spot.

In this connection, it should be noted that the inadvertent low frequency cut-off of 2 Hz, referred to previously, has distorted the signal associated with the "spot" in the recordings with an oscillating free-stream. More specifically, it is responsible for the decreasing velocity associated with the spot passage, and the minimum and rapid rise following the passage of the spot as seen, for example, in the recording for $\bar{U}_1 = 8.2$ m/s in figure 30. Apart from this extraneous effect the "spots" as shown in the various recordings of figures 30-37 exhibit the characteristic features generally associated with the passage of a turbulent "spot" (references 32-34). These are an abrupt step-up in velocity near the surface, and abrupt step-down in velocity in the outer region of the boundary layer, and an increase in "spot" duration with \bar{x} resulting from the difference in velocity at the leading and trailing interfaces of the "spot". The changes in velocity associated with the "spot" passage reflect the difference between the turbulent velocity profile within the "spot", and the laminar velocity profile in the flow surrounding the "spot". However, a cautionary comment should be introduced in regard to the "spot" shape. It is not likely that a turbulent "spot" that originates from a finite train of eddies, as in the present case, will be similar in shape to the "spot" which originates from a momentary disturbance as in references 32-34.

For a steady velocity, which is near the critical speed, U_c , random turbulent "spots" form downstream of the roughness element. This is evident from each of the recordings in figures 30-37 for which $U_1 = 8.2$ or 8.3 m/s, and $n = 0.0$ Hz. The corresponding values of Re_k are 312 and 319 for $U_1 = 8.2$ and 8.3 m/s respectively. It appears that for the steady flow condition at $\bar{x} = 61.0$ cm that the "spots" are not only much more developed in their turbulence "structure" as compared to $\bar{x} = 30.5$ cm but may have increased in number. It is not unexpected that the "spots" will grow in size as they proceed downstream,

however it is not clear whether the aforementioned differences between the "spots" at $\bar{x} = 61.0$ cm, and 30.5 cm are real or apparent. This aspect was not investigated further, however, the "spot" formation is extremely sensitive to U_1 , and it may be that the differences reflect the imprecision in U_1 .

It is seen from the steady flow condition in figures 28 and 29, at $U_1 = 8.5$ m/s ($Re_k = 337$) that the intensity of the eddies is highly modulated. This behavior provides an explanation for the random occurrence of turbulent "spots" downstream of the roughness element, although there is a continuous generation of eddies by the roughness element. It is that the eddy shedding process, not being well controlled, and being highly modulated, eddies of relatively weak intensity may damp, and not all eddies participate in the evolution of the turbulent "spot". This point of view is supported by the behavior with an oscillating free-stream at the lower values of $U_1(m)$, where $U_1(m) = \bar{U}_1 + \Delta U_1$. In the recordings for $U_1(m) = 7.86$, 7.74, and 7.68 m/s in figures 30, 34 and 35, respectively, no turbulent spots are observed, although eddy shedding is observed in the recordings for $U_1(m) = 7.74$ and 7.68 m/s in figures 28 and 29. In addition the recordings at $U_1(m) = 8.22$, 8.10, and 7.98 m/s in figures 30, 34, and 36, respectively, show evidence of intermittency, i.e. "spots" do not necessarily occur every cycle. It should be noted that the above mentioned conclusion that the recordings in figure 28 and 29 at $U_1(m) = 7.74$ and 7.68 m/s illustrate eddy shedding is inferred from the decreasing velocity fluctuation associated with the disturbance, and that no attempt was made to specifically identify the vortical nature of the disturbance. In this connection, Hall (reference 17) in his smoke visualization study of the flow behind a sphere observed that although strong periodic laminar vortices were formed at subcritical Reynolds numbers, no turbulence occurred downstream, and the vortices decayed as they propagated downstream. Although Norman did not

explicitly address this question in reference 19, Morkovin (reference 35) has commented that Norman did observe similar behavior behind a fence-type roughness element with an intensity level as high as 4 percent.

The presence of random turbulent "spots" downstream of the roughness, at about the critical velocity, provides a different view than the flow visualization studies in regard to the detailed behavior of the transitional region where transition moves rapidly upstream as shown in figure 12. The china-clay studies of references 11 and 16, and the long-exposure smoke photographs of reference 14, have led to the view that the rapid upstream movement of transition is due to the vertex of a turbulent wedge that moves rapidly forward with a slight increase in roughness Reynolds number. The view from the present study is that this transitional region consists of turbulent "spots" which increase in number with a slight increase in roughness Reynolds number. As they move downstream, the "spots" grow laterally, overtake one another, and sweep out a wedge-like boundary which gives the impression of forward-moving turbulent wedge in flow visualization studies with a relatively long-time exposure. However, at a value of Re_k , sufficiently above the critical roughness Reynolds number, the "spots" may have so increased in number, and/or the eddies being shed may have so increased in intensity, that a turbulent wedge condition consistent with the flow visualization studies has been established.

It is shown in figures 28-37 that as \bar{U}_1 increases, the duration of the turbulent "spots" as well as the duration of eddy shedding increases. It was of particular interest to examine how the duration of "spots" and eddies compared. For this purpose, the variation of $n\Delta T$ with \bar{U}_1 at $\bar{x} = 2.54, 30.5, \text{ and } 61.0 \text{ cm}$ is shown in figure 38. Within the experimental accuracy, the small differences between the duration of eddy shedding at 1 Hz and 2 Hz, at $\bar{x} = 2.54 \text{ cm}$, may be real and reflect the effect of amplitude as given by equation (4). This effect

may also influence the scatter in the data at $\bar{x} = 30.5$ cm. However, faired curves are drawn through the data in order to facilitate the comparison. It is seen that the degree of correlation increases with \bar{U}_1 . For example, at $\bar{U}_1 = 8$ m/s, the duration of the turbulent "spot" at $\bar{x} = 30.5$ cm is 0.73 the duration of eddy shedding. At $\bar{U}_1 = 9$ m/s, the duration of the turbulent "spot" at $\bar{x} = 30.5$ cm is 0.9 the duration of eddy shedding. This behavior supports the view previously expressed, i.e., that with increasing Re_k the intensity of the eddies may increase, and a greater number may participate in the development of the "spot". At $\bar{x} = 61.0$ cm, the duration of the "spot" at $\bar{U}_1 = 8.0$ and 9.0 m/s is greater than that at $\bar{x} = 30.5$ cm. This is not unexpected since the velocity of the leading edge of the "spot" is much larger than the velocity of the trailing edge, and a small difference in ΔT can represent a large difference in the size of the "spot". The high degree of correlation of the duration of turbulent "spots" with the duration of eddy shedding, coupled to the fact that when the eddy shedding is periodic with the frequency of the free-stream oscillation the turbulent "spots" also became periodic, warrant the conclusion that not only is the eddy shedding essential to the transition process, but the eddies, although modified in form, are intrinsic to the vortical structure of the turbulence.

3.4 Instability and Induced Transition

In their study of the transition process for a Blasius flow on a flat plate, Klebanoff et al. (reference 36) drew an analogy between the secondary inflectional instability occurring in the later stage of transition, and the behavior of a three-dimensional roughness element. The "hairpin" eddies described in Sections 3.2 and 3.3 are markedly similar to the eddies described in reference 36 in connection with the secondary instability. However, the eddy shedding frequency associated with the roughness, as shown in figure 17, varies

with U_1^2 rather than with $U_1^{3/2}$ as in reference 36, and the analogy may best be regarded as qualitative.

The nature of the flow about a three-dimensional roughness element which results in an inflectional velocity profile in the immediate downstream vicinity of the roughness has been well documented (references 11-21). The essential features disclosed primarily by flow visualization studies are that two sets of vortices are established at a subcritical Reynolds number. One is a closely spaced pair of spiral filaments which form in the near wake, spiral upward at the rear of the roughness, and at the height of the roughness turn and trail downstream. The other is a "horseshoe"-shaped vortex, close to the surface, which wraps around the front of the roughness forming a pair of streamwise vortices which also extend downstream. This array of vortices which results in an inflectional profile at $\bar{z} = 0.0$ cm has been observed for a variety of three-dimensional roughness geometries such as spherical, cylindrical, hemispherical, conical, and rectangular. The flow visualization studies have also yielded the observation that as the free-stream velocity is increased, a waviness appears on the vortex filaments, and this waviness increases with increasing velocity until the filaments "roll-up" into "hairpin" eddies.

The qualitative behavior revealed by the flow visualization studies manifests itself in the spanwise distributions of U and u' as shown in figure 39 and 40 respectively. The measurements were made at a distance of 14.9 roughness heights downstream of the roughness elements and for three different unit Reynolds numbers. The behavior of the frequency of eddy shedding discussed in Section 3.2 suggested that it would be more appropriate to carry out the boundary layer surveys at a given U_1/ν rather than U_1 . Consequently, U_1 was adjusted to compensate for changes in ν , and the value of U_1 noted in figure 39 is the average value for the various distributions. The unit Reynolds numbers

selected were such that one was below the critical roughness Reynolds number, one was at or slightly above critical, and one was significantly above critical. In this connection, it should be noted that the value of U_1/ν corresponding to a critical roughness Reynolds number of 325 is $4.76 \times 10^5 \text{ (m}^{-1}\text{)}$. At the subcritical Reynolds number the spanwise distributions of U clearly demonstrate the presence of the two pairs of streamwise vortices observed in the flow visualization studies. The pair of vortex filaments rotate in such a direction as to transfer momentum away from the plate at $\bar{z} = 0.0 \text{ cm}$, and the "horseshoe" vortex rotates so as to transfer momentum towards the plate at $\bar{z} = \pm 0.5d$. The spanwise distribution of u' at the subcritical Reynolds number apparently reflects a low level unsteadiness in the two sets of stationary vortices. At the higher Reynolds numbers the peak in the spanwise distributions of u' in figure 40 closely indicates the presence of the "hairpin" vortices. With increasing Reynolds number the peak increases in intensity and extends further from the surface consistent with the behavior of the "hairpin" eddy as discussed in Sections 3.2 and 3.3. It can also be inferred, within the accuracy of the spanwise distributions, that the spanwise extent of the eddy is on the order of $\bar{z}/d > \pm 0.5$, centered about $\bar{z} = 0.0 \text{ cm}$, and that the disturbed boundary layer can be separated into two regions. An outer region, $y/k \geq 1.0$, where the "hairpin" eddy is dominant, and an inner region, $y/k \leq 1.0$, where the two sets of vortices alluded to at the subcritical Reynolds number, still play a role. The latter conclusion is supported by the double peaks in the spanwise distribution of u' , close to the surface at the Reynolds numbers above critical, which have the same spanwise spacing as the peaks at the subcritical Reynolds number. The intensity of these peaks increases markedly from about 0.15 percent at the subcritical Reynolds number to about 6 percent at the highest Reynolds number. However, this increase in intensity is not necessarily inconsistent

with the presence of the two sets of vortices. The increase in intensity may reflect an increase in concentration of the vortices with increasing velocity as well as a degree of unsteadiness resulting from the interaction with the "hairpin" vortices.

The spanwise distributions of U at the higher Reynolds number, in the presence of eddy shedding, are similar in appearance to the distributions at the subcritical Reynolds number except that they exhibit a greater spanwise variation in U which extends over a greater region of the boundary layer. Be that as it may, the spanwise distributions of U can also be interpreted as being consistent with the separation of the disturbed boundary layer into outer and inner regions as outlined above. However, the "hairpin" eddies do have the same sense of rotation as the set of spiral vortices, and their orientation may be such as to make the above interpretation somewhat tenuous. Nevertheless, it is surprising that the change from a stationary set of spiral vortices to a time dependent "hairpin" eddy shedding, deduced from the flow visualization studies, does not have a greater effect on the spanwise distributions of U and u' near the surface.

In order to examine the instability question further, as well as to examine the transition to a fully developed turbulent boundary, profiles of U and u' , across the boundary layer, were measured on the centerline for different downstream positions ranging from $\bar{x} = 1.27$ to 30.5 cm. The resulting distributions for U and u' are shown in figures 41(a)-(g) and 42(a)-(g) respectively. The distributions at each \bar{x} -position, except those at $\bar{x} = 30.5$ cm were measured at five different unit Reynolds numbers, three of which were the same as for the spanwise distributions of figures 39 and 40, one was an additional unit Reynolds number below critical, and one an additional unit Reynolds number above critical.

The mean velocity profiles at $\bar{x} = 1.27$ cm in figure 41(a) are sufficiently inflectional to sustain an incipient wave type of instability which develops into a rolled-up vortex, and eddy generation at and above the critical roughness Reynolds number. The inflectional nature of the mean velocity profiles in the immediate downstream vicinity of the roughness at $\bar{x} = 1.27$ cm (7.5k), and $\bar{z} = 0.0$ cm, is illustrated in figures 43(a) and 43(b) in which they are compared with inflectional profiles for which stability calculations have been carried out. In figure 43(a) the mean velocity profiles at unit Reynolds up to and including the unit Reynolds number which is slightly above critical are compared with the Lin profile (reference 37) for a two-dimensional mixing layer in which one fluid is at rest. Similarly, in figure 43(b) the same profiles are compared with the Hartree profile (reference 38) for a two-dimensional separated layer. The measurements of mean velocity, close to the surface, and which are nearly constant, reflect the behavior of a hot-wire in a separated region, and the momentum thickness, θ , was obtained by extrapolating the distributions smoothly to zero at the surface. The boundary layer profiles were matched to the mixing layer distribution at $U/U_1 = 0.5$, and it is seen from the comparison, as well as from the comparison in figure 43(b), that the inflection is sufficiently close to the wall that the instability may be regarded as being more characteristic of a wall-bounded flow rather than a free-shear layer, but one which is specific to the geometry of the roughness, and the Reynolds number. This is supported by the variation of frequency with U_1^2 , at least for the size of roughness elements herein investigated, whereas a free-shear layer would imply a variation with $U_1^{3/2}$. In addition, the mixing layer, and the separated laminar boundary layer have their inflection at $U/U_1 = 0.5$. The presence of the separated region tends to obscure the inflection point in the boundary layer profiles. However, the corresponding distributions of u' at $\bar{x} = 1.27$ cm in figure 42(a) indicate a

maximum in u' at $y/k = 1.34$. It is reasonable to assume that this position, for a resulting instability, is the point of inflection. The corresponding value of U/U_1 , averaged over the three unit Reynolds numbers, is 0.34 which at $U_1 = 8.3$ m/s yields 6.5 mm for the wavelength of the instability. From this point of view, the instability at the critical Reynolds number is strongly nonlinear with u'/U_1 of about 6 percent, and the "hairpin" eddy developing within one or two wavelengths. This rapid development of the "hairpin" eddy is not inconsistent with an inflectional instability when it is compared to the two to three wavelengths, observed in references 36 and 39, over which the nonlinear behavior of three-dimensional Tollmien-Schlichting waves resulted in the generation of "hairpin" eddies. However, in the latter case the wavelengths were very much longer.

The distributions of u' indicate that at the subcritical Reynolds numbers the observed instability may behave linearly, i.e. governed by linear stability theory. At $U_1/\nu = 4.13 \times 10^5 (\text{m}^{-1})$ the maximum in u'/U_1 increases from 1.0 percent at $\bar{x} = 1.27$ cm to 1.8 percent at $\bar{x} = 2.54$ cm, and then damps with increasing distance downstream. At the lower Reynolds number of $3.54 \times 10^5 (\text{m}^{-1})$ the maximum in u'/U_1 at $\bar{x} = 1.27$ cm is 0.65 percent, and the nature of the distribution is such as to indicate that this represents a small degree of amplified disturbance above the background disturbances. However, in contrast to the higher Reynolds number, it exhibits no further growth and damps with distances further downstream. It was shown in reference 39 that a relatively weak three-dimensional Tollmien-Schlichting wave with an intensity level of 2 percent may still behave linearly. It is therefore reasonable to infer that the instabilities at the subcritical Reynolds numbers are also behaving linearly. In this connection, it is of interest, despite the three-dimensionality of the instability, to compare the unstable frequency observed at

$U_1/\nu = 4.13 \times 10^5 (\text{m}^{-1})$ with the two-dimensional stability calculations of references 40 and 41 for the separated boundary layer and mixing layer respectively. The pertinent nondimensional frequency parameters, $2\pi f\nu/U_1^2$ and $2\pi f\theta/U_1$ are 68×10^{-5} for the separated layer, and 0.20 for the mixing layer. The corresponding Reynolds numbers based on displacement thickness and momentum thickness, R_{δ^*} and R_θ , are 1170 and 300. At $2\pi f\nu/U_1^2 = 68 \times 10^{-5}$, Branch II of the stability diagram for the separated layer is at $R_{\delta^*} = 1,000$. At $R_{\delta^*} = 1170$, the unstable frequency, at $U_1/\nu = 4.13 \times 10^5 (\text{m}^{-1})$, is barely outside the unstable region. At $2\pi f\theta/U_1 = 0.20$ and $R_\theta = 300$, the unstable frequency is within the instability region for the mixing layer which has as its outer bound $2\pi f\theta/U_1 = 0.27$. Comparison of the unstable frequencies at the higher Reynolds numbers is moot since they are regarded as behaving nonlinearly. However, it is evident that with increasing Reynolds number the unstable frequencies extend further into the damped region for the separated layer. As for the mixing layer comparison, the unstable frequency at the Reynolds number slightly above critical is still within the unstable region, but at $U_1/\nu = 5.97 \times 10^5 (\text{m}^{-1})$ and $6.81 \times 10^5 (\text{m}^{-1})$ the unstable frequencies are outside the zone of instability.

The purpose of the foregoing comparison with the stability calculations is not to imply any direct correspondence, but is solely for the purpose of evaluating whether the profiles in the immediate downstream vicinity of the roughness may be sufficiently inflectional to undergo the observed instabilities. The "strength" of the inflection and its position relative to the surface are the significant criteria in assessing, at least qualitatively, the instability of an inflectional profile in a wall-bounded flow. In general, increased proximity of the inflection to the surface tends to have a stabilizing effect, whereas, an increase in the "strength" of the inflection is destabilizing. Inasmuch as it has been previously assumed that the instability

is essential inviscid, i.e. that the inflection is at the critical layer, the inflection should be the governing criterion. It is seen in figures 43(a) and (b) that the measured profiles are more inflectional than either the Hartree or mixing layer profiles, and it can be concluded that the measured profiles are sufficiently inflectional to undergo the observed instabilities. In this connection it would be helpful to have a stability calculation, albeit two-dimensional, of a profile that is representative of the measured profile. There is also an indication from the measured profiles in figures 43(a) and (b) that the strength of the inflection may increase with increasing Reynolds number. This may contribute to the very rapid increase in amplification, shown in figure 42(a), for the corresponding range of Reynolds numbers.

The foregoing discussion has attempted to characterize the instability resulting from a three-dimensional roughness element as an inflectional instability. In lieu of any theoretical calculations for evaluating three-dimensional instabilities in three-dimensional flows, the rationalization has taken the liberty of comparison with the theoretical guidelines existing for two-dimensional instabilities in two-dimensional flows, and a reasonable case for inflectional instability has been made. The sensitivity of the eddy shedding frequencies to background disturbances, and their nondimensional scaling, as discussed in Section 3.2, also provide indirect evidence for an inflectional instability. The consideration of an inflectional instability provides a simple model for the behavior of a three-dimensional roughness element. The critical roughness Reynolds number reflects the separation into linear and nonlinear instabilities. In the linear range, at subcritical Reynolds numbers, the disturbance, although it may be initially amplified, cannot sustain itself. It can dissipate laterally, and damp as it travels downstream into more stable regions where the mean flow profiles become less and

less inflectional, as evidenced by the profiles in figure 41. At some Reynolds number the instability becomes nonlinear. In this range the disturbance can no longer be characterized by linear theory. A frequency which may be stable according to linear theory may well be unstable when it is nonlinear. The amplification in the nonlinear range of Reynolds numbers is extremely rapid, and the instability results in a rolled-up vortex. As concluded in Section 3.3, this vortex is intrinsic to the transition process. The final onset of turbulence results from vortical instability, and the complex vortex-vortex interaction of the shedding vortices with the pre-existing stationary vortices.

The above model, however, does not explicitly account for the observations of Hall (reference 17), and Morkovin (reference 35) referred to in Section 3.3, i.e. the occurrence of "hairpin" eddies with an intensity level as high as 4 percent which develop and decay without the onset of turbulence. This behavior implies a narrow range of nonlinearity with Reynolds number for which the resulting vortices, and vortex-vortex interaction are not unstable. The intensity level of 4 percent is consistent with this possibility, and the distributions of intensity in figure 42(a). In any event, this aspect merits further investigation, not only to ascertain its role in the context of the present investigation, but in view of its importance in understanding the vortex dynamics involved in the onset of turbulence. In the same vein, it is not evident that the formation of the "hairpin" eddies from a rolling up of the spiral vortex filaments can be reconciled with an inflectional instability. If the flow visualization is to be taken literally, then the evolution of the "hairpin" eddies involves a vortical instability. On the other hand, their formation from an inflectional instability would involve nonlinear development of an initial Rayleigh instability, and the "hairpin" eddies may well be generated by a time-dependent concentration of spanwise vorticity, and not by an

altered state of the spiral vortex filaments. One may speculate that the vagaries of flow visualization do not provide an insight into the realities of such distinctions. For example, is the flow tracer "captured" by one set of vortices at the expense of the other thus resulting in an apparent transition from the spiral vortex filaments to the "hairpin" eddies? It is evident that this aspect also merits further investigation in order to arrive at a proper understanding of the induced transition to turbulent flow.

The critical behavior of a three-dimensional roughness element in inducing transition to turbulent flow is clearly demonstrated by the distributions of U and u' at the various Reynolds numbers. At subcritical Reynolds numbers the distributions return to that which would exist without the roughness present. In figure 44 the mean velocity distributions at the various \bar{x} -positions for the subcritical Reynolds numbers, and the Reynolds number which is slightly above critical, are compared nondimensionally with the mean velocity profile measured without the roughness. The distance, \bar{x} , required to return to the undisturbed condition is dependent on the Reynolds number. At unit Reynolds numbers of 3.54×10^5 , and $4.13 \times 10^5 (\text{m}^{-1})$, for example, the recovery occurs in $\bar{x} = 12.7$ and 20.3 cm respectively. At the Reynolds number which is just above critical the mean velocity distributions are indicative of transitional flow consisting of intermittent turbulent "spots". The changes in profile shape with \bar{x} reflect an increase in the percent of time that the flow is turbulent with increasing \bar{x} consistent with the downstream growth of turbulent "spots". However, at this Reynolds number the flow condition is extremely sensitive to Reynolds number. The distributions of u' at this Reynolds number reflect this sensitivity in their variation with \bar{x} .

As discussed in Section 3.3 the turbulent "spots" are initiated closer to the roughness with increasing Reynolds number until at some Reynolds number a

wedge of turbulence may be regarded as being attached to the roughness. Since a finite distance is required for the instability, the wedge of turbulence, albeit in close proximity to the roughness, is not actually attached. At a unit Reynolds number of $6.81 \times 10^5 (\text{m}^{-1})$, which is the highest for which the distributions were measured, the corresponding Re_k is 550, and the wedge of turbulence has its origin at $\bar{x} = 5.08 \text{ cm}$. It is evident from the progressive changes in the distributions of U and u' with \bar{x} , at the two highest Reynolds numbers, that the transition to a turbulent state characteristic of a "fully developed" turbulent boundary layer is initiated near the surface. In this connection, it should be noted that the turbulence at the origin of the wedge, or at its point of initiation has in general not been characterized. In the present case, turbulence is characterized solely by the u -fluctuation having a continuous spectrum. The turbulence, according to this definition, begins near the surface, moves out in y with increasing \bar{x} , but is not characteristic of "fully developed" turbulence until $\bar{x} = 30.5 \text{ cm}$. This is seen in figure 45 in which the mean velocity distributions at various \bar{x} for unit Reynolds numbers of 5.97×10^5 and $6.81 \times 10^5 (\text{m}^{-1})$ are compared with a turbulent boundary layer profile measured by Purtell et al (reference 42). The position at which the turbulence in the wedge becomes characteristic of a "fully developed" boundary layer is examined in figure 46 in which the distributions of u' at $\bar{x} = 20.3$ and 30.5 cm at a unit Reynolds number of $6.81 \times 10^5 (\text{m}^{-1})$ are compared with a distribution from reference 42 for a turbulent boundary layer at about the same Reynolds number. The measurements of Purtell et al were made with a linearized hot-wire response whereas the present measurements were not. However, the magnitude of the difference between the distributions is such that attributing the difference to the method of measurement is questionable. Either, it is due to other experimental uncertainties, or is real. The latter is a strong

possibility. The equivalence of Reynolds numbers based in one case on velocity, and in the other on distance has not been thoroughly evaluated for a turbulent boundary. Involved herein is the question of "new" vs. "aged" turbulence. The present measurements were made at a much larger U_1 than the measurements of Purtell et al, whereas the latter were made at what may be considered a much larger \bar{x} . In view of these uncertainties it is concluded that the turbulence as well as the mean velocity, are characteristic of a "fully developed" turbulent boundary layer at $\bar{x} = 30.5$ cm. The values of \bar{x} are not scaled with k since there is not adequate evidence that such scaling is appropriate. The position in the wedge at which the turbulence becomes characteristic of a "fully developed" boundary layer is observed in the present study to move upstream with increasing Reynolds number but whether an asymptotic \bar{x}/k is reached has, to date, not been established nor has the effect of roughness size, shape, and position on such scaling been determined. This question of scaling merits further investigation, and it is apparent that considerable care should be given to the state of a "tripped" boundary layer in order to ascertain the degree to which it is free of distortion.

4. Summary and Conclusions

An experimental investigation is described which is directed toward extending the technical database and improving our understanding of the manner in which single three-dimensional roughness elements induce earlier transition from laminar to turbulent flow in boundary layers. The investigation was carried out primarily with hemispherical roughness elements in a well characterized zero-pressure gradient laminar boundary layer on a flat plate. The critical roughness Reynolds number, Re_k , at which turbulence may be regarded

as originating from the roughness, was experimentally determined for the hemispherical elements herein considered to be independent of roughness size and position. The value of Re_k based on the roughness height and the velocity in the boundary layer at the height of the roughness was 325. The dependence of Re_k on roughness shape and aspect ratio, as well as its imprecision in correlating the behavior of single roughness elements, is demonstrated. It is shown that the critical behavior of three-dimensional roughness elements and the associated Re_k are a consequence of the critical onset of an eddy generating process. The effect of a steady and an oscillatory free-stream velocity on the eddy shedding behavior was also investigated. The results demonstrate that the eddy shedding frequency varies linearly with the square of the free-stream velocity, and is also functionally dependent on the ratio of roughness height to position. In this connection, it appears that the boundary layer displacement thickness at the roughness position, without the roughness present, is a more appropriate length scale for characterizing the Strouhal behavior than the customarily used roughness height. It is also shown that roughness shape and aspect ratio influence the Strouhal behavior. It is concluded that the eddies resulting from the eddy shedding process are essential and directly involved in the transition process. They may be regarded as being elemental "structures" of the turbulence generated by the complex interaction of the shedding vortices with the pre-existing stationary vortices that lie near the surface and are inherent to the flow about a three-dimensional obstacle in a laminar boundary layer. The mean and fluctuating flow fields were measured on the centerline at different positions downstream of a hemispherical roughness element which had a height of 1.7 mm and was positioned at 91.4 cm from the leading edge of the flat plate. The measurements were made at Reynolds numbers which were below and above critical. Such measurements not only extend the technical database for

characterizing roughness element behavior, but also illustrate that considerable care should be given to the state of the "tripped" boundary layer in order to ascertain the degree to which it is free of "distortion". These measurements also permitted within the limitations imposed by present stability theory, an evaluation of whether an inflectional instability may be the fundamental mechanism underlying the behavior of three-dimensional roughness elements. It is concluded that the behavior of three-dimensional roughness elements is consistent with such an instability. However, further investigation is required in order to reconcile this view with the observations from the flow visualization studies.

5. Acknowledgment

The authors wish to express their appreciation to Mr. L. M. Sargent and Mr. S. Woo for their assistance in the processing of data, and the preparation of figures. The authors are deeply grateful to Mrs. S. Johnson for her invaluable assistance in the preparation of the manuscript and figures. The authors are also indebted to Mr. E. Thompson of the Arnold Engineering Development Center for his support in initiating the investigation, and to Dr. K. Kushman of the Arnold Engineering Development Center for his support, encouragement and patience during the course of the investigation.

References

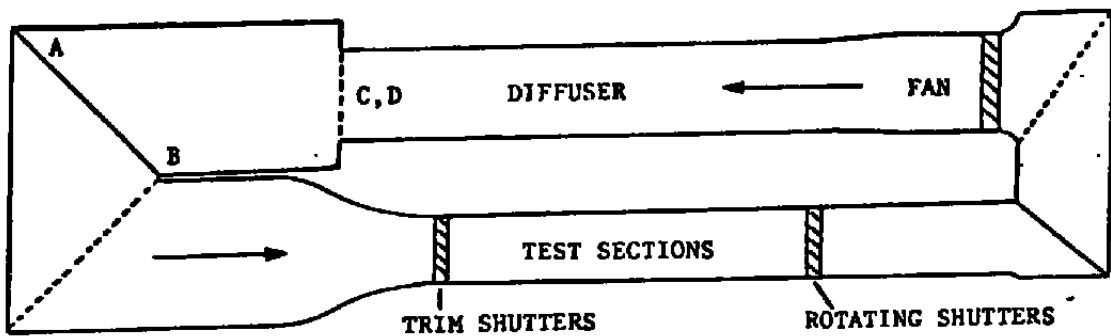
1. R. Betchov, and W. O. Criminale, Jr., Stability of Parallel Flows, Academic Press, New York, 1967.
2. I. Tani, Boundary-Layer Transition, Ann. Rev. Fluid Mech., Vol. 1, p. 169, 1969.
3. M. V. Morkovin, Critical Evaluation of Transition from Laminar to Turbulent Shear Layers with Emphasis on Hypersonically Traveling Bodies, Air Force Flight Dyn. Lab. Tech. Rep. AFOL-TR-68-149, March 1969.
4. J. T. Stuart, Nonlinear Stability Theory, Ann. Rev. Fluid Mech., Vol. 3, p. 349, 1971.
5. E. Reshotko, Boundary-layer Stability and Transition, Ann. Rev. Fluid Mech., Vol. 8, p. 311, 1976.
6. P. S. Klebanoff and Z. W. Diehl, Some Features of Artificially Thickened Turbulent Boundary Layers, NACA Report 1110, 1952 or NACA TN 2475, 1951.
7. A. M. O. Smith and D. W. Clutter, The Smallest Height of Roughness Capable of Affecting Boundary Layer Transition, Jour. Aerospace Sci., Vol. 26, No. 4, p. 229, April 1959.
8. I. Tani, Effect of a Two-Dimensional and Isolated Roughness on Laminar Flow, Boundary Layer and Flow Control, edited by G. V. Lachmann, Pergamon Press, New York, Vol. 2, p. 637, 1961.
9. P. S. Klebanoff, G. B. Schubauer and K. D. Tidstrom, Measurements on the Effect of Two-Dimensional and Three-Dimensional Roughness Elements on Boundary Layer Transition, Jour. Aero. Sci., Vol. 22, No. 11, p. 803, November 1955.
10. P. S. Klebanoff and K. D. Tidstrom, Mechanism by which a Two-Dimensional Roughness Element Induces Boundary-Layer Transition, Phys. Fluids, Vol. 15, No. 7, p. 1173, July 1972.

11. N. Gregory and W. S. Walker, The Effect of Transition of Isolated Surface Exorescences in the Boundary Layer, Aero. Res. Council, Rept. and Mem., No. 2779, 1956.
12. J. Weske, Experimental Study of Detail Phenomena of Transition in Boundary Layers, Tech. Note BN91, Inst. Fluid Dyn. and App. Math., Univ. Maryland, February 1957.
13. I. Tani, A. Komoda, Y. Komatsu, and M. Iuchi, Boundary Layer Transition by Isolated Roughness, Aero. Res. Inst., Tokyo Univ., Report No. 375, November 1962.
14. M. Mochizuki, Smoke Observation on Boundary Layer Transition Caused by a Spherical Roughness Element, Jour. Phys. Soc. Japan, Vol. 16, No. 5, p. 995, May 1961.
15. M. Mochizuki, Hot-Wire Investigations of Smoke Patterns Caused by a Spherical Roughness Element, Natur. Sci. Rept., Ochanomizu Univ., Tokyo, Japan, Vol. 12, No. 2, 1961.
16. T. Matsui, Transition in a Laminar Boundary Layer Due to an Isolated Roughness Element, Res. Rept. No. 12, Faculty of Engineering, Gifu University, Gifu, Japan, 1962.
17. G. R. Hall, Interaction of the Wake from Bluff Bodies with an Initially Laminar Boundary Layer, AIAA Journal, Vol. 5, No. 8, p. 1386, August 1967.
18. Y. Furuya and M. Miyata, Visual Studies on the Wake of a Roughness Element Proximate to a Wall, Memoirs of the Faculty of Engineering, Nagoya University, Vol. 24, No. 2, p. 278, November 1972.
19. R. S. Norman, On Obstacle Generated Secondary Flows in Laminar Boundary Layers and Transition to Turbulence, Ph.D. Thesis, Illinois Institute of Technology, 1972.

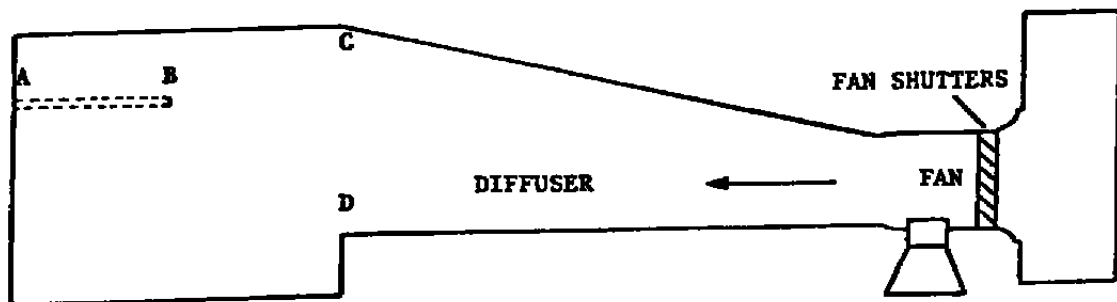
20. A. K. Gupta, Some Observations in the Wake of a Small Vertical Cylinder Attached to a Flat Plate, *Phys. Fluids*, Vol. 23, No. 1, p. 221, January 1980.
21. M. S. Acarlar and C. R. Smith, An Experimental Study of Hairpin-Type Vortices as a Potential Flow Structure of Turbulent Boundary Layers, Lehigh University Report FM-5, October 1984.
22. P. S. Klebanoff, Effect of Free-Stream Turbulence on a Laminar Boundary Layer, *Bull. Am. Phys. Soc.*, Vol. 10, No. 11, p. 1323, November 1971.
23. L. Schiller, Strömung in Rohren, *Handbuch der Experimentalphysik*, Vol. 4, Pt. 4, p. 189, Leipzig, 1932.
24. L. K. Loftin, Effects of Specific Types of Surface Roughness in Boundary-Layer Transition, NACA ACR L5J29a, February 1946.
25. L. Klanfer and T. R. Owen, The Effect of Isolated Roughness on Boundary Layer Transition, R.A.E. Tech. Memo. No. Aero. 355, March 1953.
26. F. R. Hama, An Efficient Tripping Device, *Jour. Aero. Sci.*, Vol. 24, No. 3, p. 236, March 1957.
27. I. Wygnanski and R. A. Petersen, Coherent Motion in Excited Free Shear Flows, AIAA-85-0539, AIAA Shear Flow Control Conference, March 12-14, 1985.
28. F. R. Hama, Streaklines in a Perturbed Shear Flow, *Phys. Fluids*, Vol. 5, p. 644, June 1962.
29. R. S. Norman and M. V. Morkovin, A Mechanism of Transition Downstream of an Isolated 3-D Roughness, *Bull. Am. Phys. Soc.*, Vol. 17, No. 11, p. 1081, November 1972.
30. I. Tani, Three-Dimensional Aspects of Boundary-Layer Transition, *Proc. Indian Acad. Sci., (Engg. Sci.)*, Vol. 4, Pt. 2, p. 219, August 1981.
31. P. G. Hill and A. H. Stenning, Laminar Boundary Layers in Oscillating Flow, *Trans. ASME, Series D, Jour. Basic Engg.*, Vol. 82, p. 595, 1960.

32. G. B. Schubauer and P. S. Klebanoff, Contributions on the Mechanics of Boundary-Layer Transition, NACA TN 3489, September 1955, also NACA Rept. 1289, 1956.
33. I. Wygnanski, M. Sokolov, and D. Friedman, On a Turbulent Spot in a Laminar Boundary Layer, Jour. Fluid Mech., Vol. 78, part 4, p. 785, December 1976.
34. B. Cantwell, D. Coles and P. Dimotakis, Structure and Entrainment in the Plane of Symmetry of a Turbulent Spot, Jour. Fluid Mech., Vol. 87, part 4, p. 641, August 1978.
35. M. Morkovin, Bypass Transition to Turbulence and Research Desiderata, CP-2386, Transition in Turbines Symposium, NASA Lewis Research Center, May 15-16, 1984.
36. P. S. Klebanoff, K. D. Tidstrom, and L. M. Sargent, The Three-Dimensional Nature of Boundary Layer Instability, Jour. Fluid Mech., Vol. 12, part 1, p. 1, January 1962.
37. C. C. Lin, On the Stability of the Laminar Mixing Region Between Two Parallel Streams in a Gas, NACA TN 2887, January 1953.
38. D. R. Hartree, On an Equation Occurring in Falkner and Skan's Approximate Treatment of the Equations of the Boundary Layer, Proc. Cambridge Phil. Soc. 33, 223, 1937.
39. P. S. Klebanoff, and K. D. Tidstrom, Evolution of Amplified Waves Leading to Transition in a Boundary Layer with Zero Pressure Gradient, NASA TN D-195, September 1959.
40. A. R. Wazzan, T. T. Okamura and A. M. O. Smith, Spatial and Temporal Stability Charts for the Falkner-Skan Boundary Layer Profiles, McDonnell Douglas Report No. DAC-67086, September 1968.
41. M. Lessen, On Stability of Free Laminar Boundary Layer Between Parallel Streams, NACA Rept. 979, March 1950.

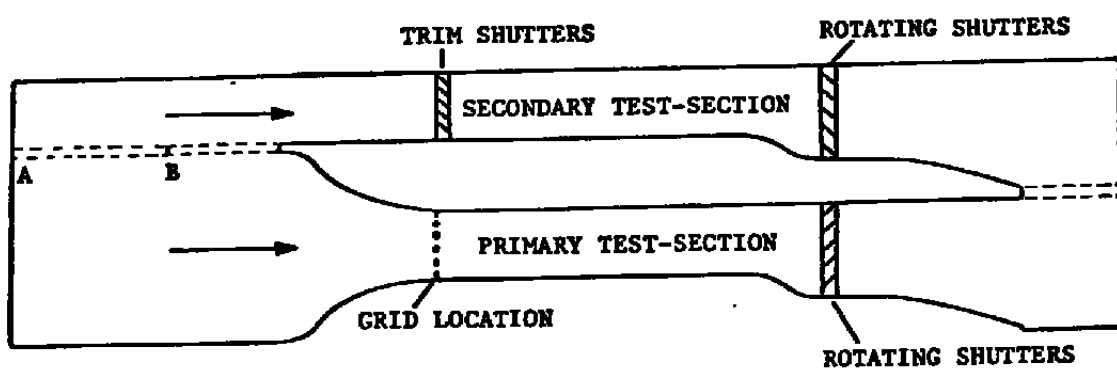
42. L. P. Purtell, P. S. Klebanoff and F. T. Buckley, Turbulent Boundary at Low Reynolds Number, Phys. Fluids, Vol. 24, p. 802, May 1981.



a. Plan view



b. Return duct



c. Primary and secondary ducts

Figure 1. Schematic drawing of Unsteady Flow Facility.

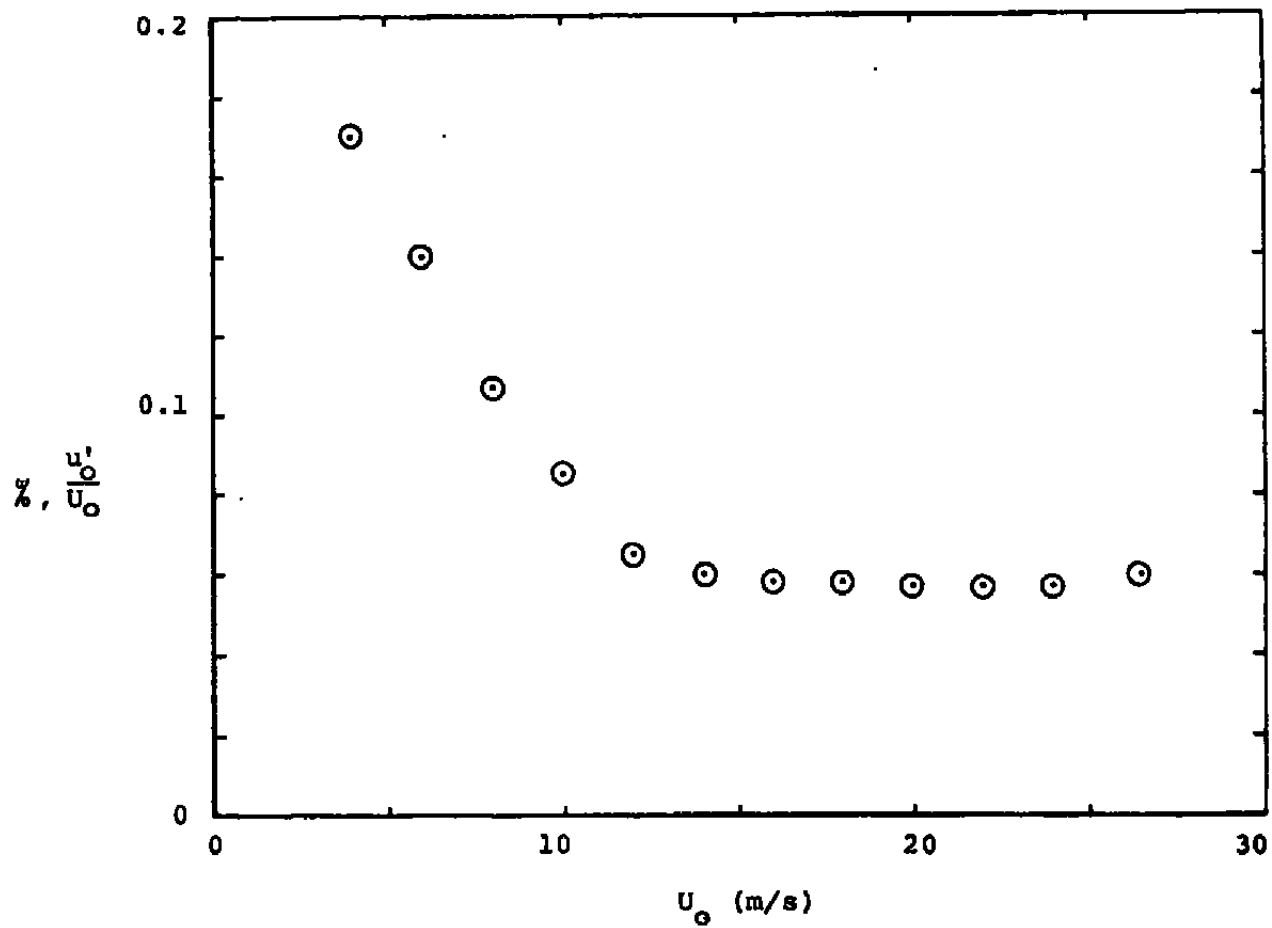


Figure 2. Turbulence intensity upstream of flat plate.

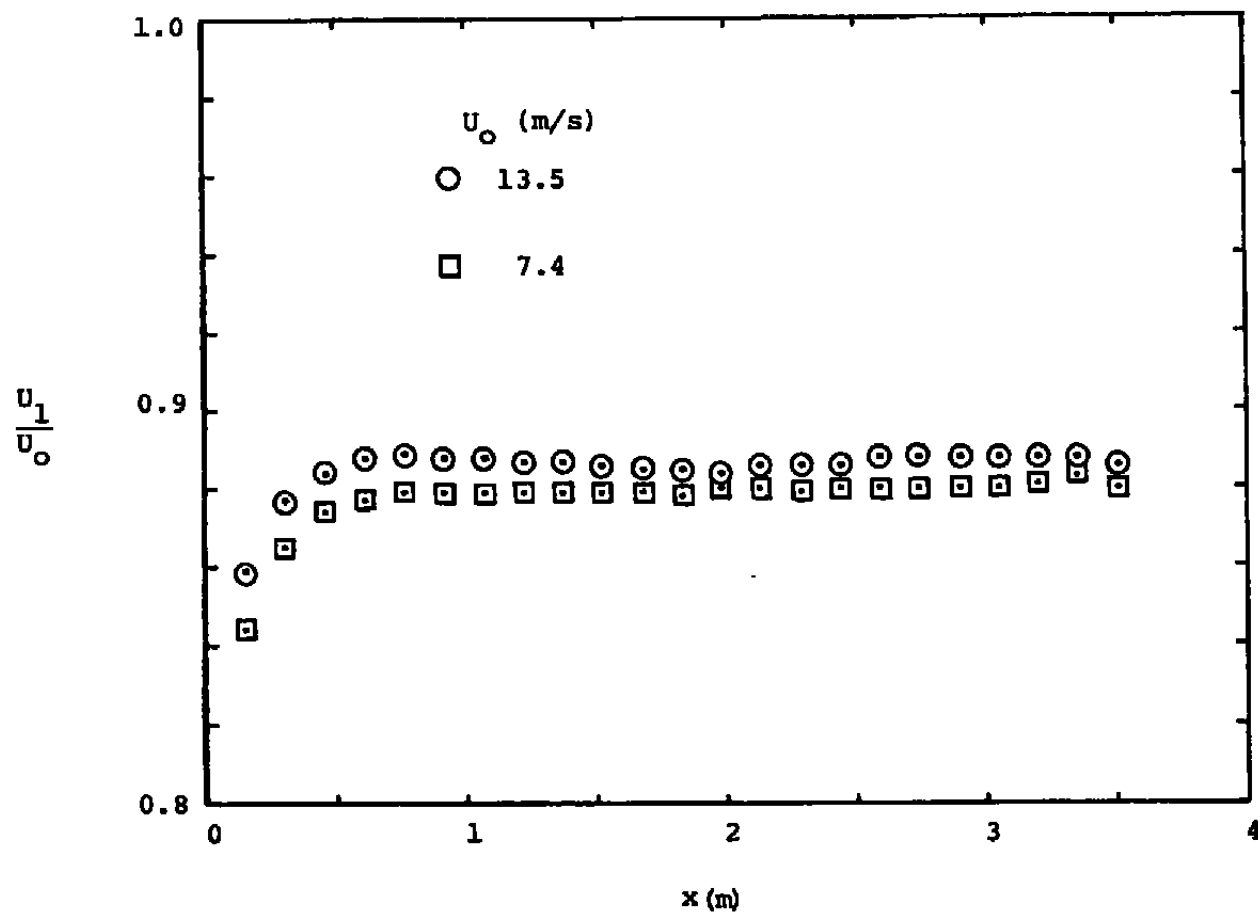


Figure 3. Distribution of freestream velocity along flat plate.

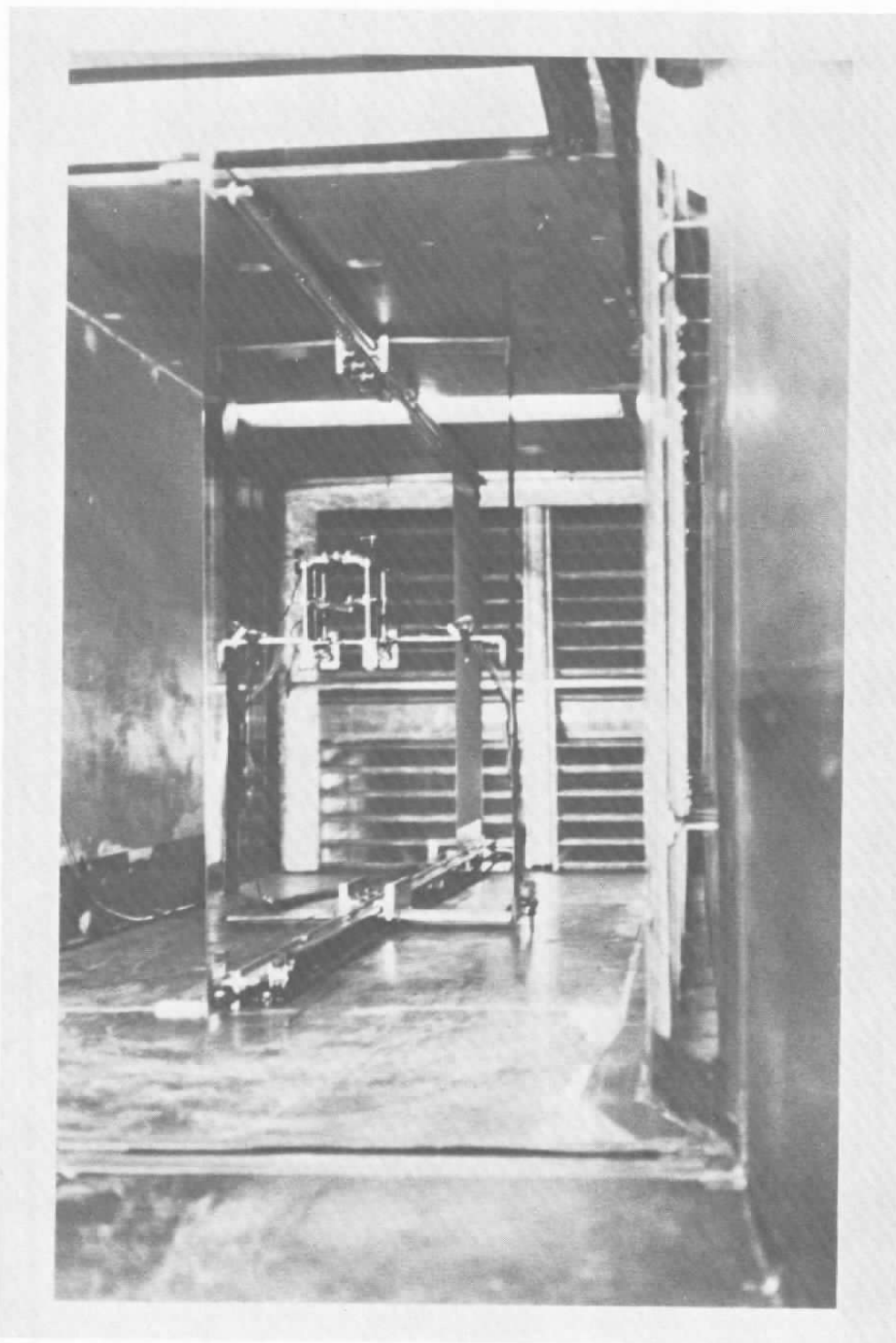
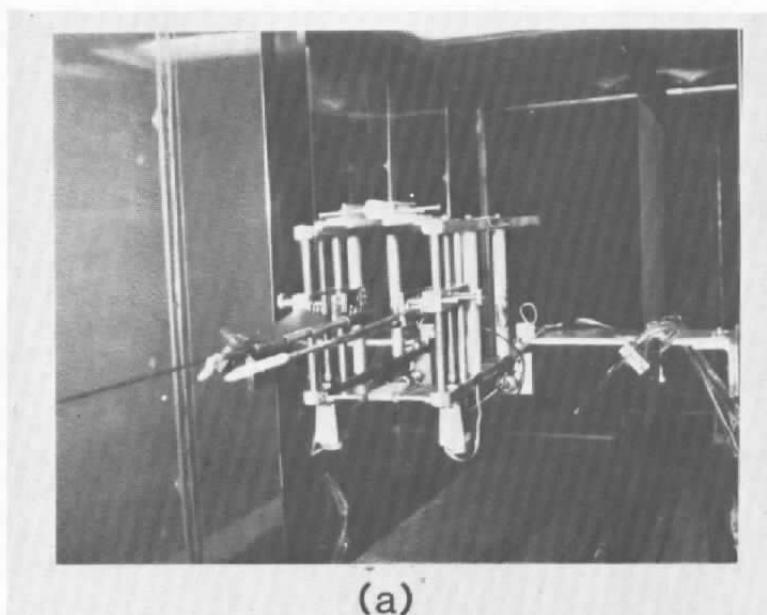
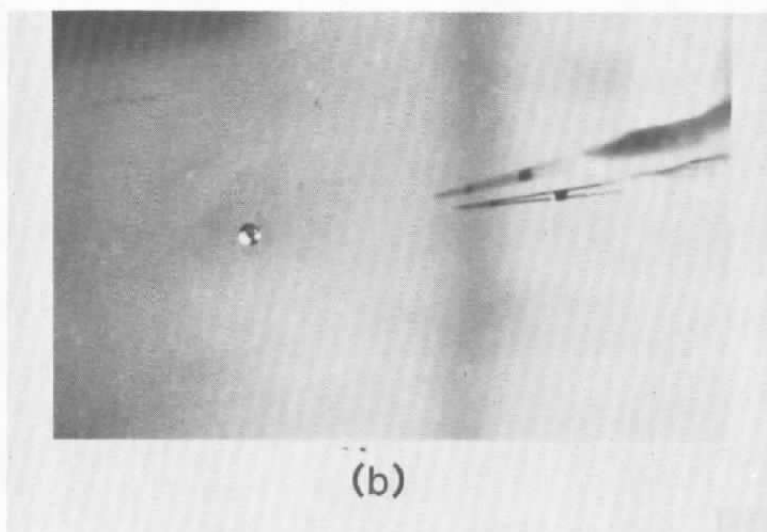


Figure 4. Photographs of the overall experimental arrangement.



a. Traversing mechanism



b. Roughness element, and hot-wire probe
Figure 5. Close-up view of experimental arrangement.

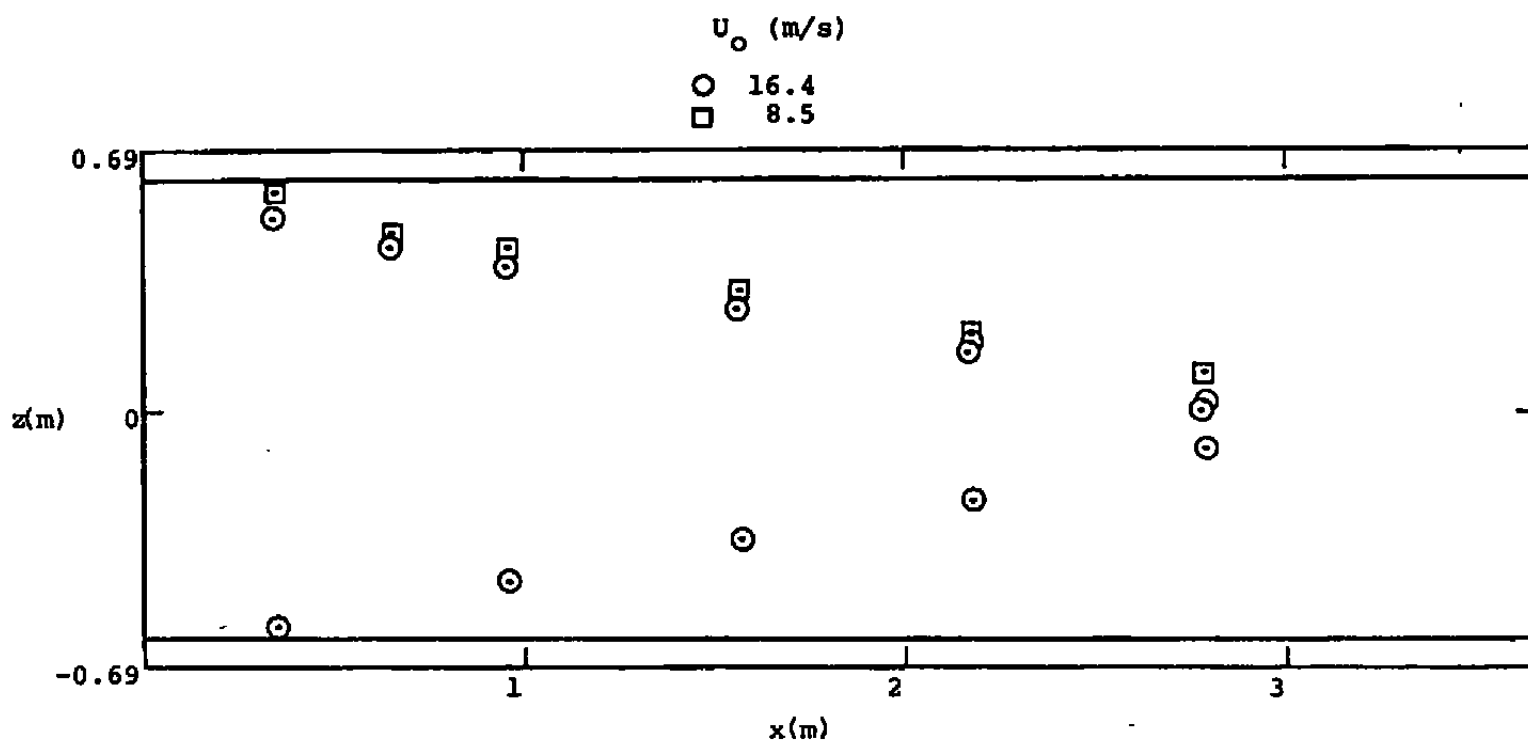


Figure 6. Transverse contamination along flat plate.

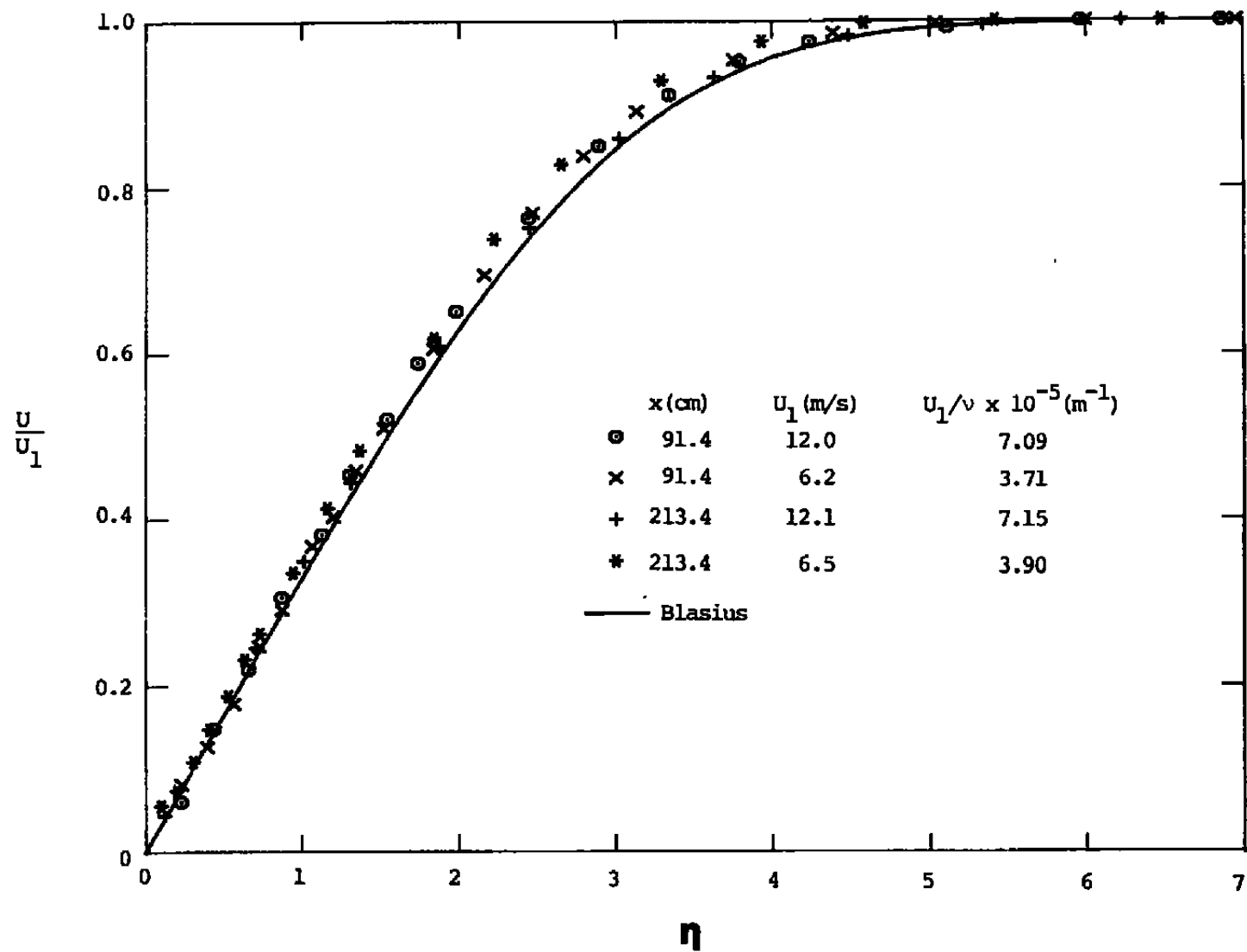


Figure 7. Mean-velocity profiles without roughness.

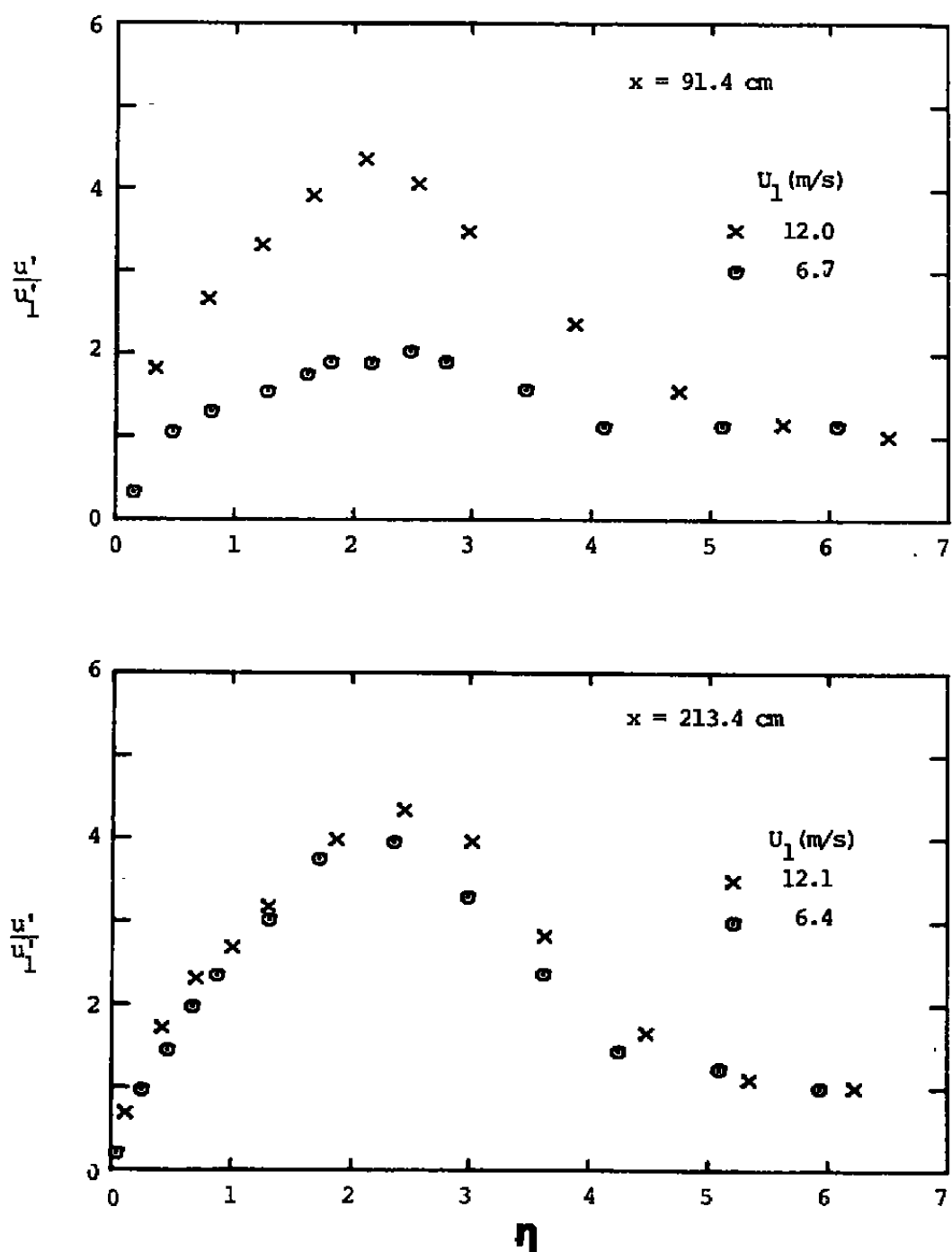


Figure 8. Intensity of u-fluctuation without roughness.

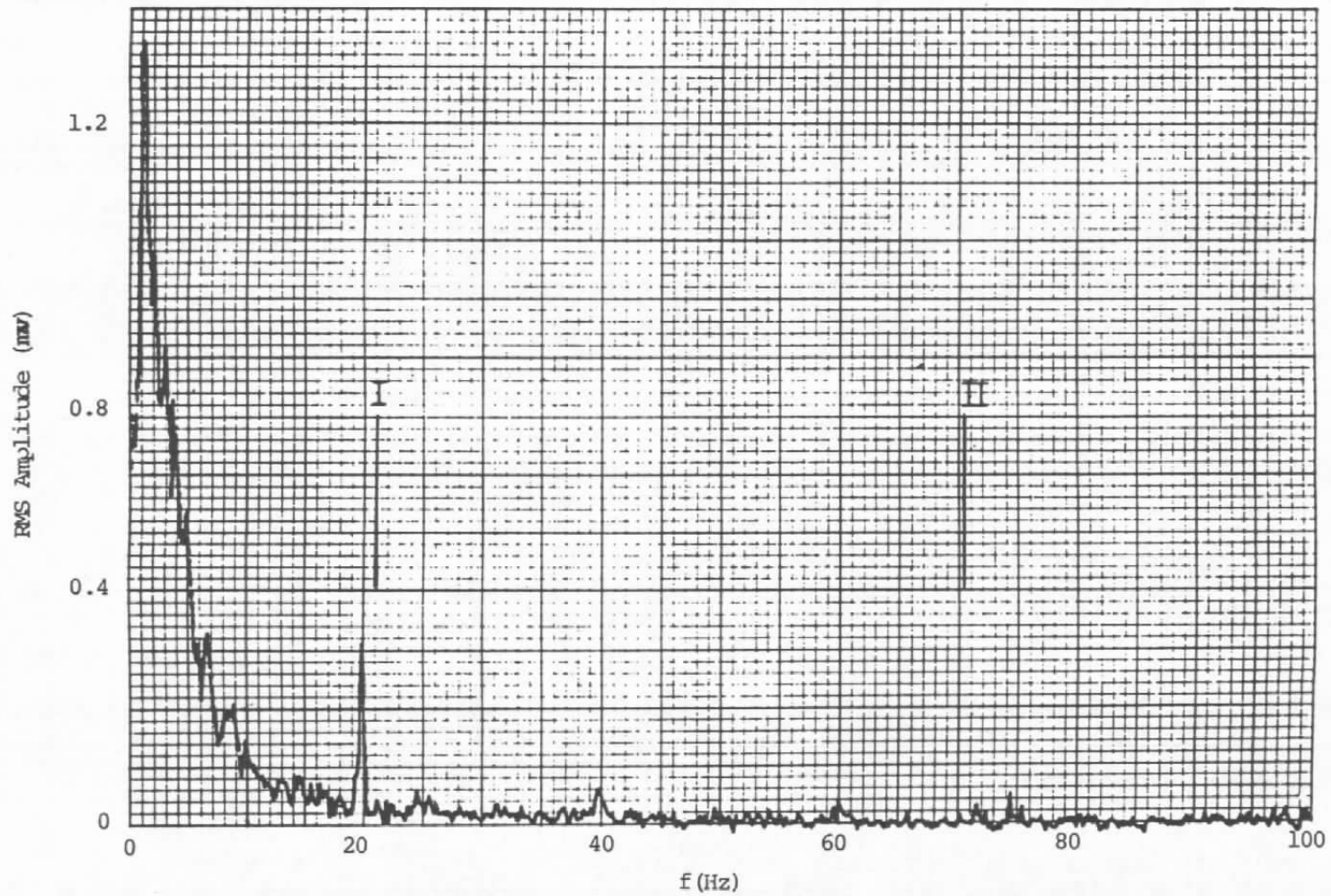


Figure 9. Spectrum of u -fluctuation in boundary layer without roughness.

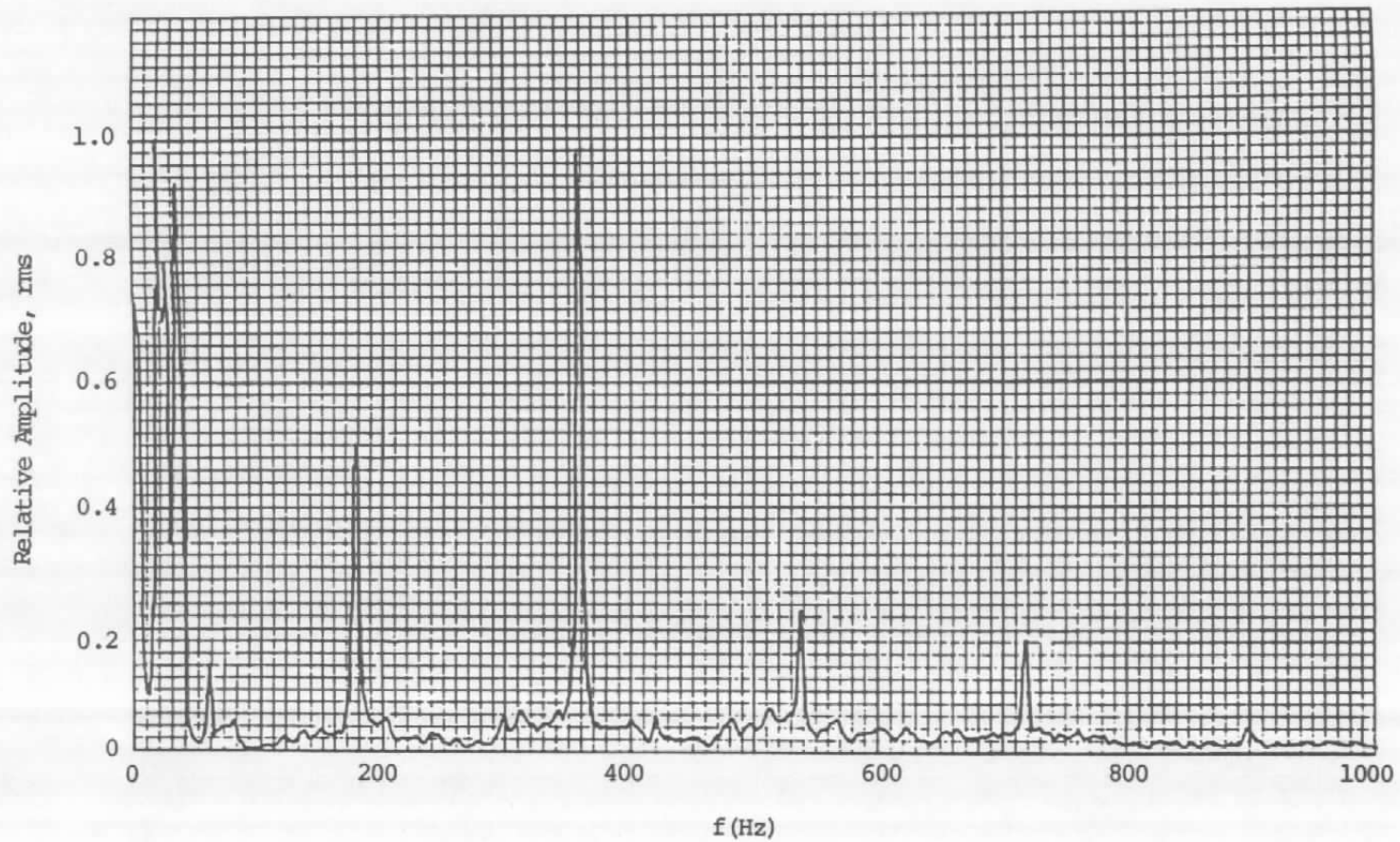


Figure 10. Spectrum of u-fluctuation in the freestream.

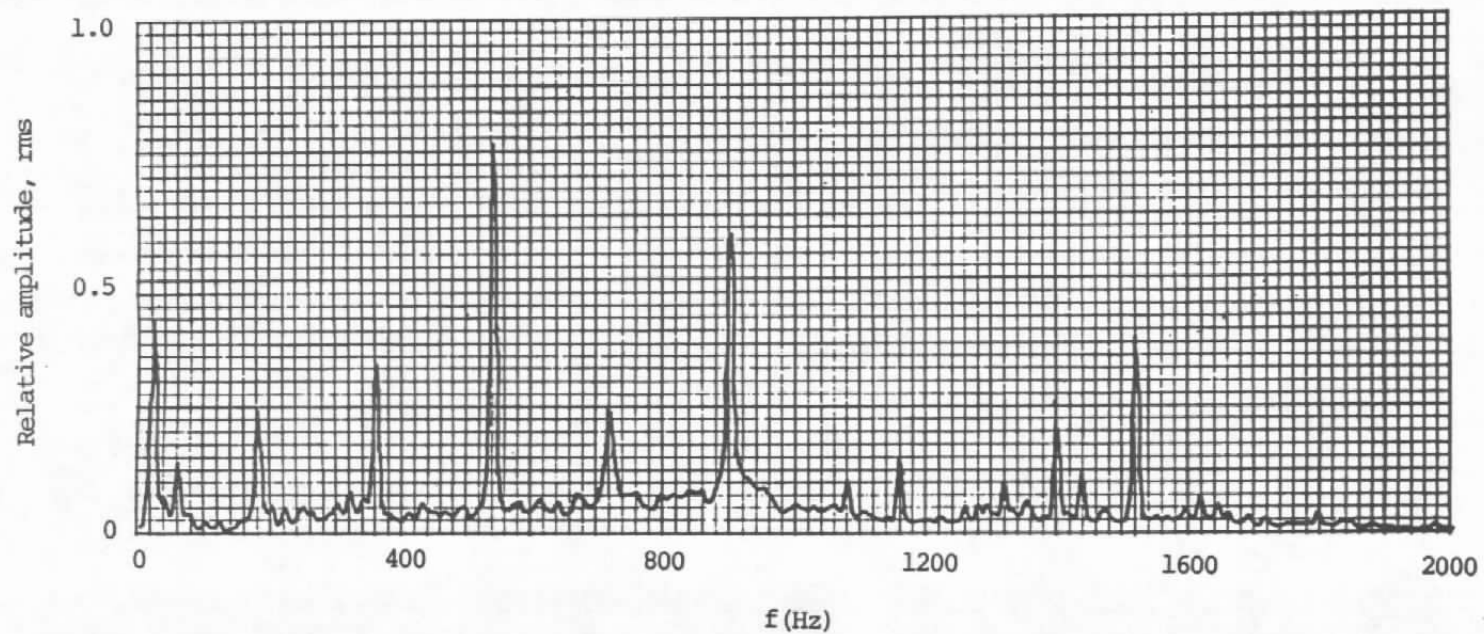


Figure 11. Spectrum of the output of an accelerometer attached to the fan housing.

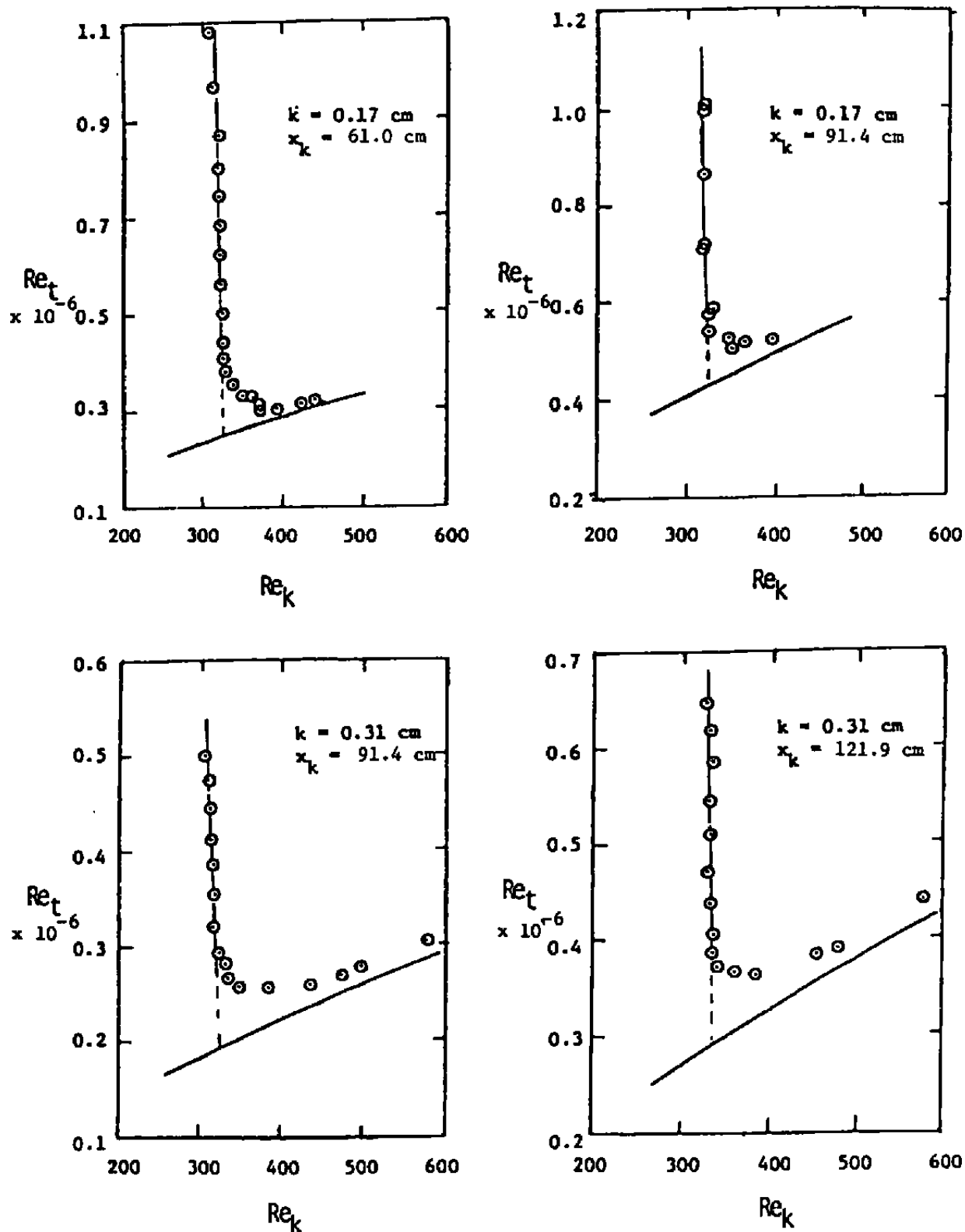


Figure 12. Variation of Reynolds number of transition with roughness Reynolds number for hemispherical roughness elements.

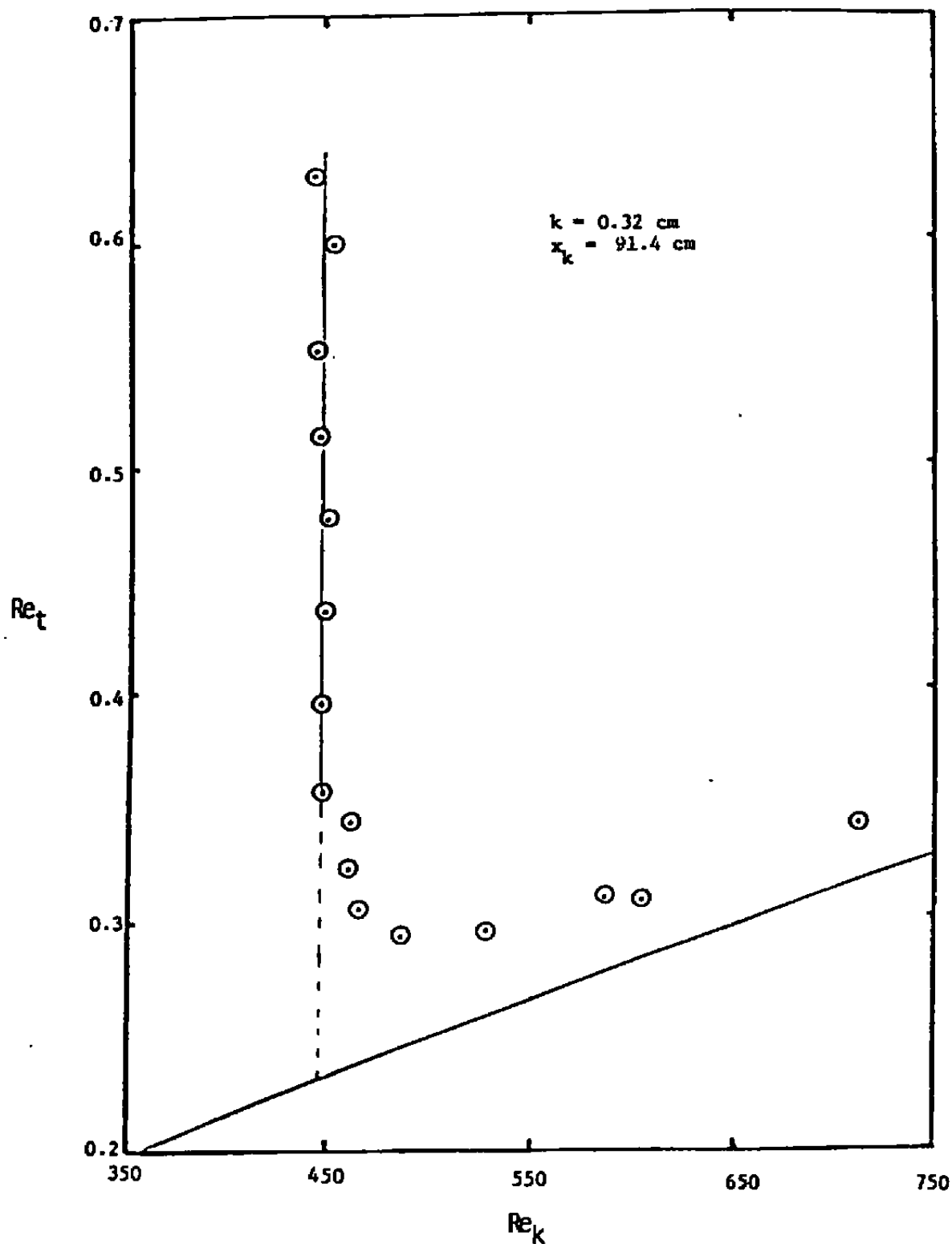


Figure 13. Variation of Reynolds number of transition with roughness Reynolds number for a cylindrical roughness element.

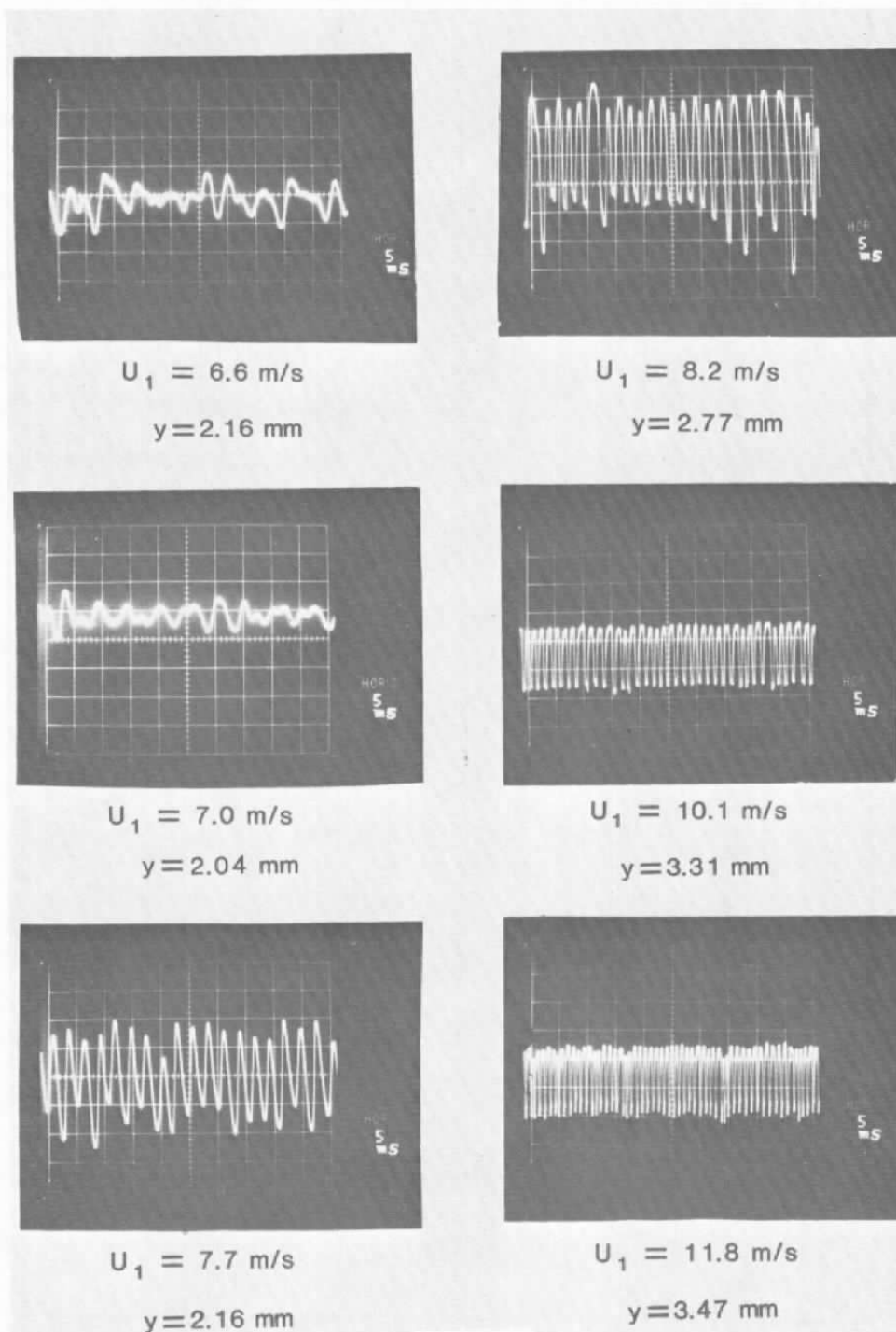


Figure 14. Oscillograms of u -fluctuation downstream of a hemispherical roughness element illustrating variation in frequency with freestream velocity; $k = 1.7$ mm, $x_k = 91.4$ cm, $\bar{x} = 2.54$ cm, $\bar{z} = 0.0$ cm.

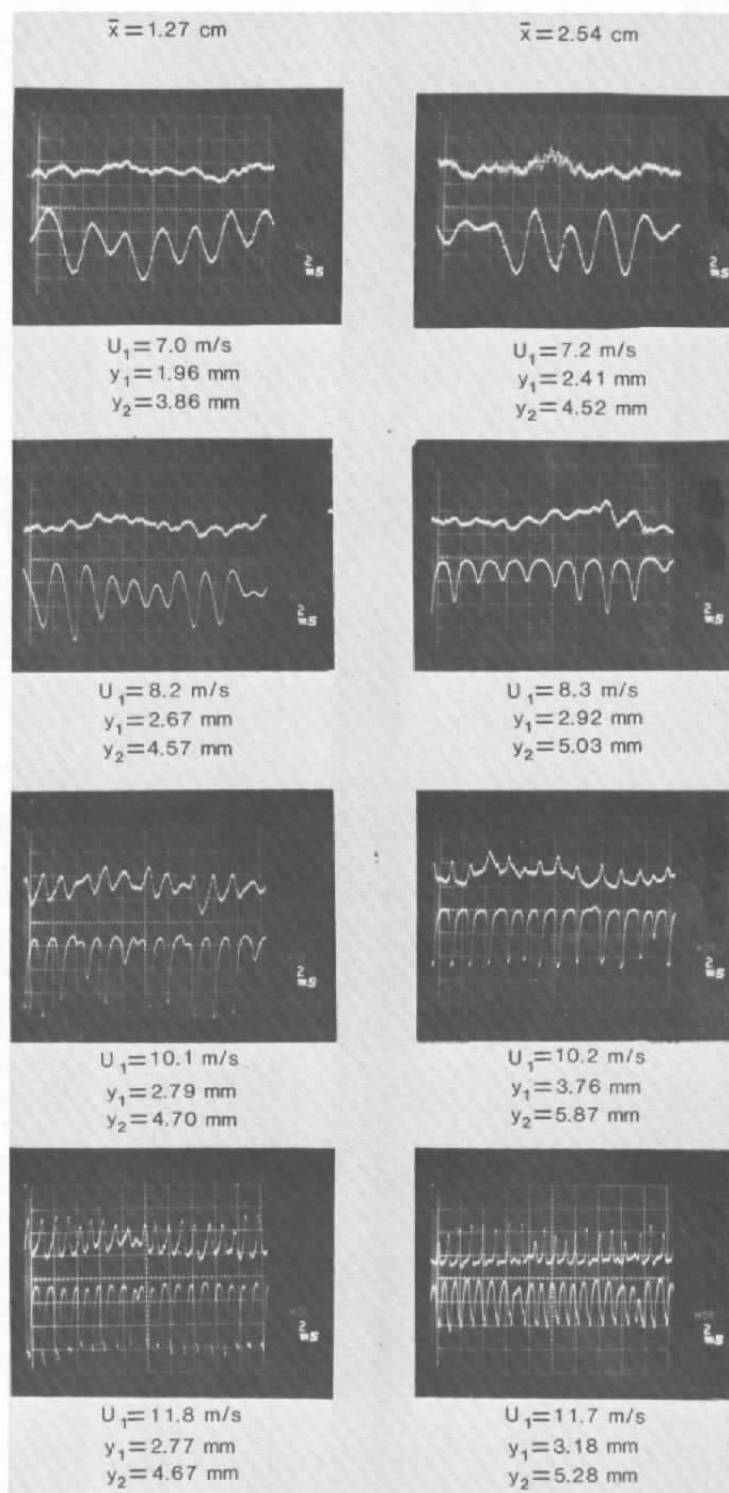


Figure 15. Oscillograms of simultaneous u -fluctuations downstream of a hemispherical roughness element illustrating phase in y -direction; $k = 1.7$ mm, $x_k = 91.4$ cm, $\bar{z} = 0.0$ cm.

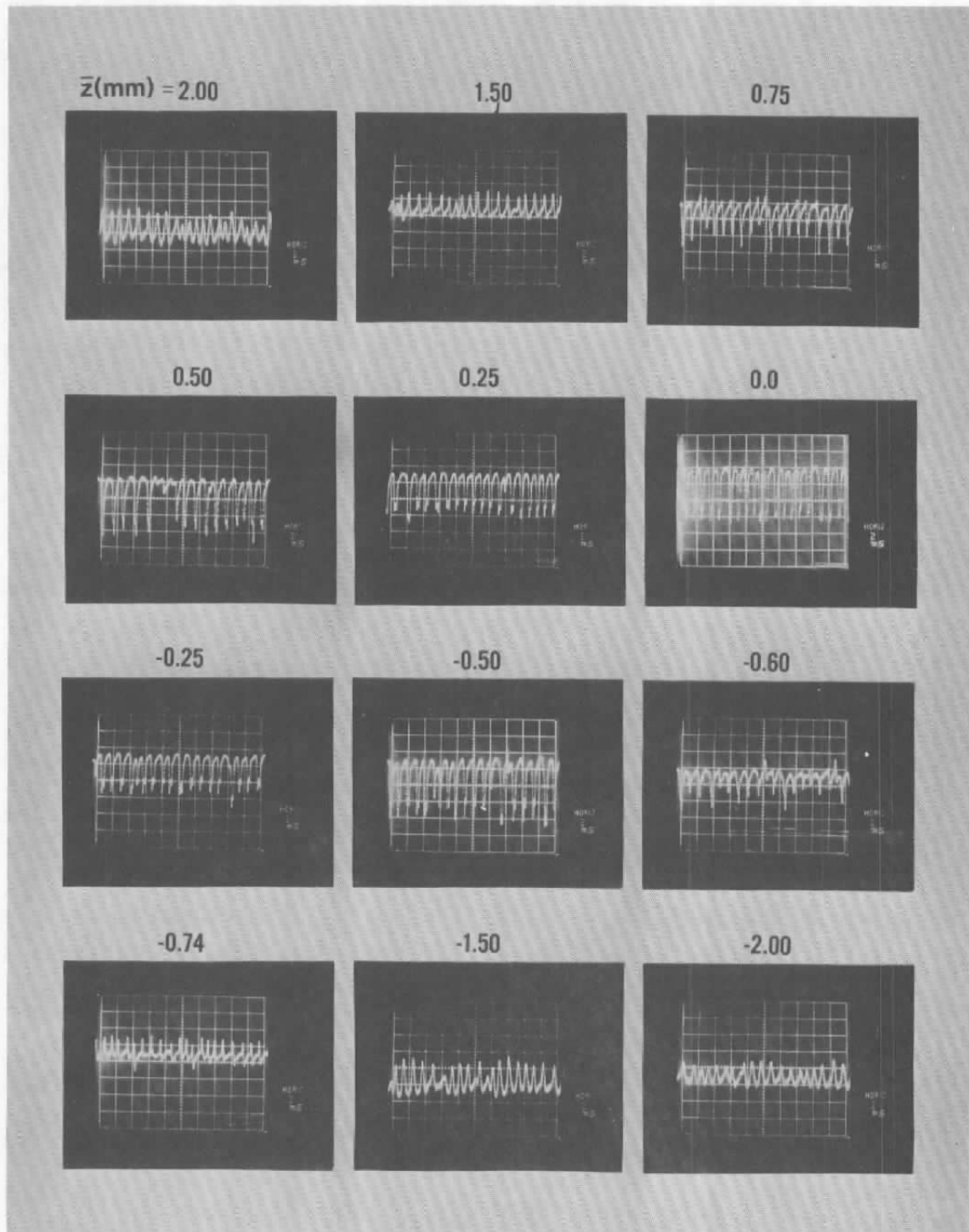


Figure 16. Oscillograms of simultaneous u -fluctuation downstream of a hemispherical roughness element illustrating phase in z -direction; $k = 1.7 \text{ mm}$, $x_k = 1.27 \text{ cm}$, $\bar{x} = 1.27 \text{ cm}$, $y = 3.18 \text{ mm}$.

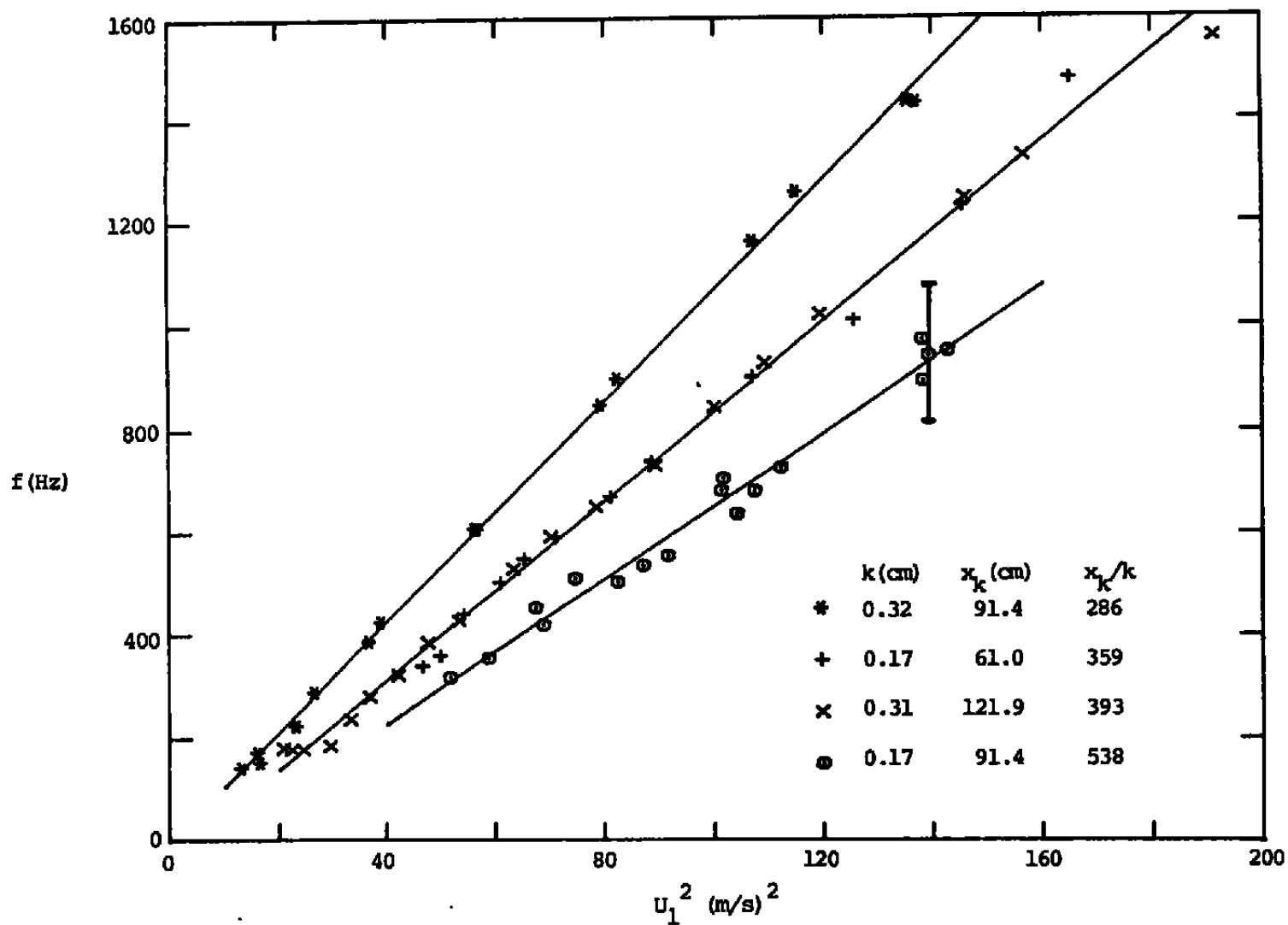


Figure 17. Variation of eddy shedding frequency with freestream velocity for hemispherical roughness elements of different size and position.

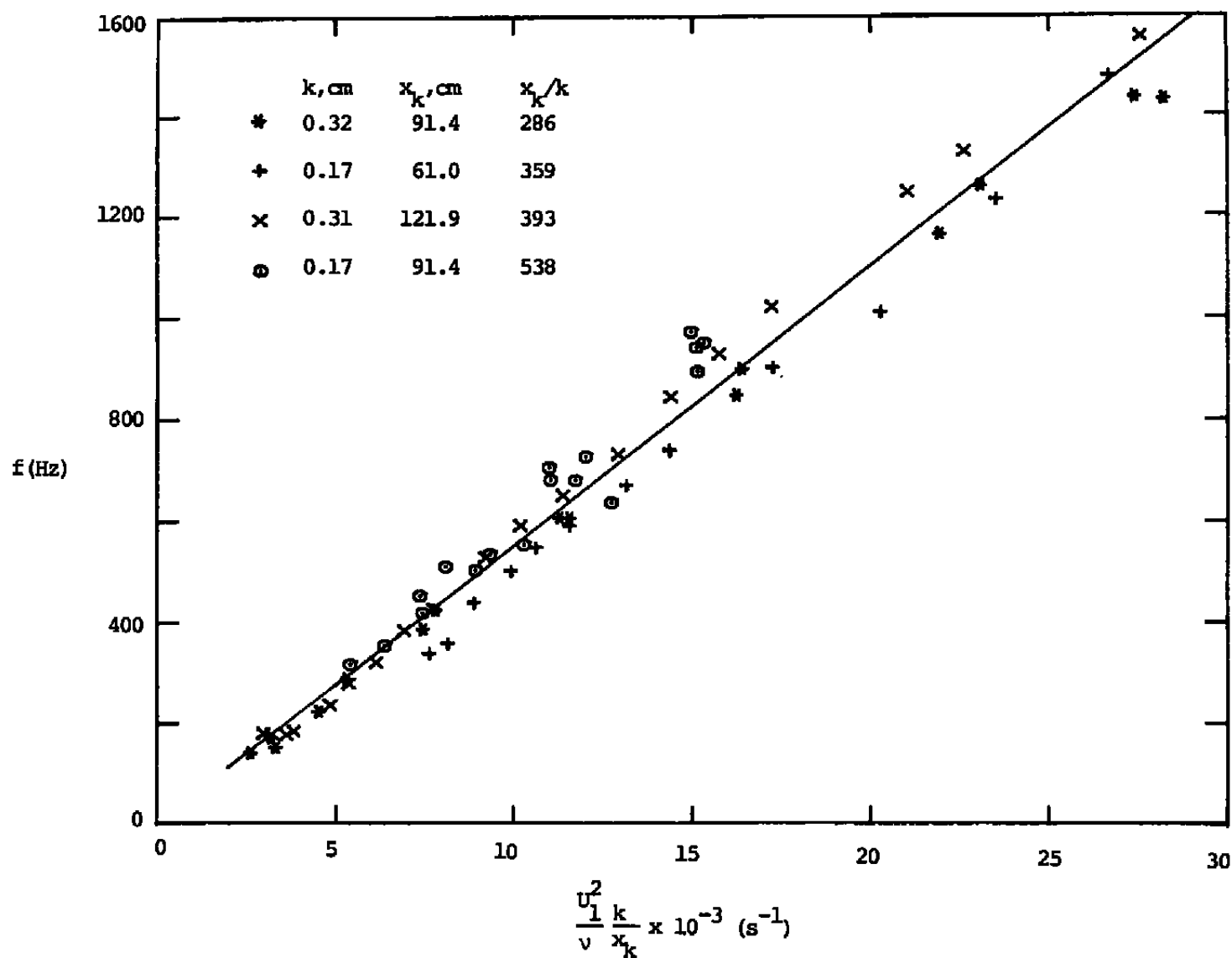


Figure 18. Scaling of data of figure 17 with k/x_k and ν .

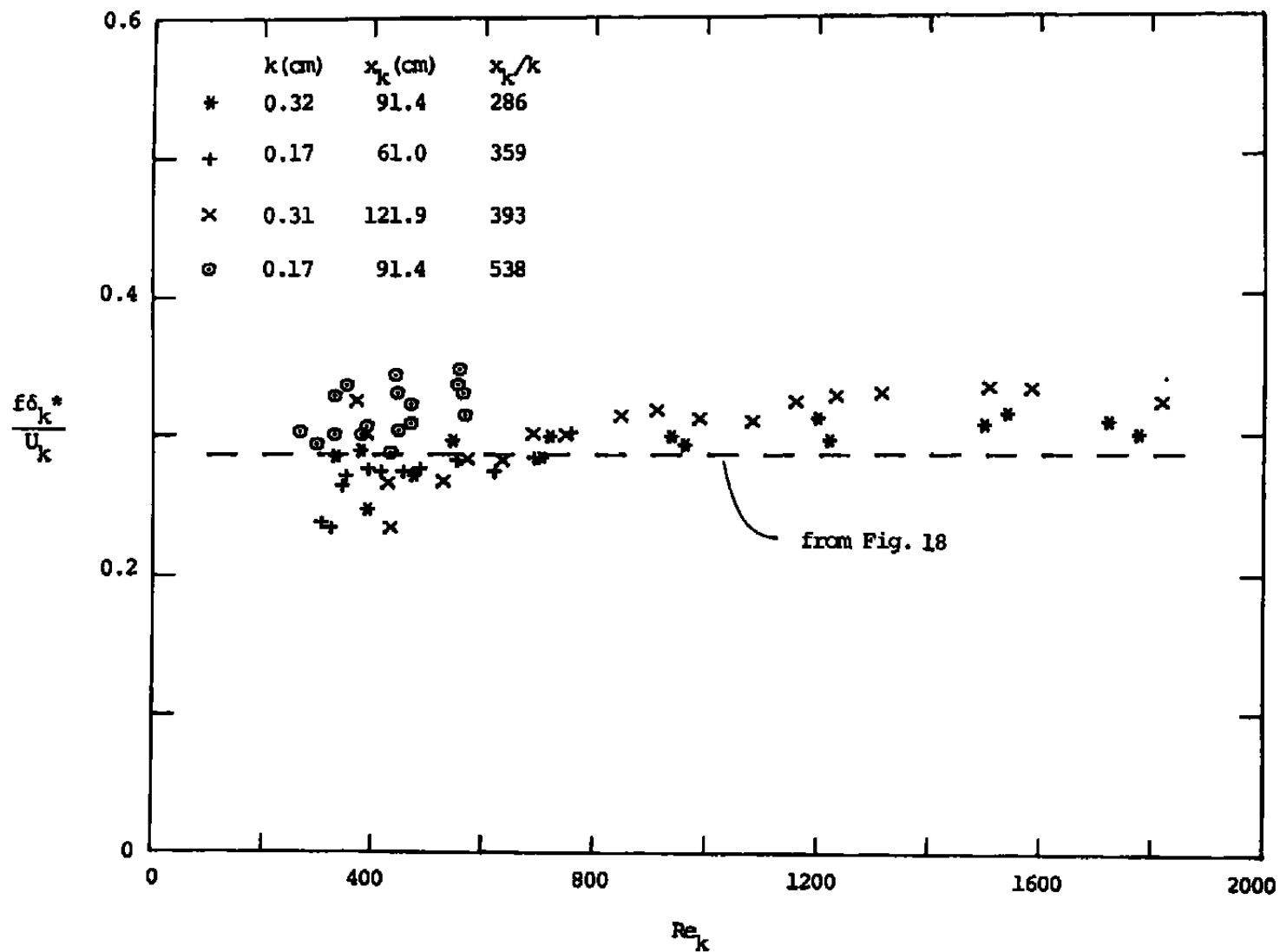


Figure 19. Strouhal behavior for hemispherical roughness elements with boundary layer scaling.

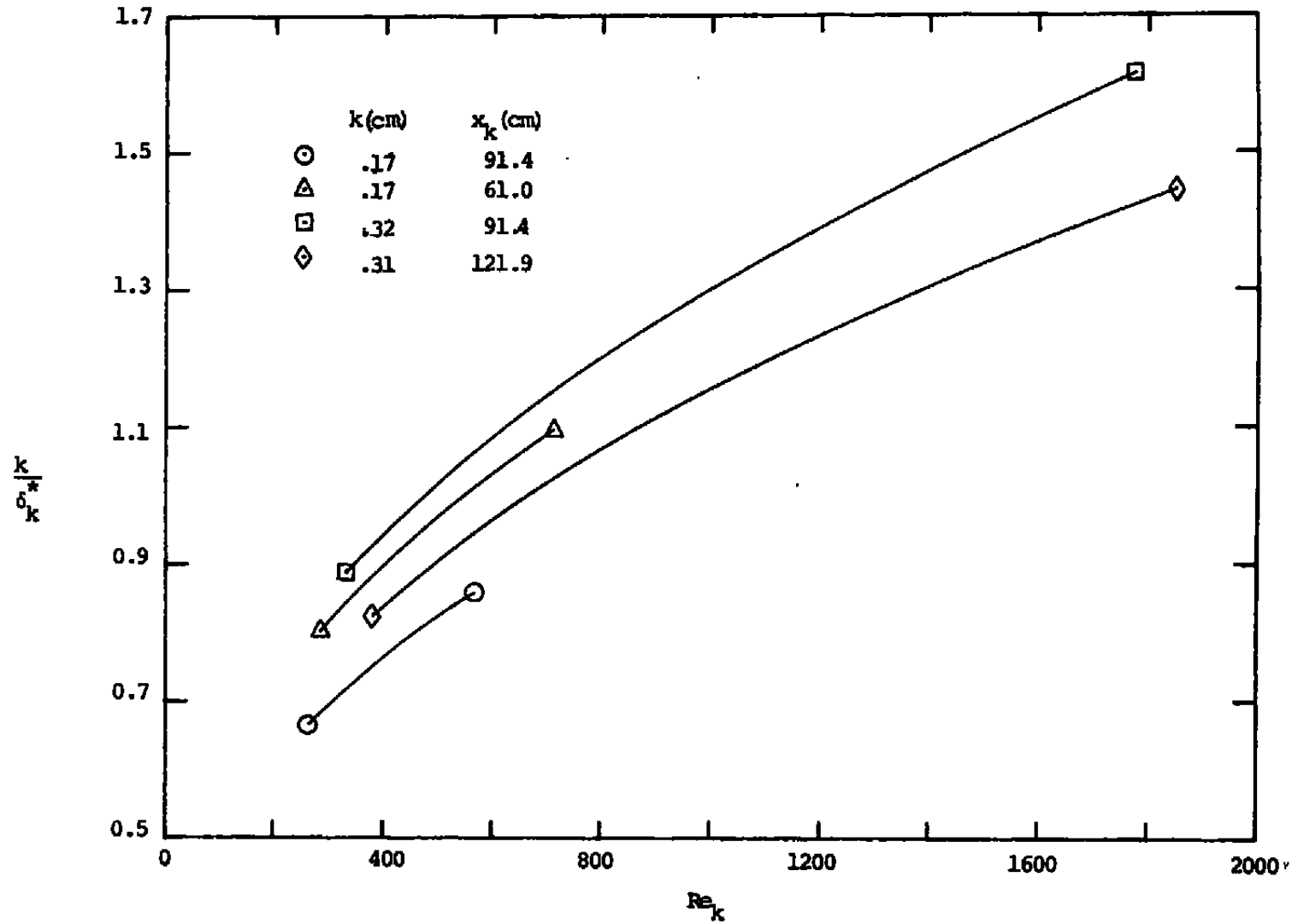


Figure 20. Variation of k/δ_k^* with roughness Reynolds number for hemispherical roughness elements of different size and position.

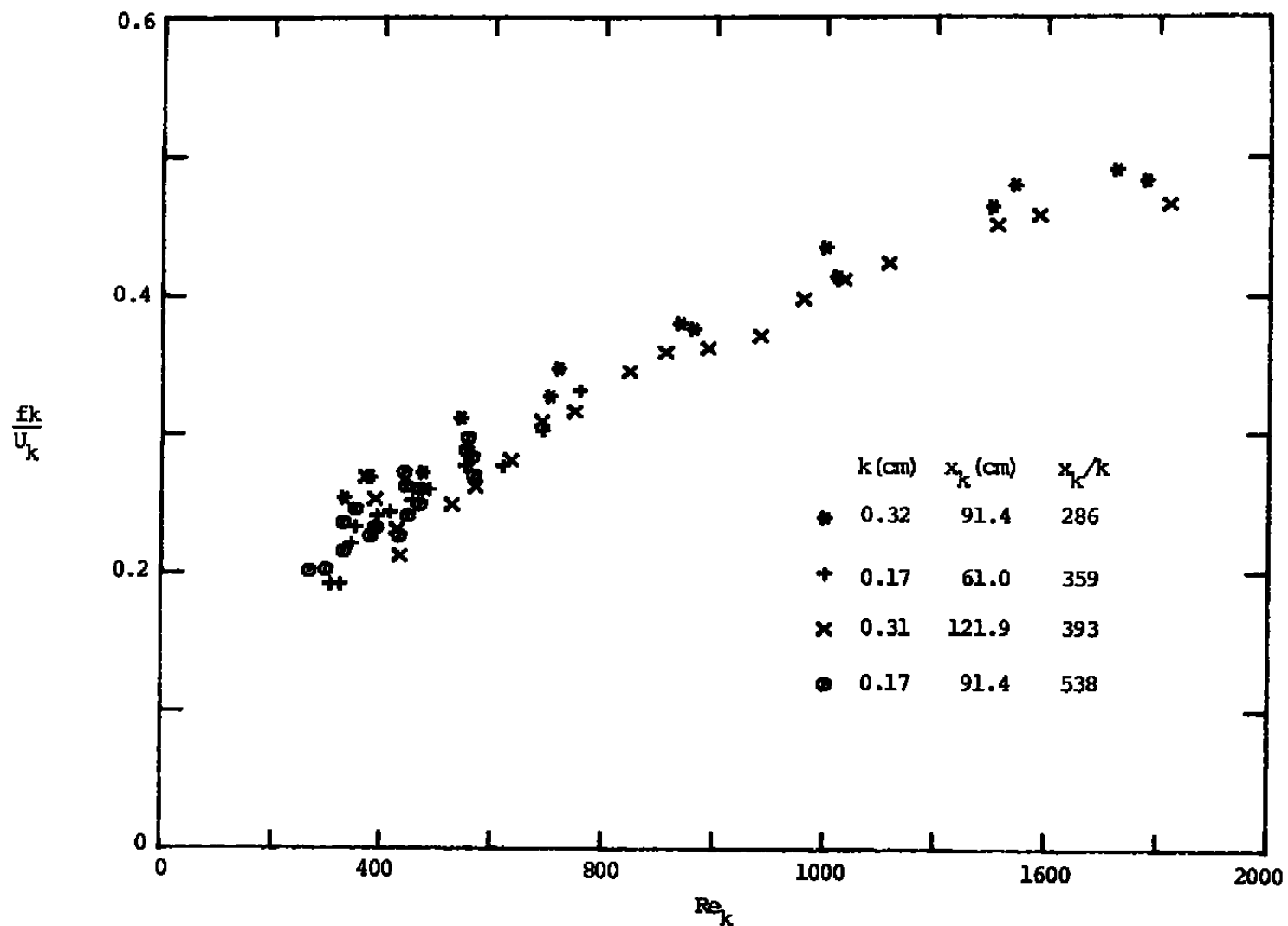


Figure 21. Strouhal behavior for hemispherical roughness elements with geometric scaling.

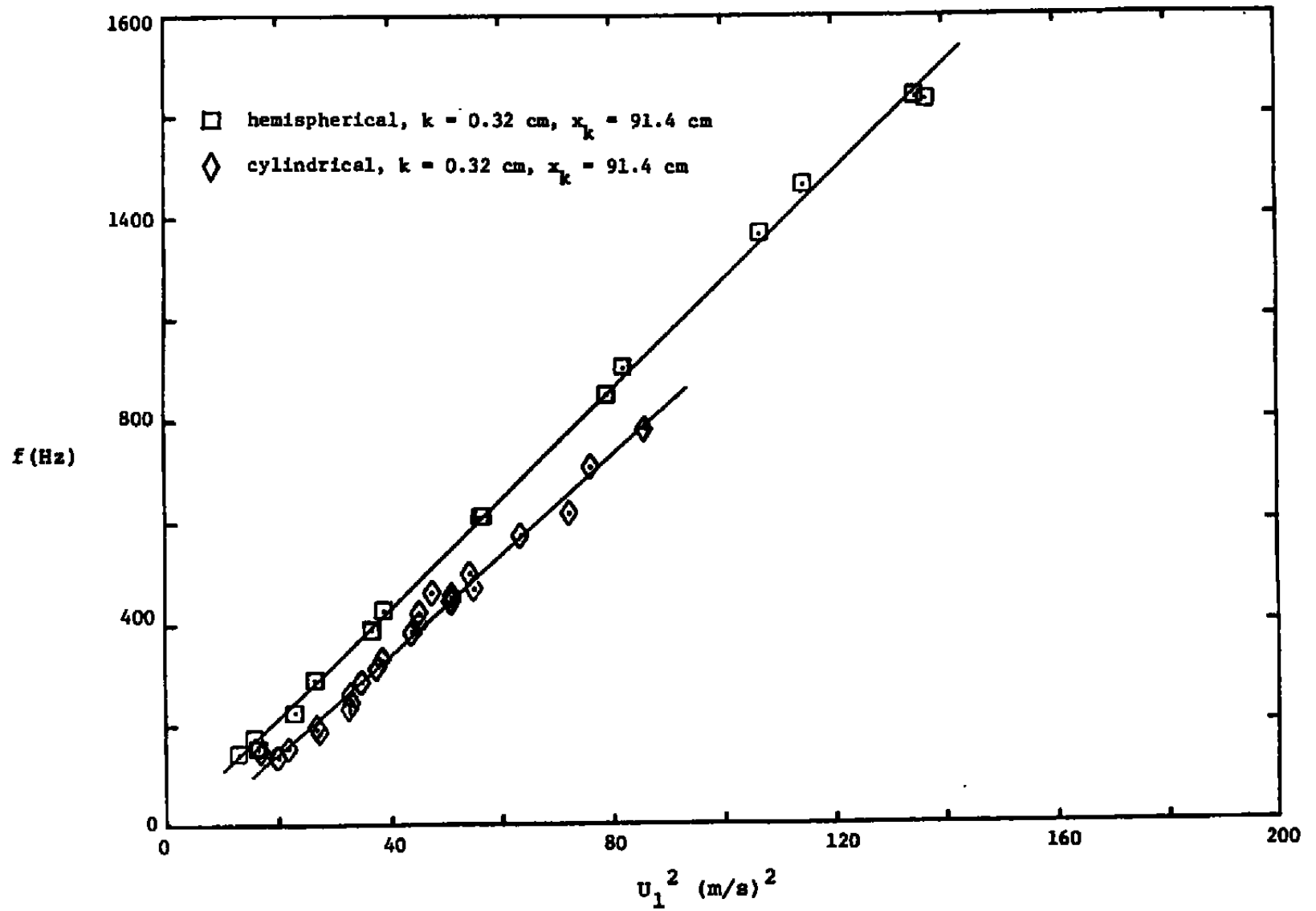


Figure 22. Comparison of variation of eddy shedding frequency with freestream velocity for a hemispherical and a cylindrical roughness element.

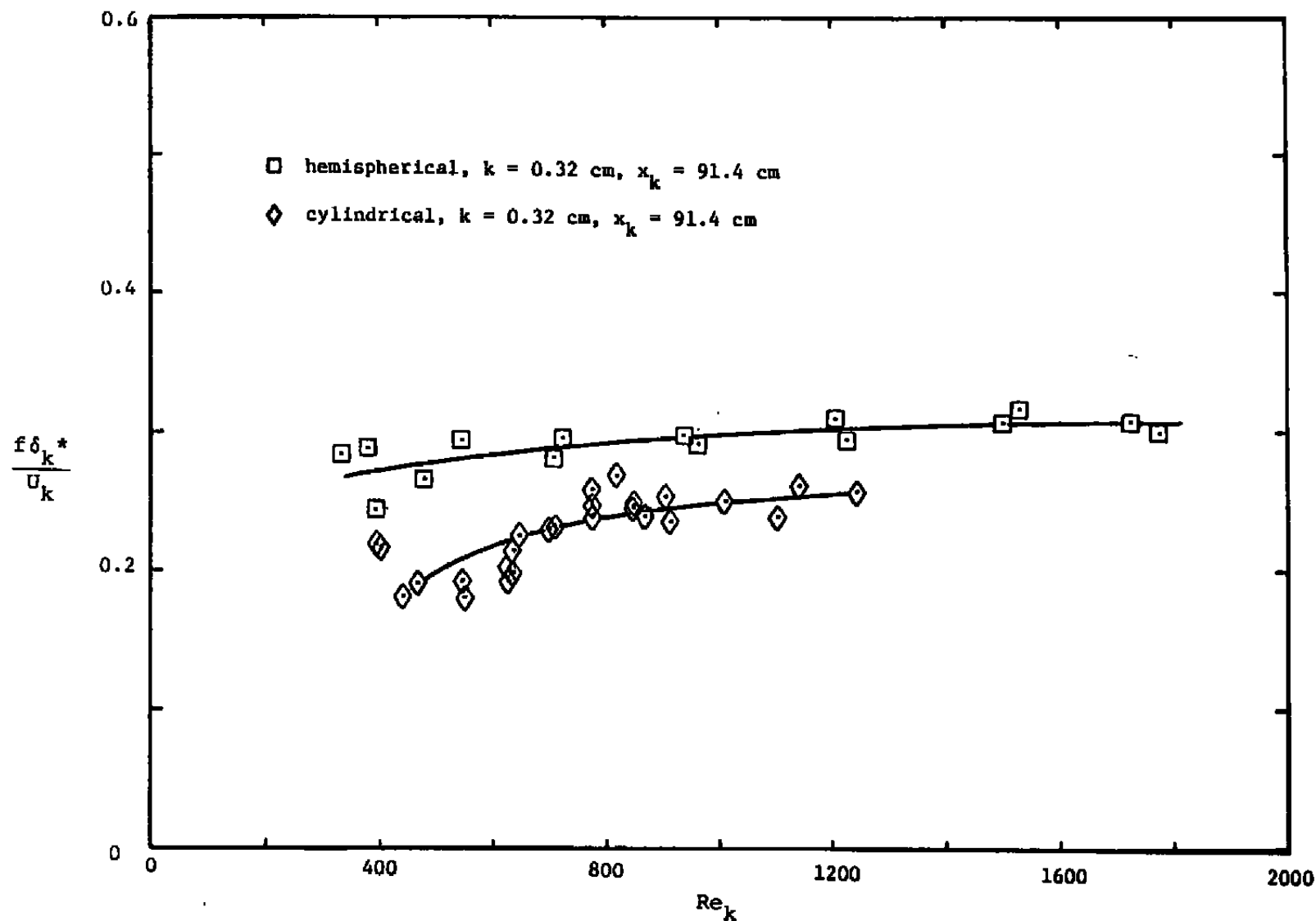


Figure 23. Comparison of Strouhal behavior for a hemispherical and a cylindrical roughness element.

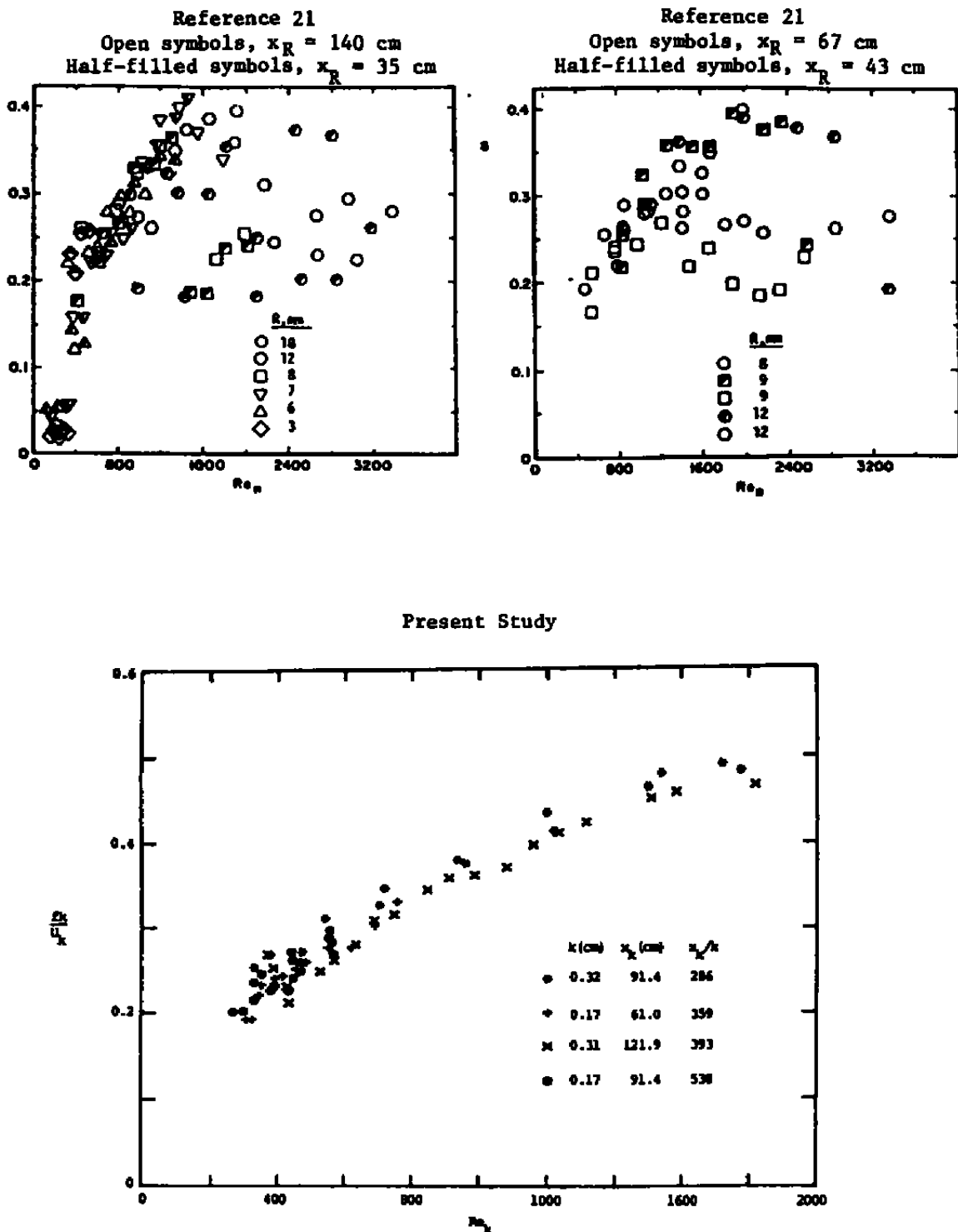


Figure 24. Comparison of Strouhal behavior for hemispherical roughness elements observed in the present study with the observations of Strouhal behavior in reference 21.

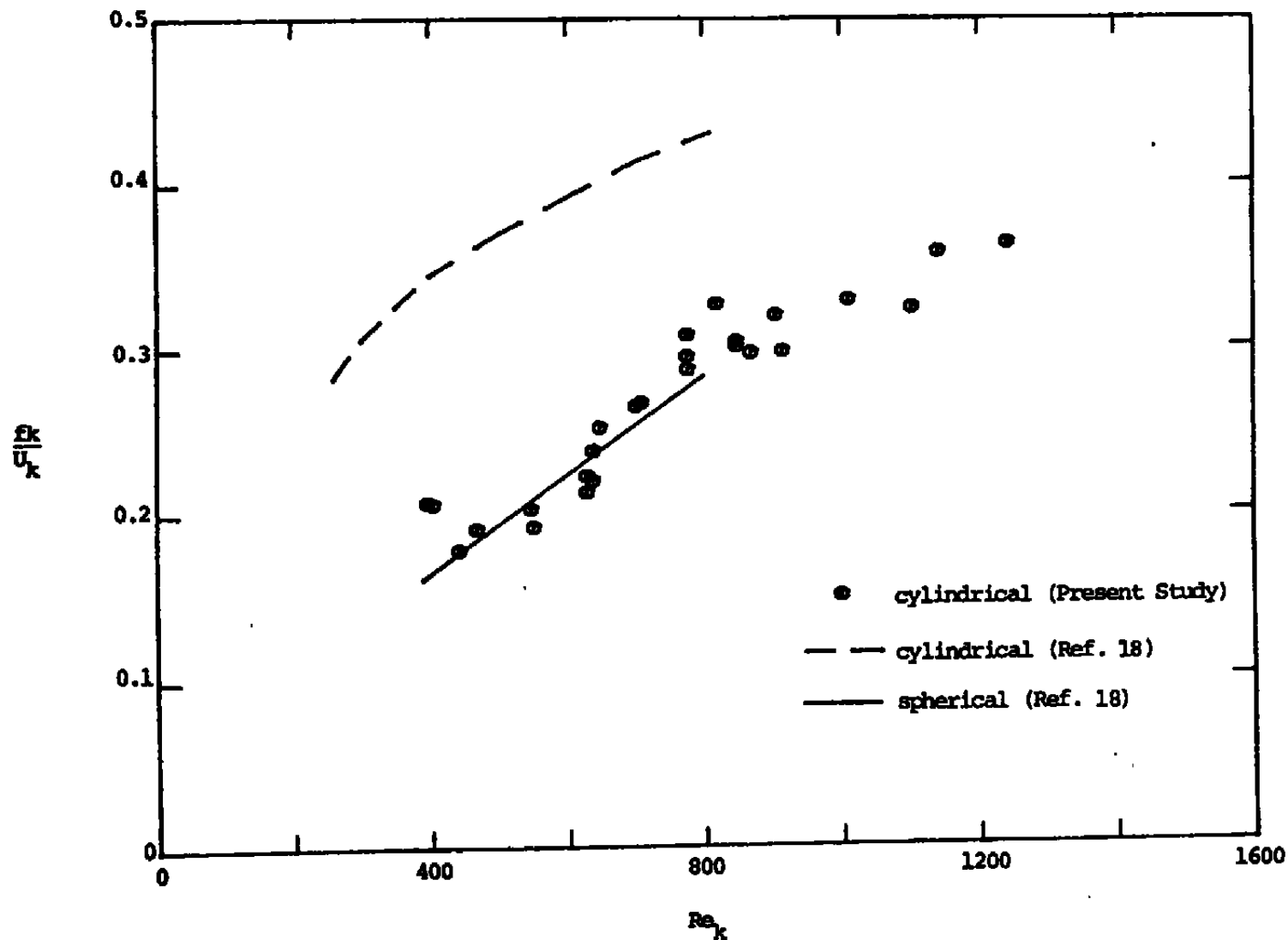


Figure 25. Comparison of Strouhal behavior for a cylindrical roughness element observed in the present study with the observations of Strouhal behavior in reference 18.

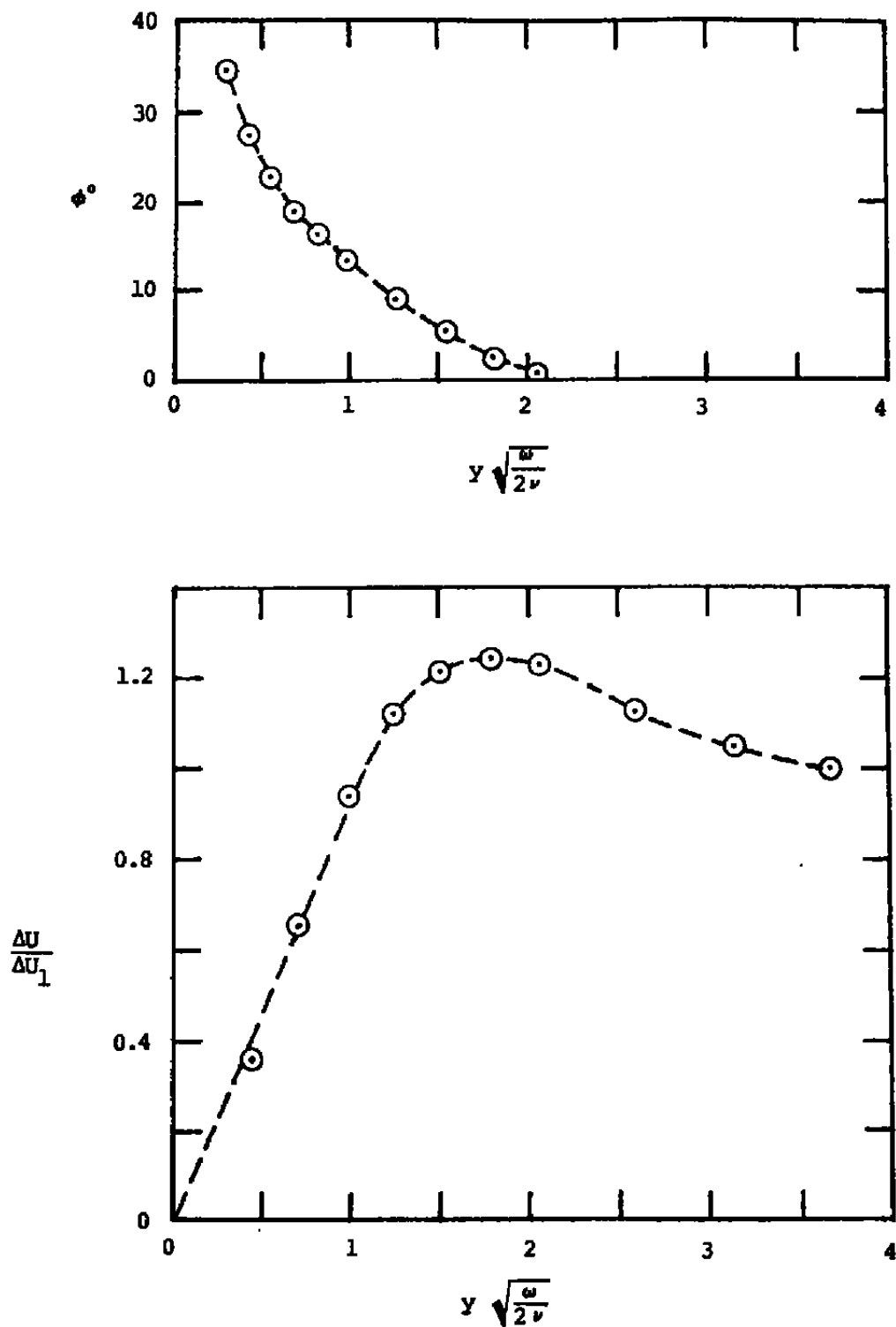


Figure 26. Phase and amplitude response of the laminar boundary layer without roughness to a freestream oscillation; $U_1 = 6.8$ m/s, $x = 94$ cm, $n = 1.0$ Hz.

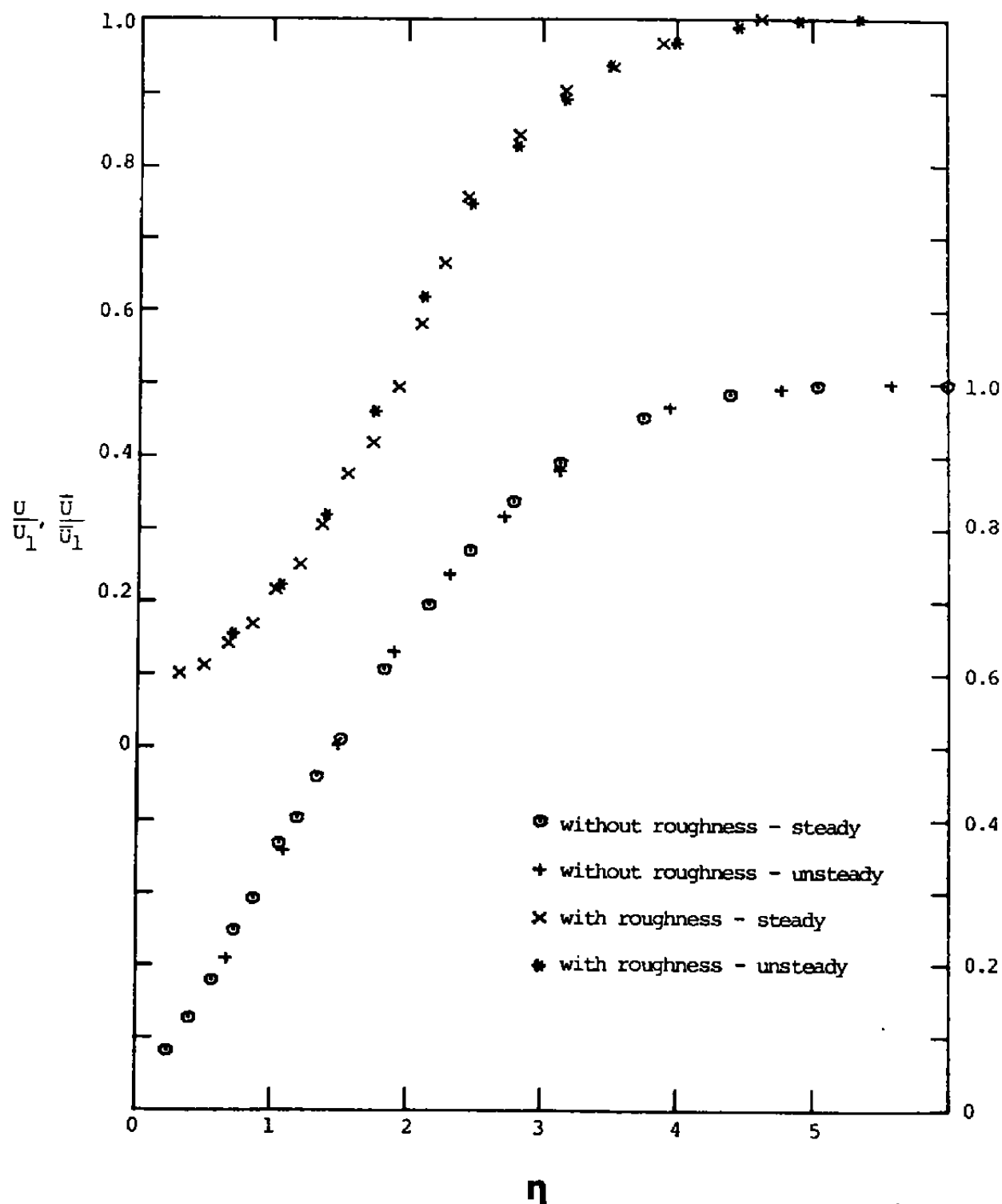


Figure 27. Comparison of mean-velocity profiles for steady and unsteady flow with and without a roughness element.

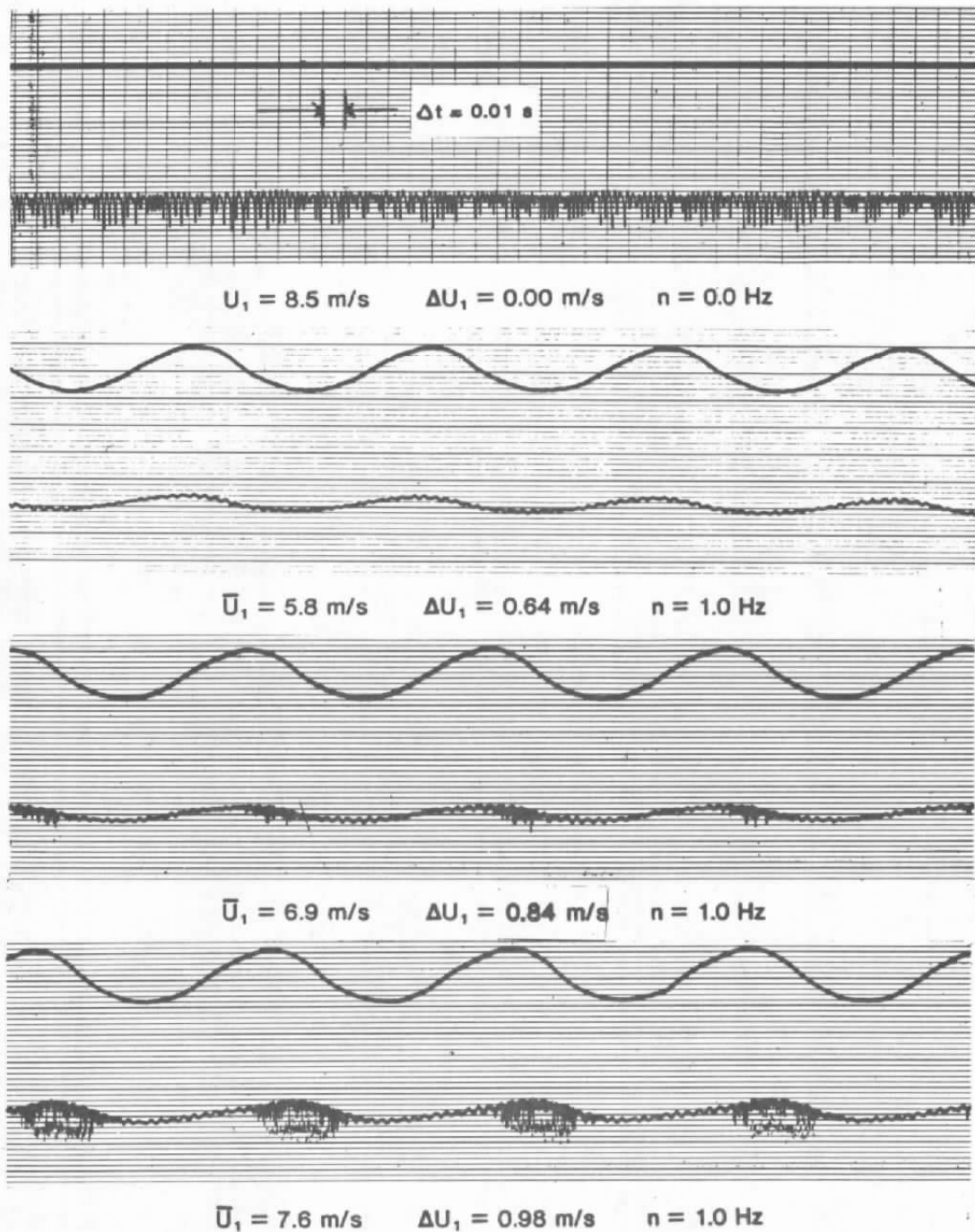
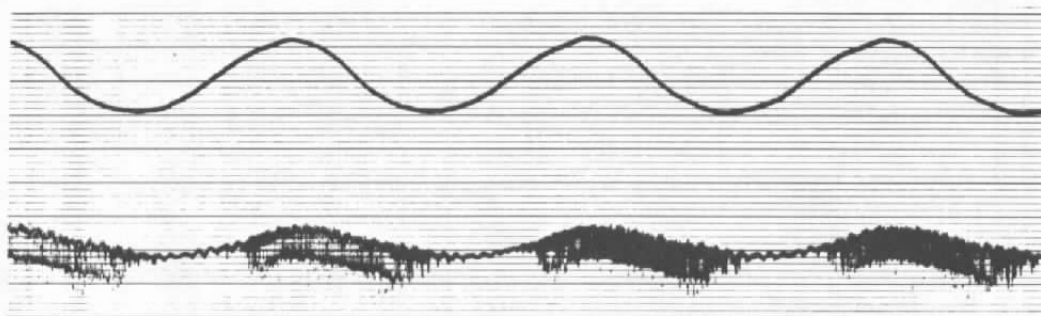
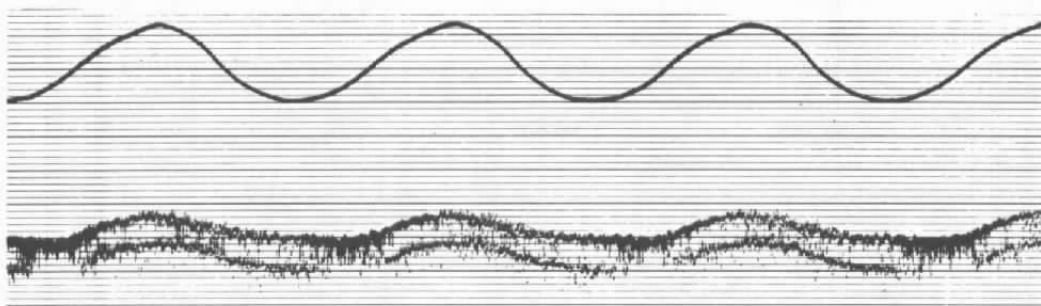


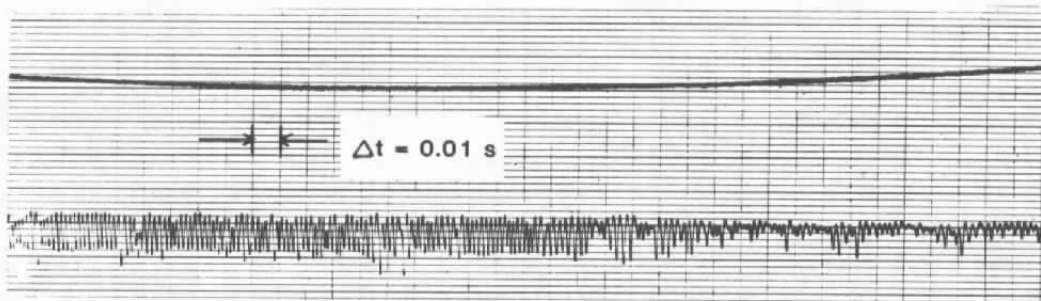
Figure 28. Strip-chart recordings of simultaneous u -fluctuations in an oscillatory freestream, and in the boundary layer downstream of a hemispherical roughness element; $k = 1.7 \text{ mm}$, $x_k = 91.4 \text{ cm}$, $\bar{x} = 2.54 \text{ cm}$, $y = 3.18 \text{ mm}$, $\bar{z} = 0.0 \text{ cm}$.



$$\bar{U}_1 = 8.7 \text{ m/s} \quad \Delta U_1 = 1.20 \text{ m/s} \quad n = 1.0 \text{ Hz}$$



$$\bar{U}_1 = 9.7 \text{ m/s} \quad \Delta U_1 = 1.38 \text{ m/s} \quad n = 1.0 \text{ Hz}$$



$$\bar{U}_1 = 9.6 \text{ m/s} \quad \Delta U_1 = 1.36 \text{ m/s} \quad n = 1.0 \text{ Hz}$$

Figure 28. Concluded.

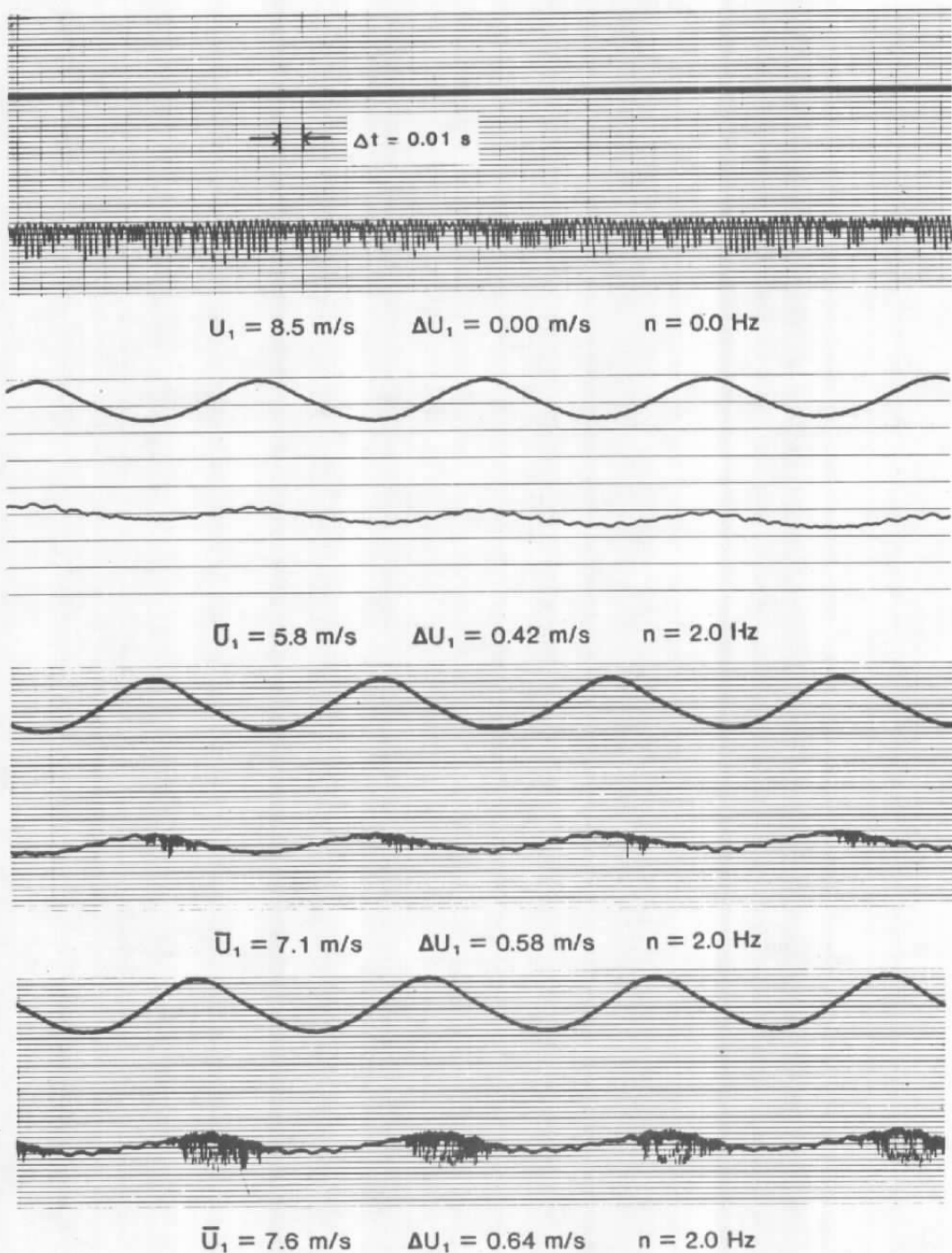
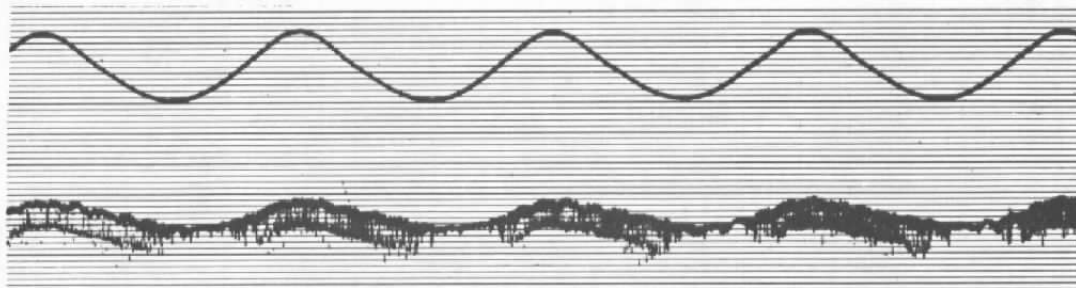
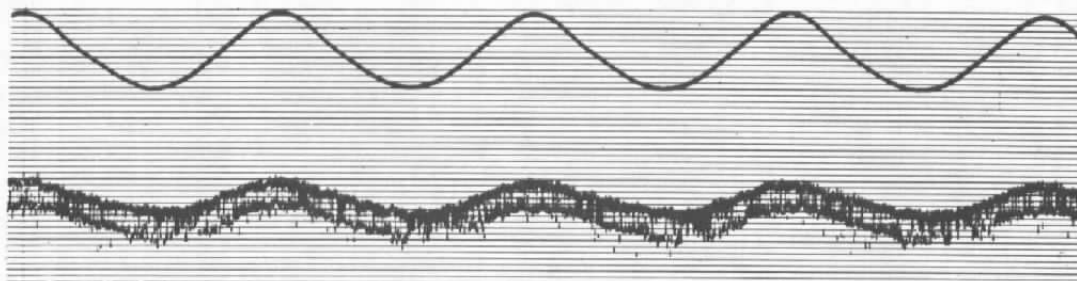


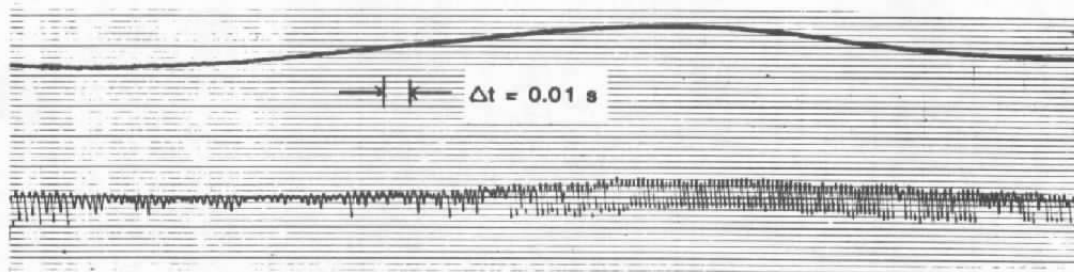
Figure 29. Strip-chart recordings of simultaneous u -fluctuations in an oscillatory freestream, and in the boundary layer downstream of a hemispherical roughness element; $k = 1.7 \text{ mm}$, $x_k = 91.4 \text{ cm}$, $\bar{x} = 2.54 \text{ cm}$, $y = 3.18 \text{ mm}$, $\bar{z} = 0.0 \text{ cm}$.



$\bar{U}_1 = 8.7 \text{ m/s}$ $\Delta U_1 = 0.78 \text{ m/s}$ $n = 2.0 \text{ Hz}$



$\bar{U}_1 = 9.6 \text{ m/s}$ $\Delta U_1 = 0.89 \text{ m/s}$ $n = 2.0 \text{ Hz}$



$\bar{U}_1 = 9.6 \text{ m/s}$ $\Delta U_1 = 0.89 \text{ m/s}$ $n = 2.0 \text{ Hz}$

Figure 29. Concluded.

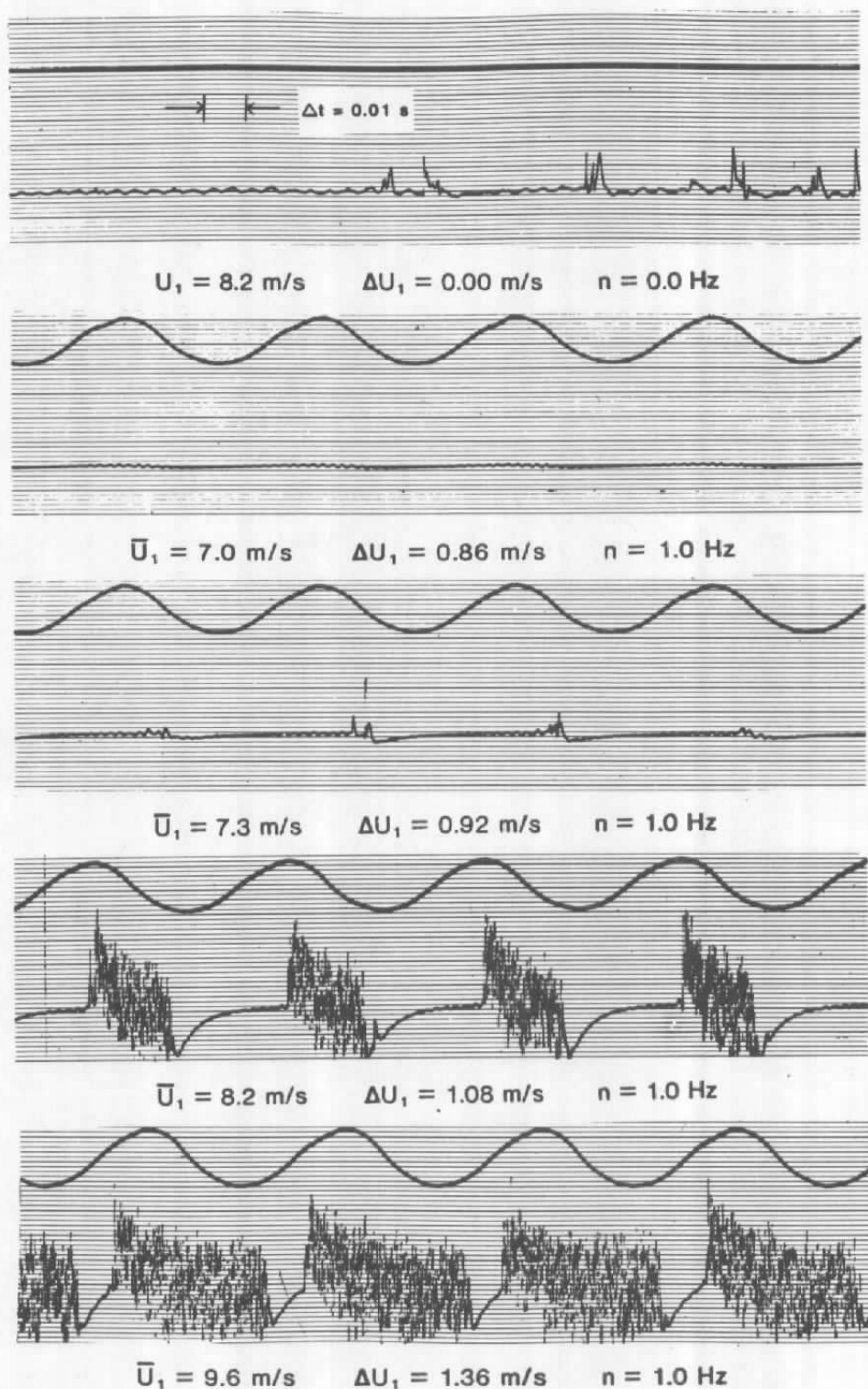


Figure 30. Strip-chart recordings of simultaneous u -fluctuations in an oscillatory freestream, and in the boundary layer downstream of a hemispherical roughness element; $k = 1.7 \text{ mm}$, $x_k = 91.4 \text{ cm}$, $\bar{x} = 30.5 \text{ cm}$, $y = 0.61 \text{ mm}$, $\bar{z} = 0.0 \text{ cm}$.

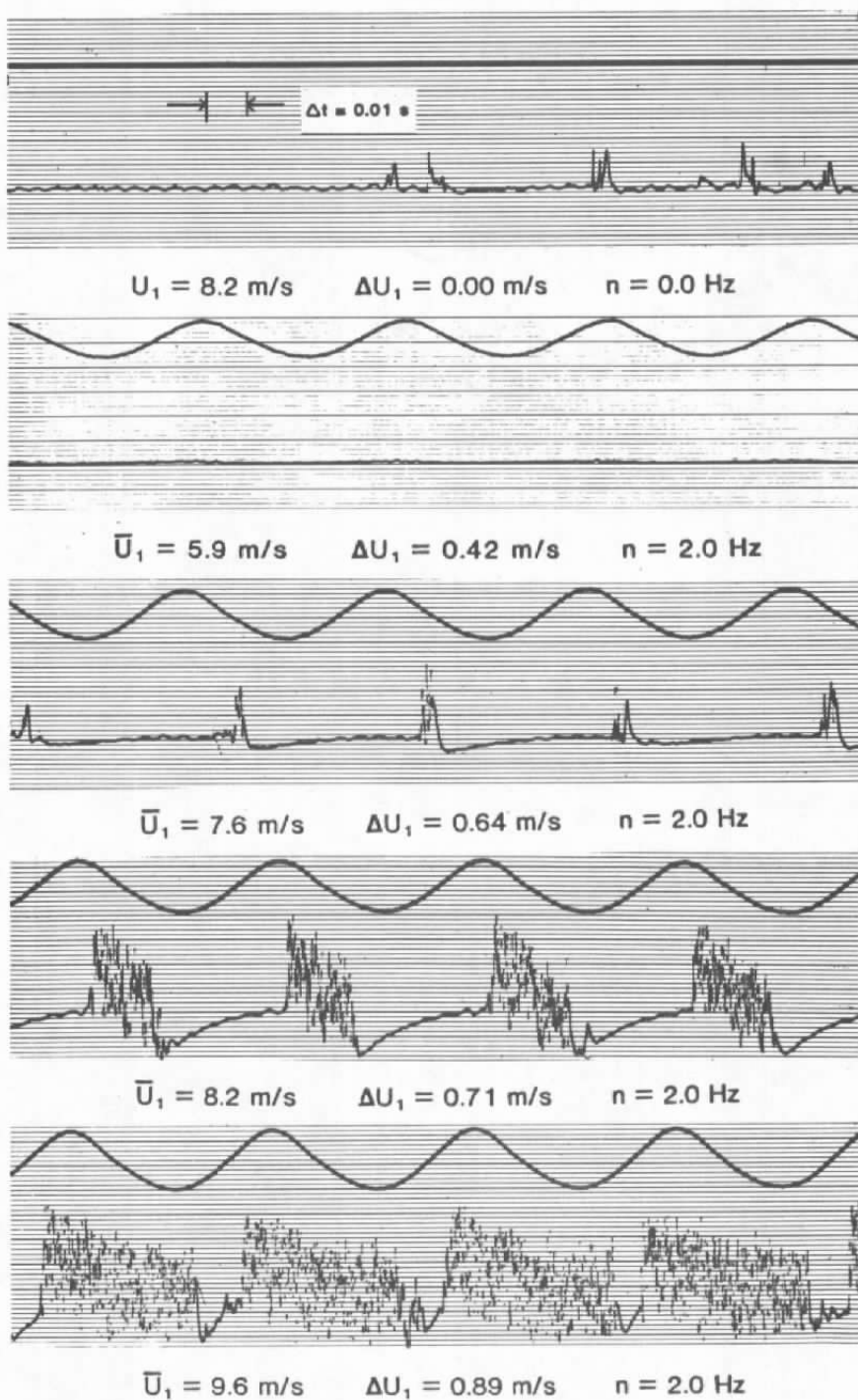


Figure 31. Strip-chart recordings of simultaneous u -fluctuations in an oscillatory freestream, and in the boundary layer downstream of a hemispherical roughness element; $k = 1.7 \text{ mm}$, $x_k = 91.4 \text{ cm}$, $\bar{x} = 30.5 \text{ cm}$, $y = 0.61 \text{ mm}$, $\bar{z} = 0.0 \text{ cm}$.

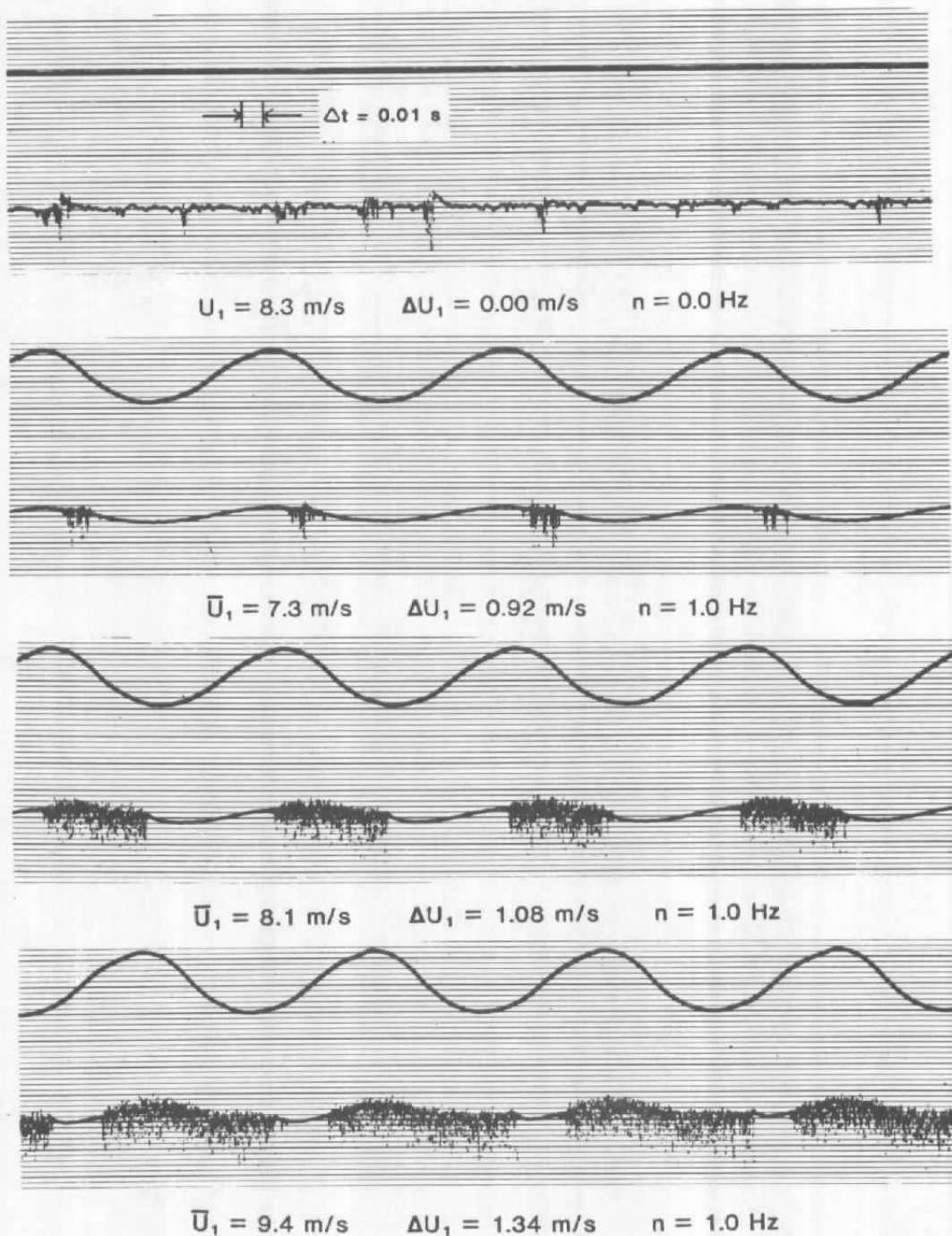


Figure 32. Strip-chart recordings of simultaneous u -fluctuations in an oscillatory freestream, and in the boundary layer downstream of a hemispherical roughness element; $k = 1.7 \text{ mm}$, $x_k = 91.4 \text{ cm}$, $\bar{x} = 30.5 \text{ cm}$, $y = 6.35 \text{ mm}$, $\bar{z} = 0.0 \text{ cm}$.

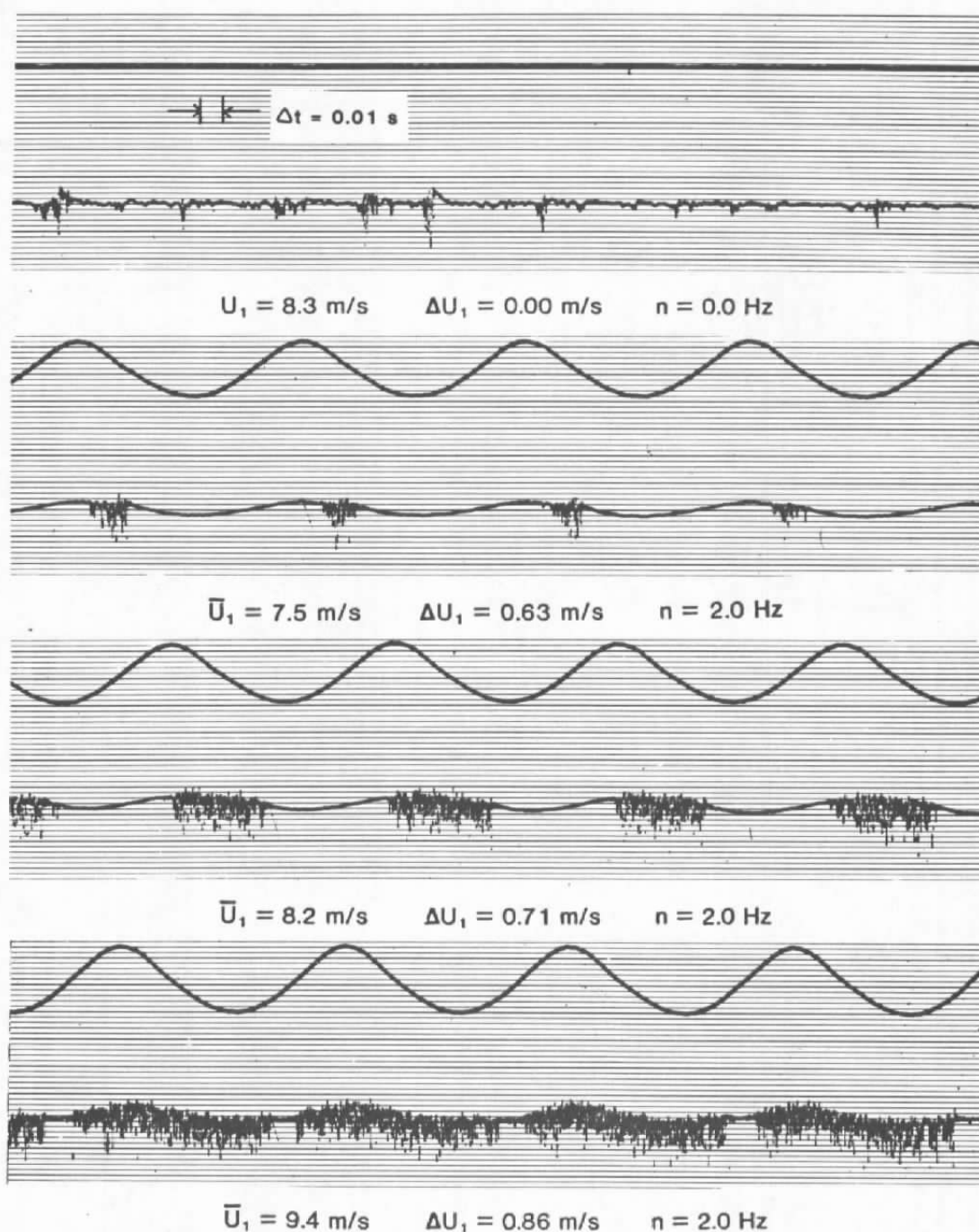


Figure 33. Strip-chart recordings of simultaneous u -fluctuations in an oscillatory freestream, and in the boundary layer downstream of a hemispherical roughness element; $k = 1.7 \text{ mm}$, $x_k = 91.4 \text{ cm}$, $\bar{x} = 30.5 \text{ cm}$, $y = 6.35 \text{ mm}$, $\bar{z} = 0.0 \text{ cm}$.

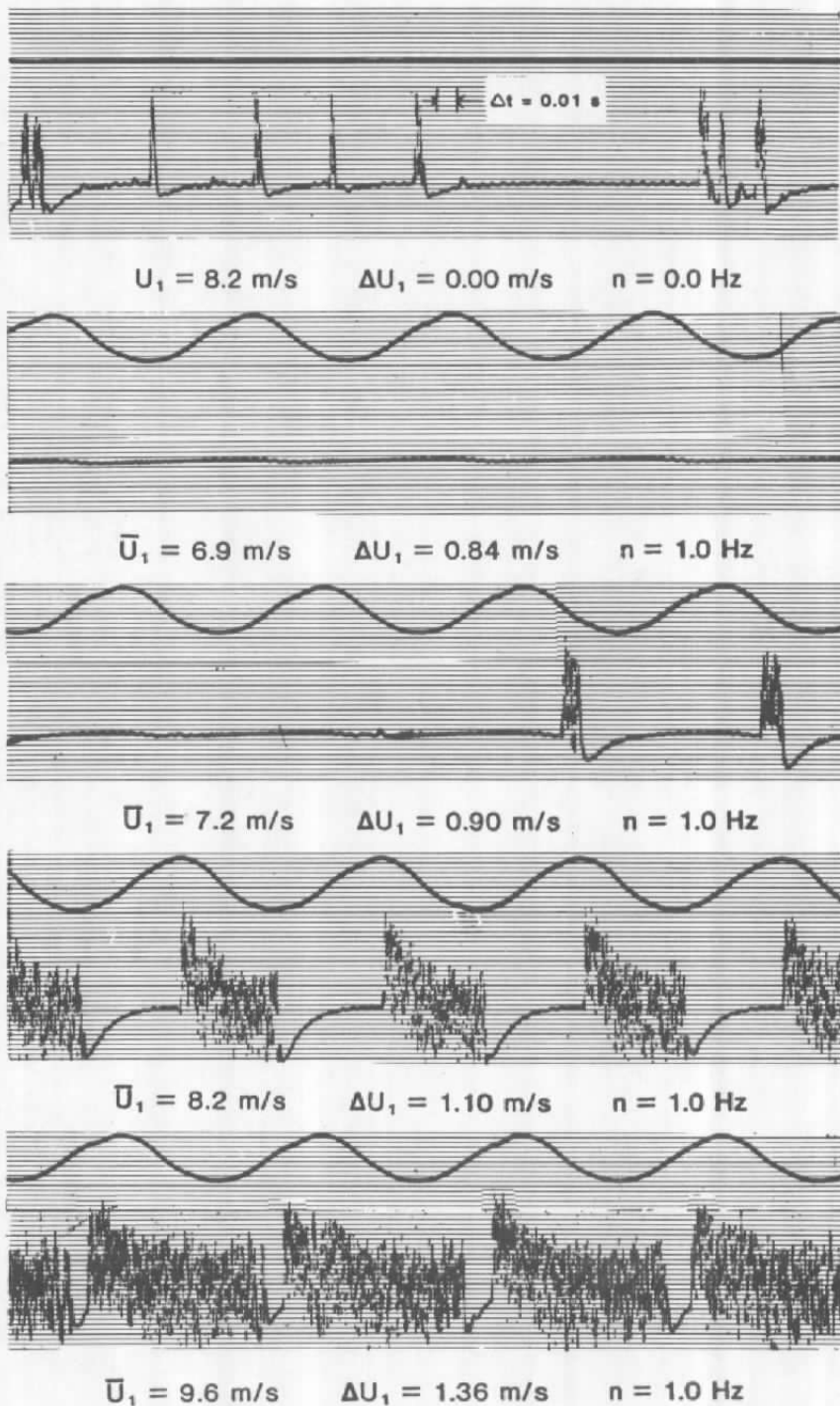


Figure 34. Strip-chart recordings of simultaneous u -fluctuations in an oscillatory freestream, and in the boundary layer downstream of a hemispherical roughness element; $k = 1.7 \text{ mm}$, $x_k = 91.4 \text{ cm}$, $\bar{x} = 61.0 \text{ cm}$, $y = 0.61 \text{ mm}$, $\bar{z} = 0.0 \text{ cm}$.

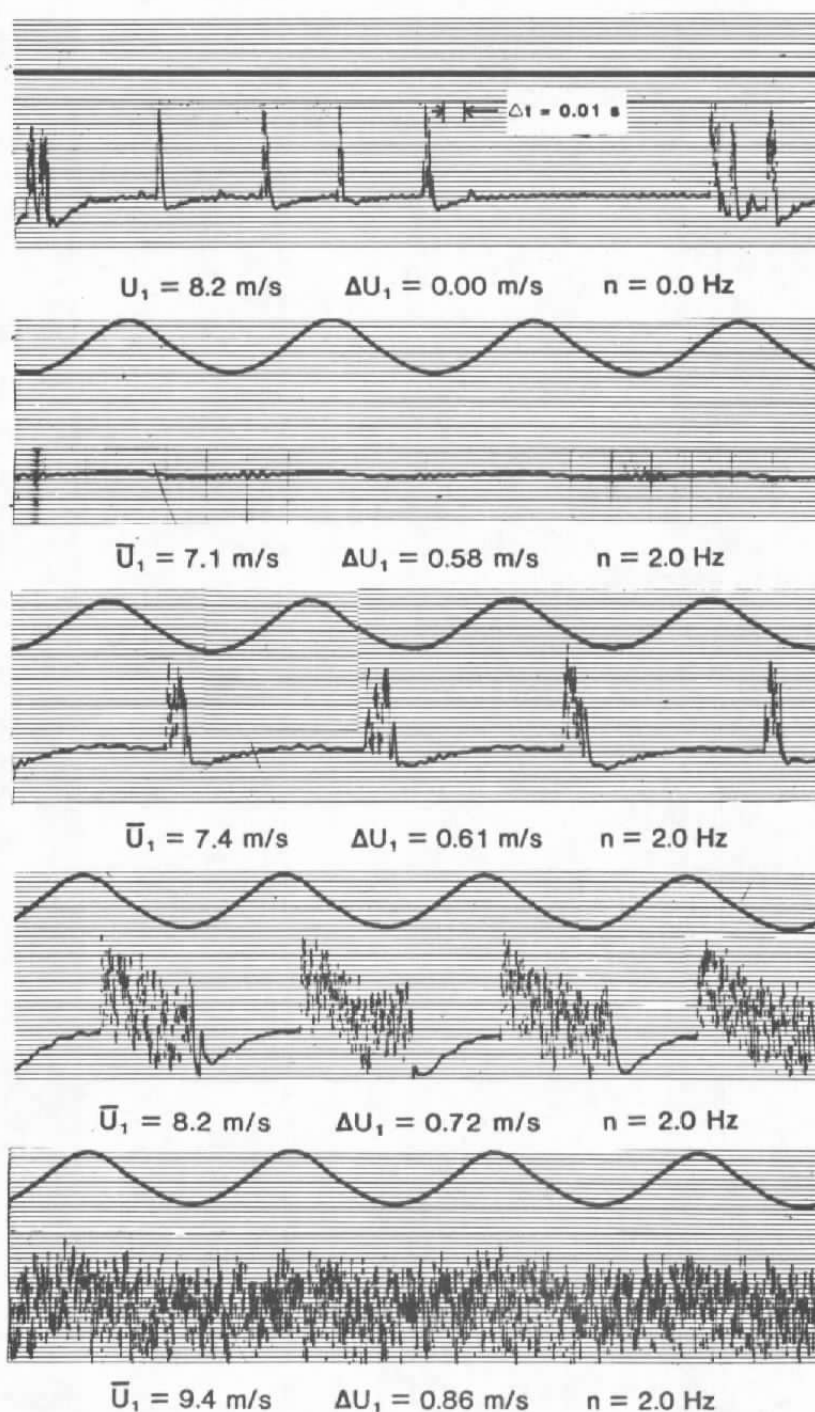


Figure 35. Strip-chart recordings of simultaneous u -fluctuations in an oscillatory freestream, and in the boundary layer downstream of a hemispherical roughness element; $k = 1.7 \text{ mm}$, $x_k = 91.4 \text{ cm}$, $\bar{x} = 61.0 \text{ cm}$, $y = 0.61 \text{ mm}$, $\bar{z} = 0.0 \text{ cm}$.

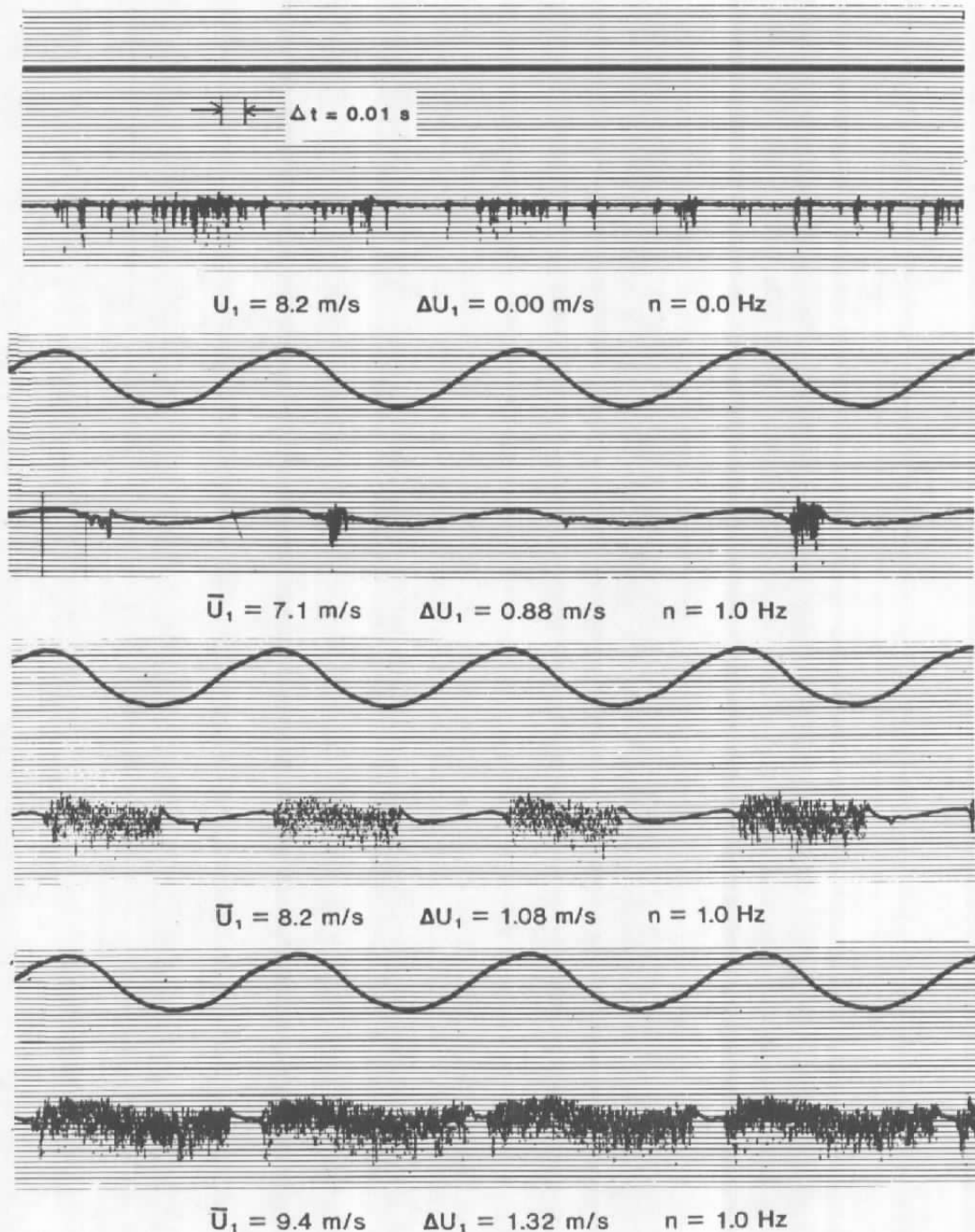


Figure 36. Strip-chart recordings of simultaneous u -fluctuations in an oscillatory freestream, and in the boundary layer downstream of a hemispherical roughness element; $k = 1.7 \text{ mm}$, $x_k = 91.4 \text{ cm}$, $\bar{x} = 61.0 \text{ cm}$, $y = 6.35 \text{ mm}$, $\bar{z} = 0.0 \text{ cm}$.

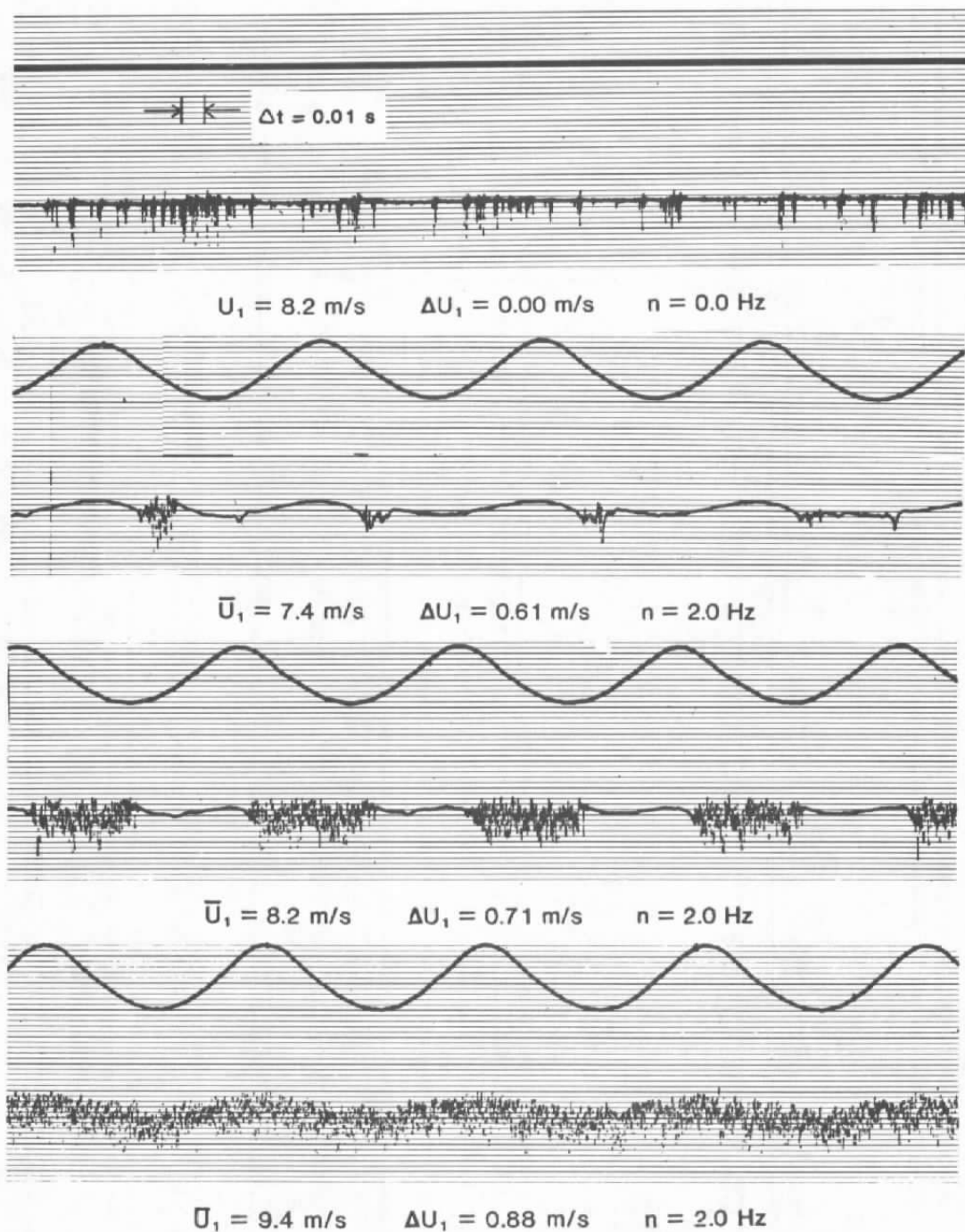


Figure 37. Strip-chart recordings of simultaneous u -fluctuations in an oscillatory freestream, and in the boundary layer downstream of a hemispherical roughness element; $k = 1.7 \text{ mm}$, $x_k = 91.4 \text{ cm}$, $\bar{x} = 61.0 \text{ cm}$, $y = 6.35 \text{ mm}$, $\bar{z} = 0.0 \text{ cm}$.

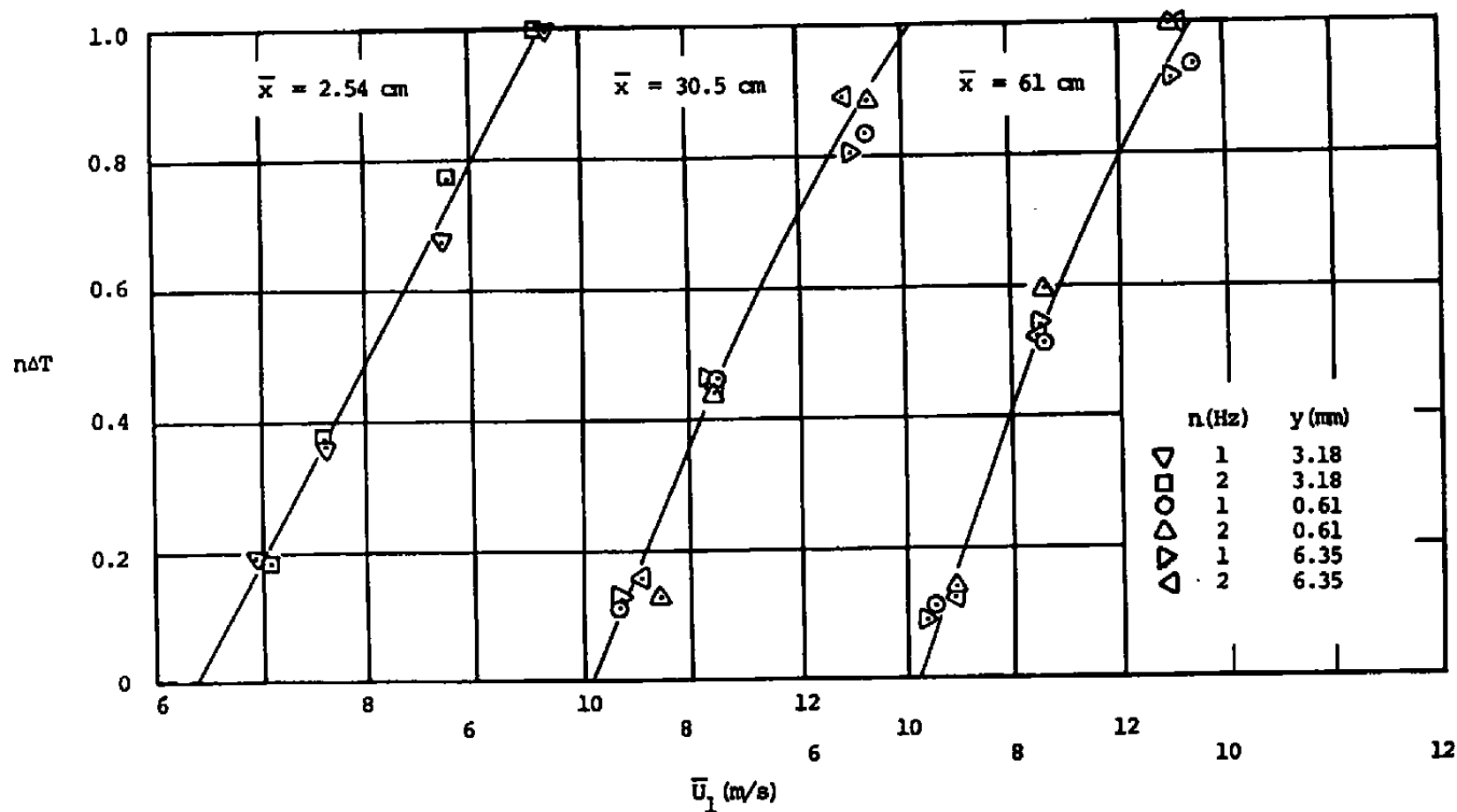


Figure 38. Comparison of the duration of eddy shedding with the duration of resulting turbulent "spot."

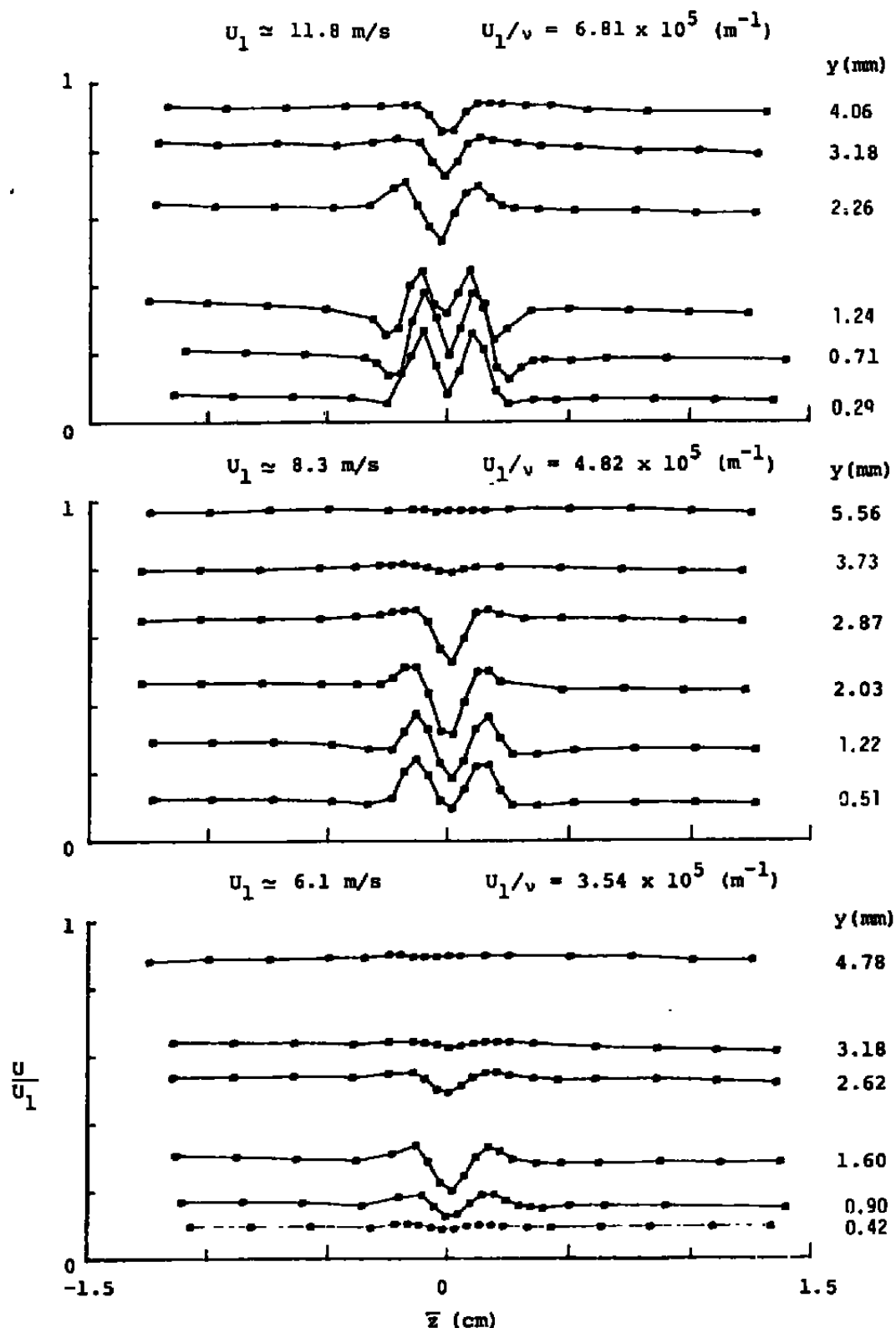


Figure 39. Spanwise distributions of mean velocity at various positions from the surface for varying unit Reynolds number; $k = 1.7 \text{ mm}$, $x_k = 91.4 \text{ cm}$, $\bar{x} = 2.54 \text{ cm}$.

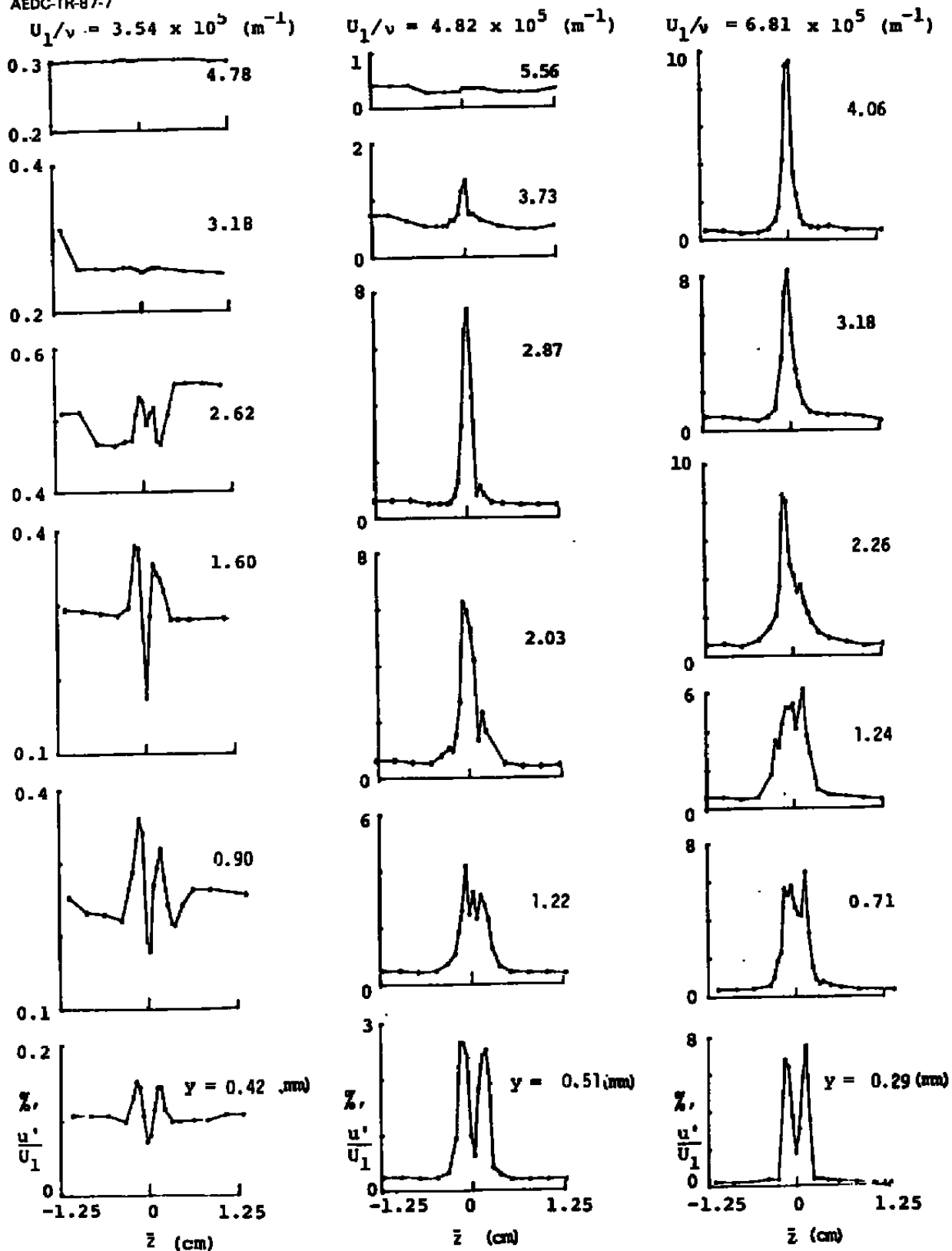
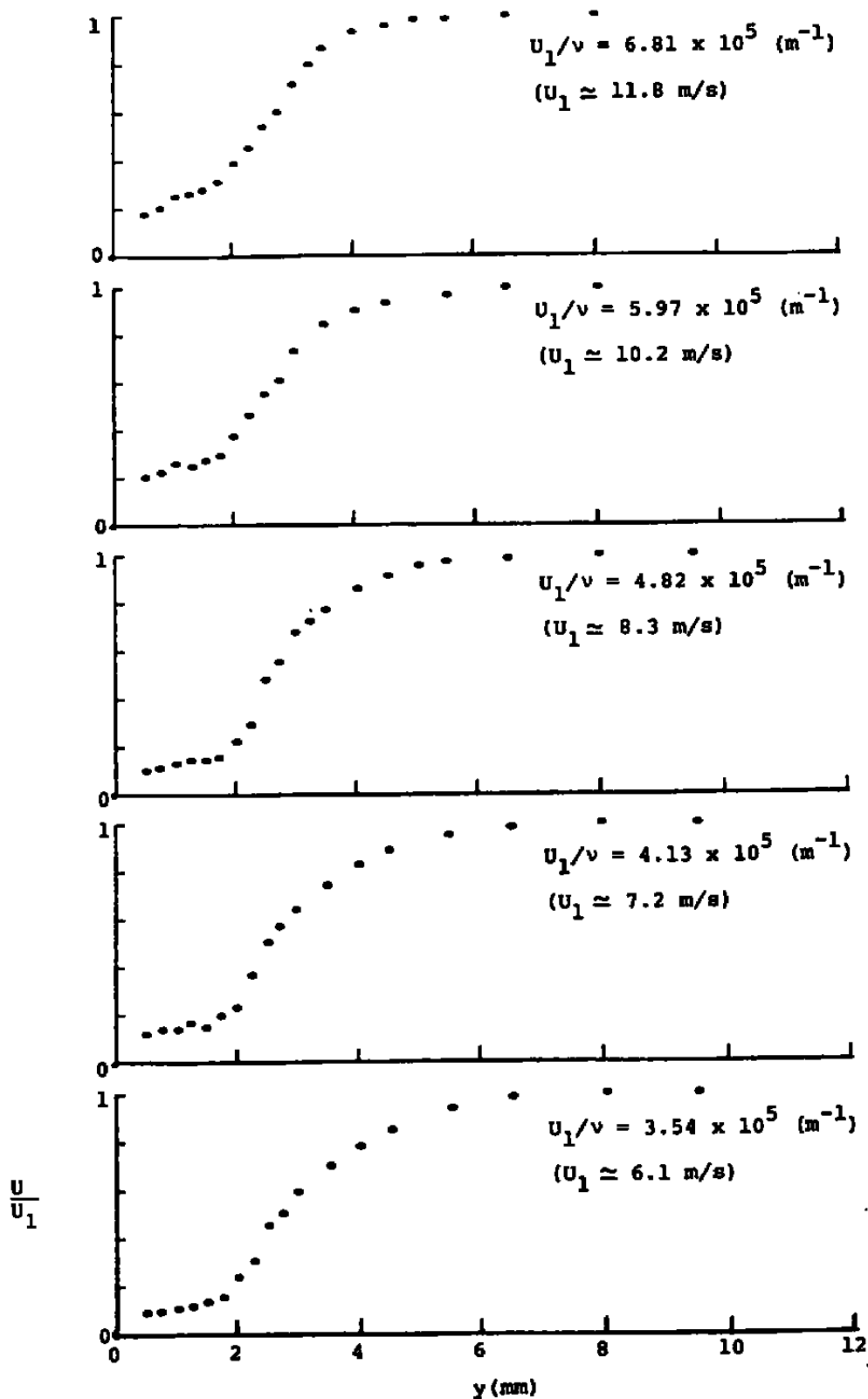
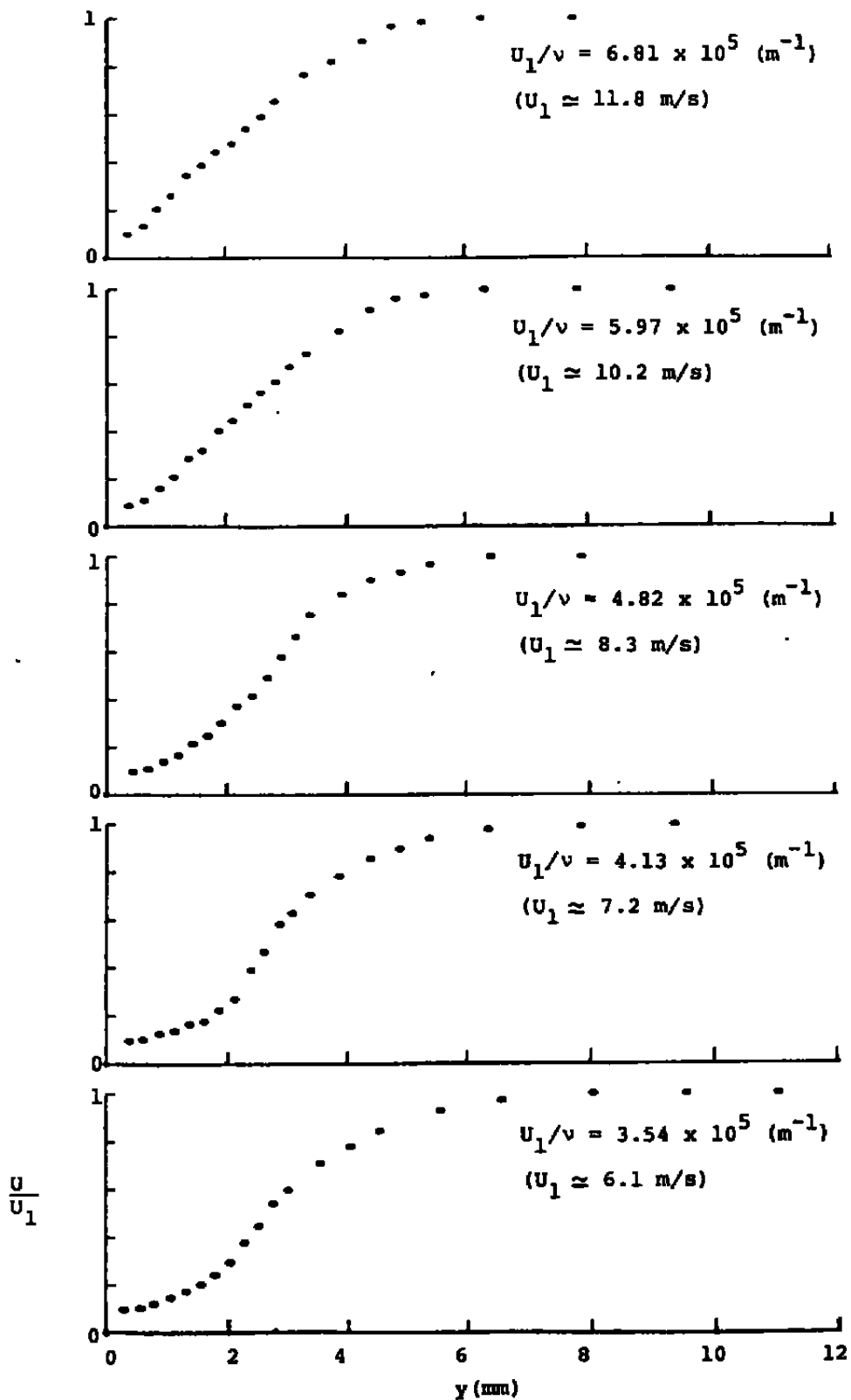


Figure 40. Spanwise distributions of the intensity of u -fluctuation at various positions from the surface for varying unit Reynolds number; $k = 1.7 \text{ mm}$, $x_k = 91.4 \text{ cm}$, $\bar{x} = 2.54 \text{ cm}$.

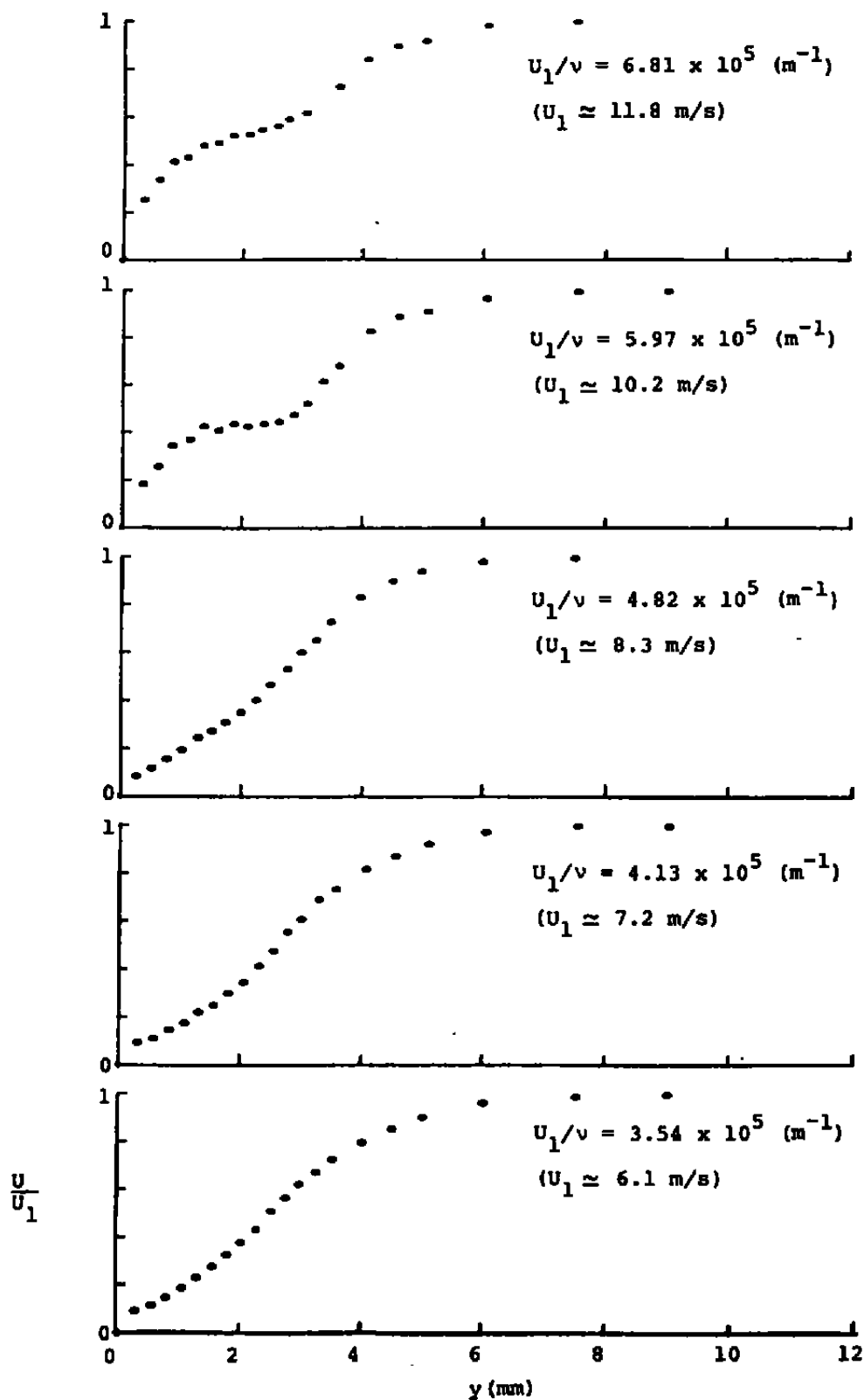


a. $\bar{x} = 1.27$ cm

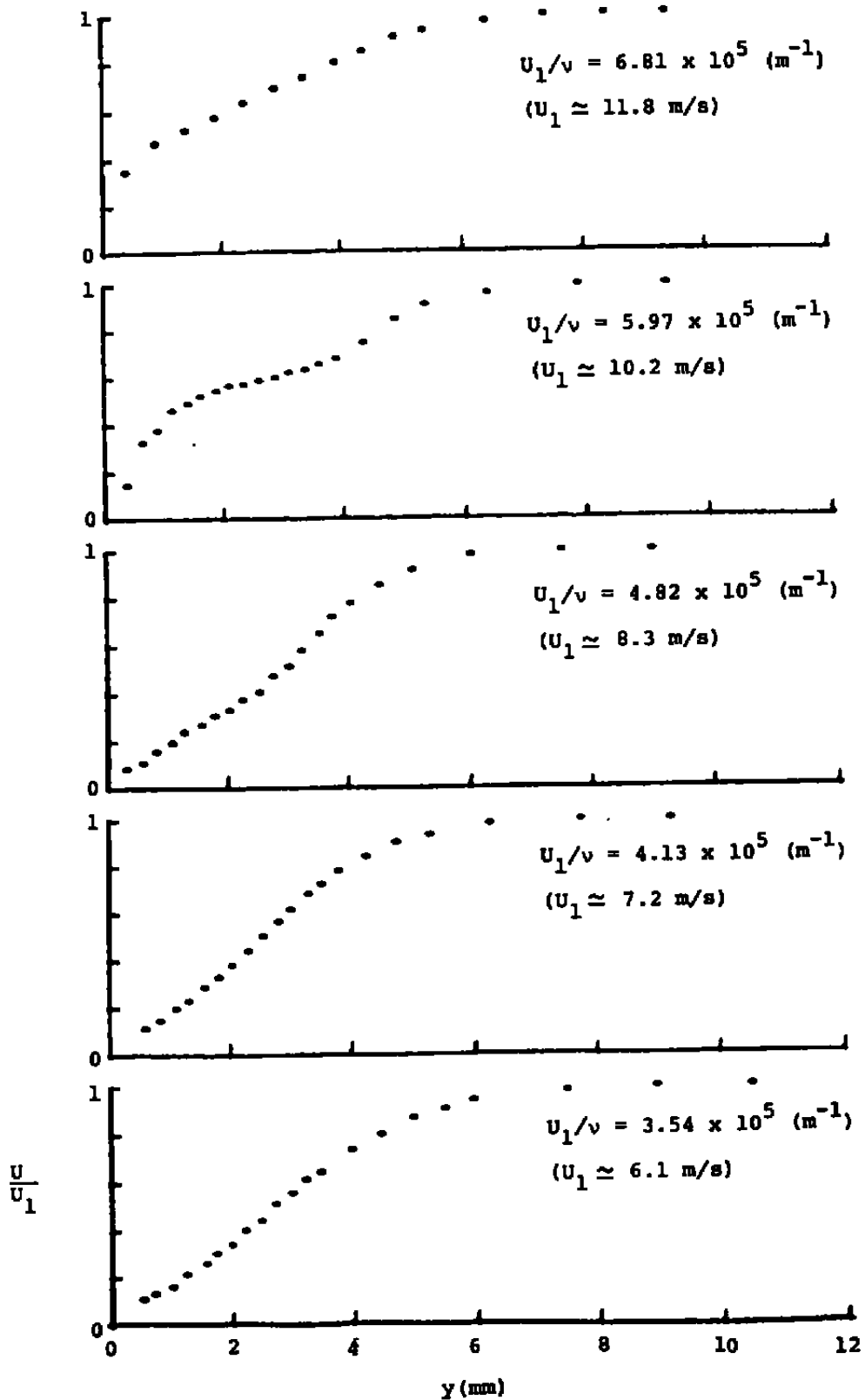
Figure 41. Mean-velocity distributions for varying unit Reynolds number; $k = 1.7$ mm, $x_k = 91.4$ cm, $\bar{z} = 0.0$ cm.



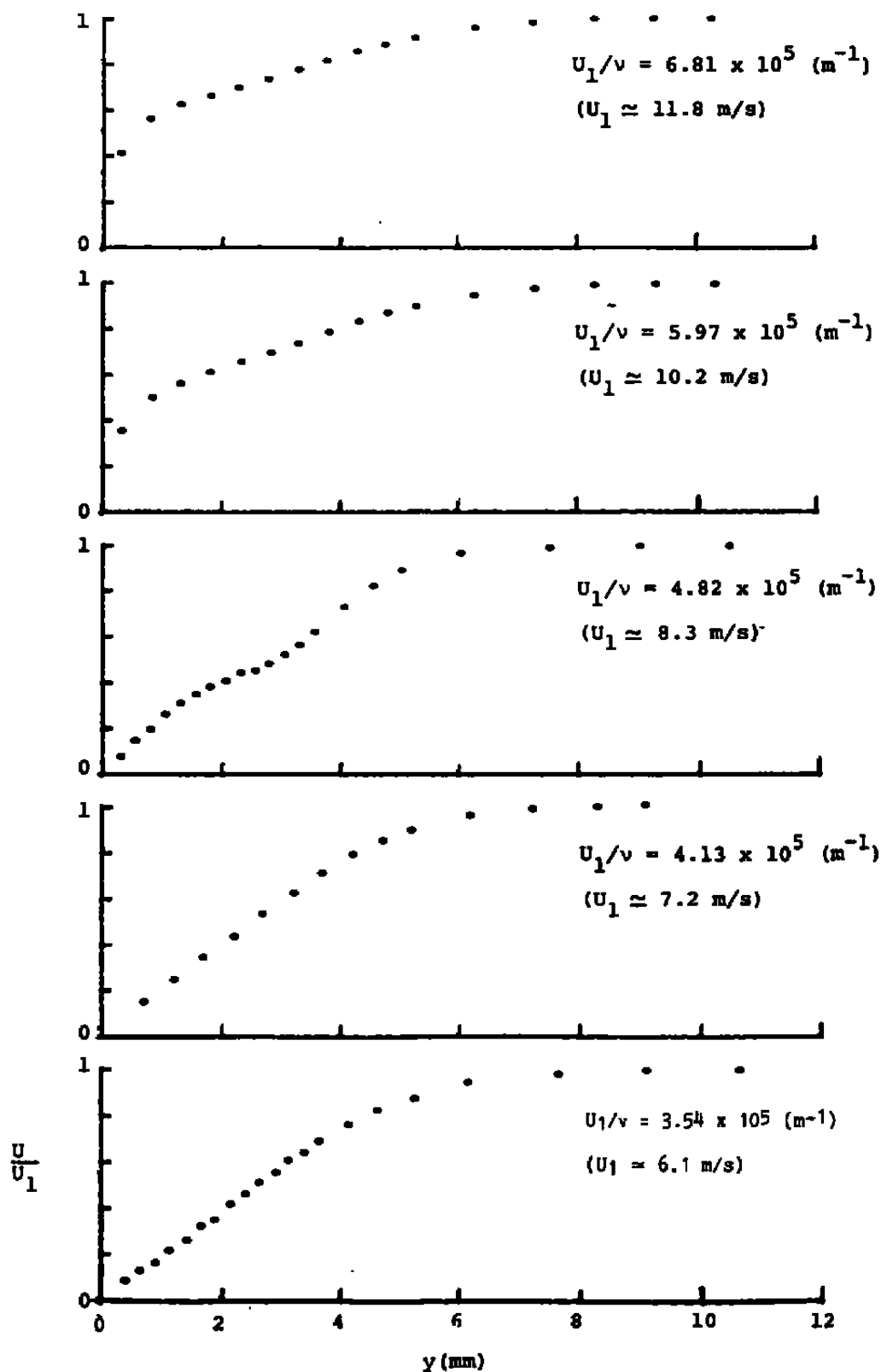
b. $\bar{x} = 2.54$ cm
Figure 41. Continued.



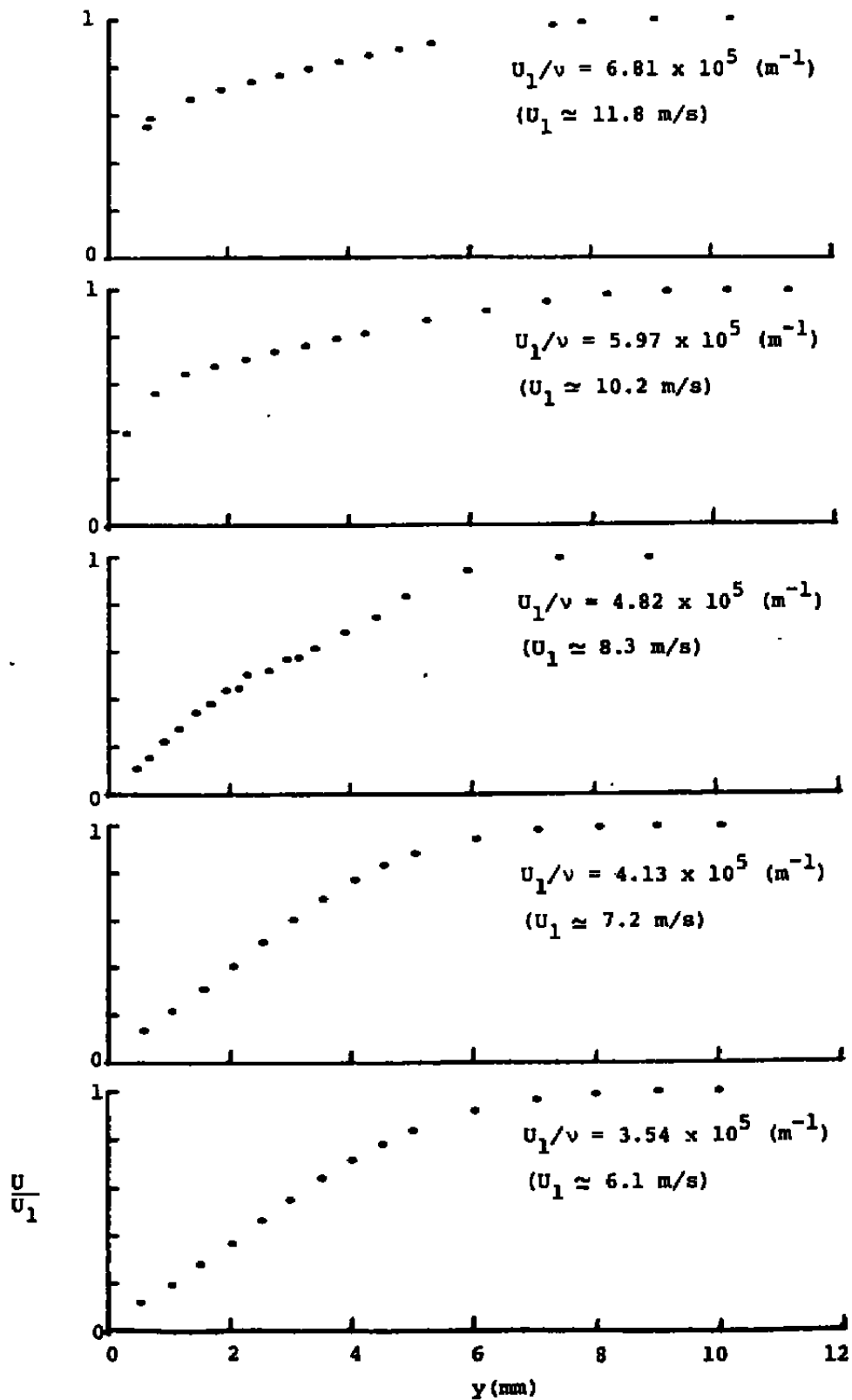
c. $\bar{x} = 5.08 \text{ cm}$
Figure 41. Continued.



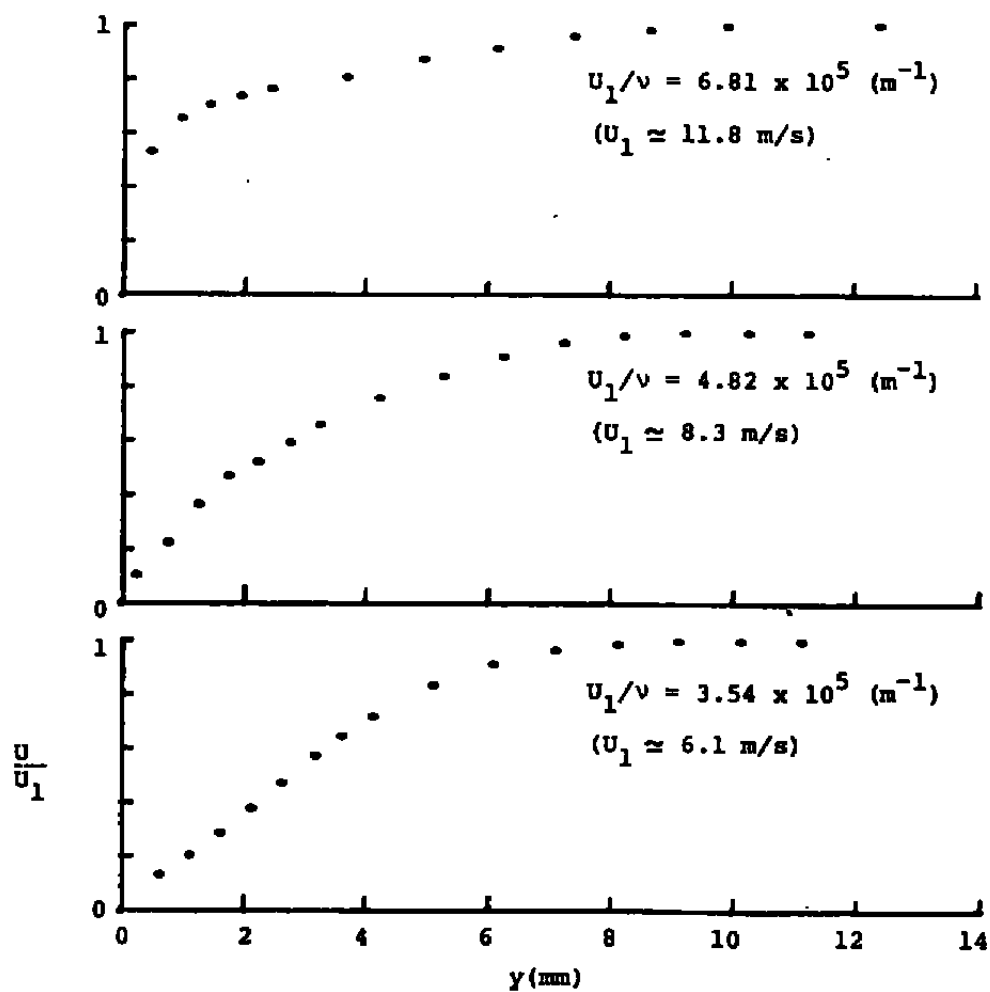
d. $\bar{x} = 7.62 \text{ cm}$
Figure 41. Continued.



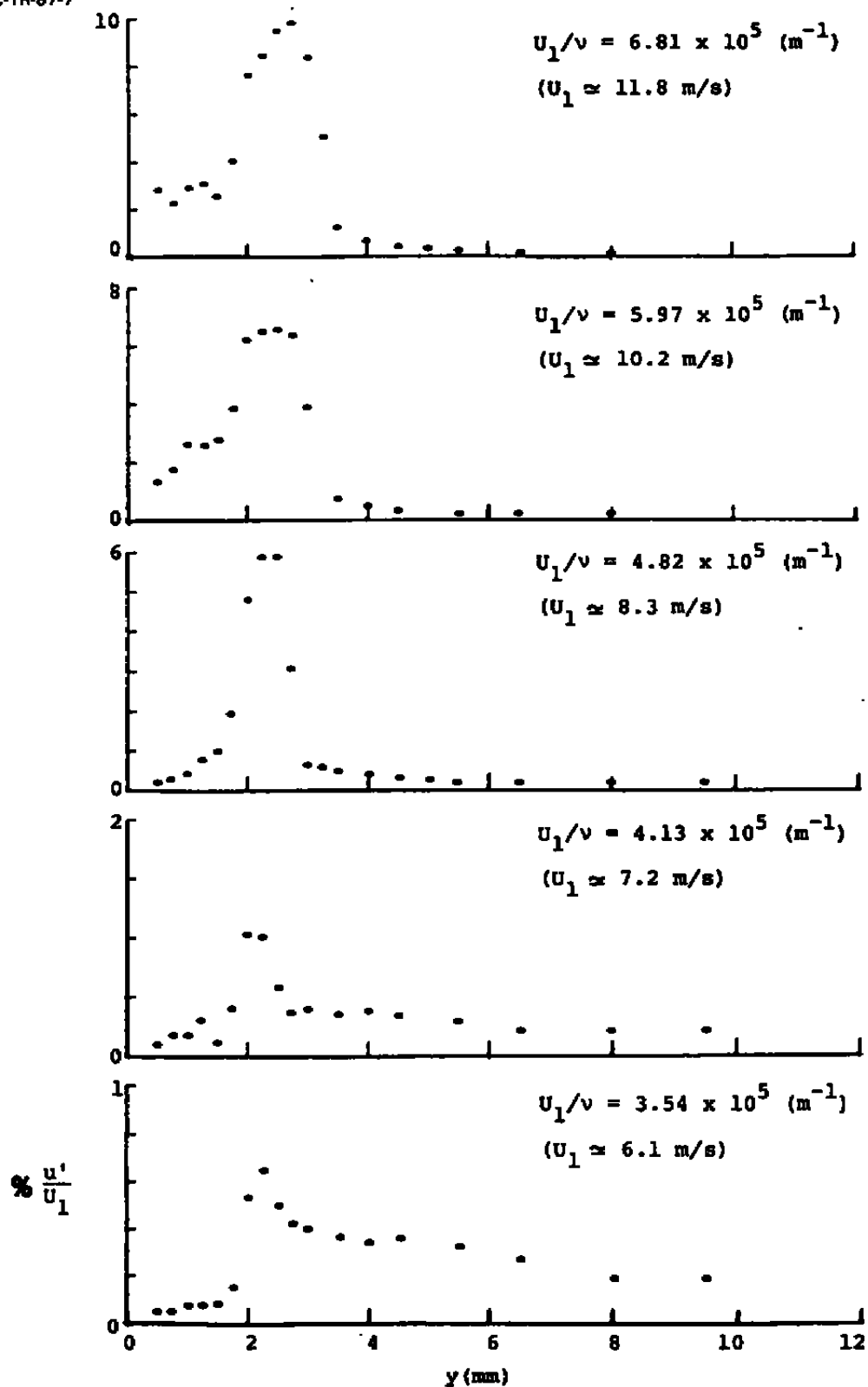
e. $\bar{x} = 12.7 \text{ cm}$
 Figure 41. Continued.



f. $\bar{x} = 20.3 \text{ cm}$
 Figure 41. Continued.

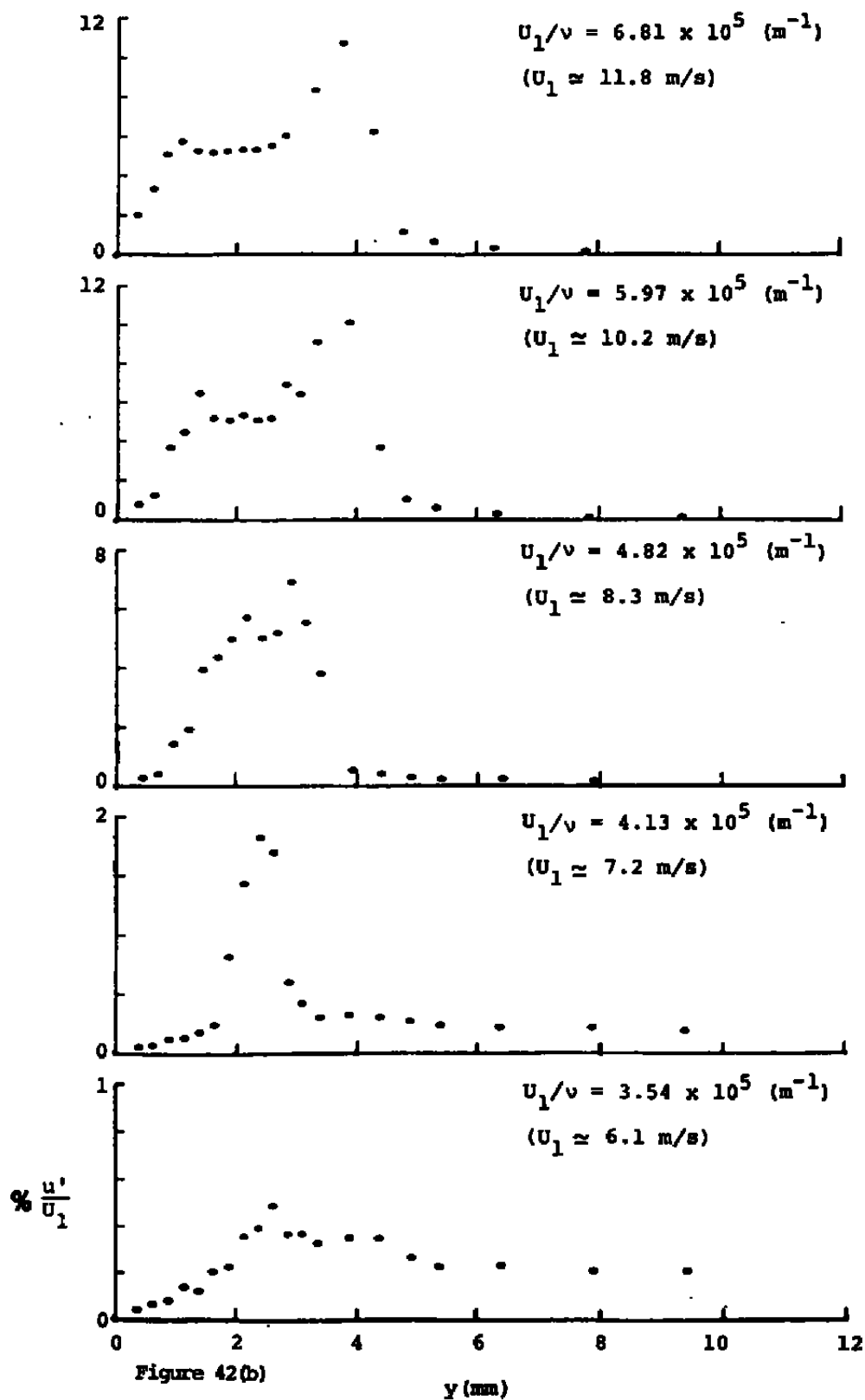


g. $\bar{x} = 30.5 \text{ cm}$
Figure 41. Concluded.

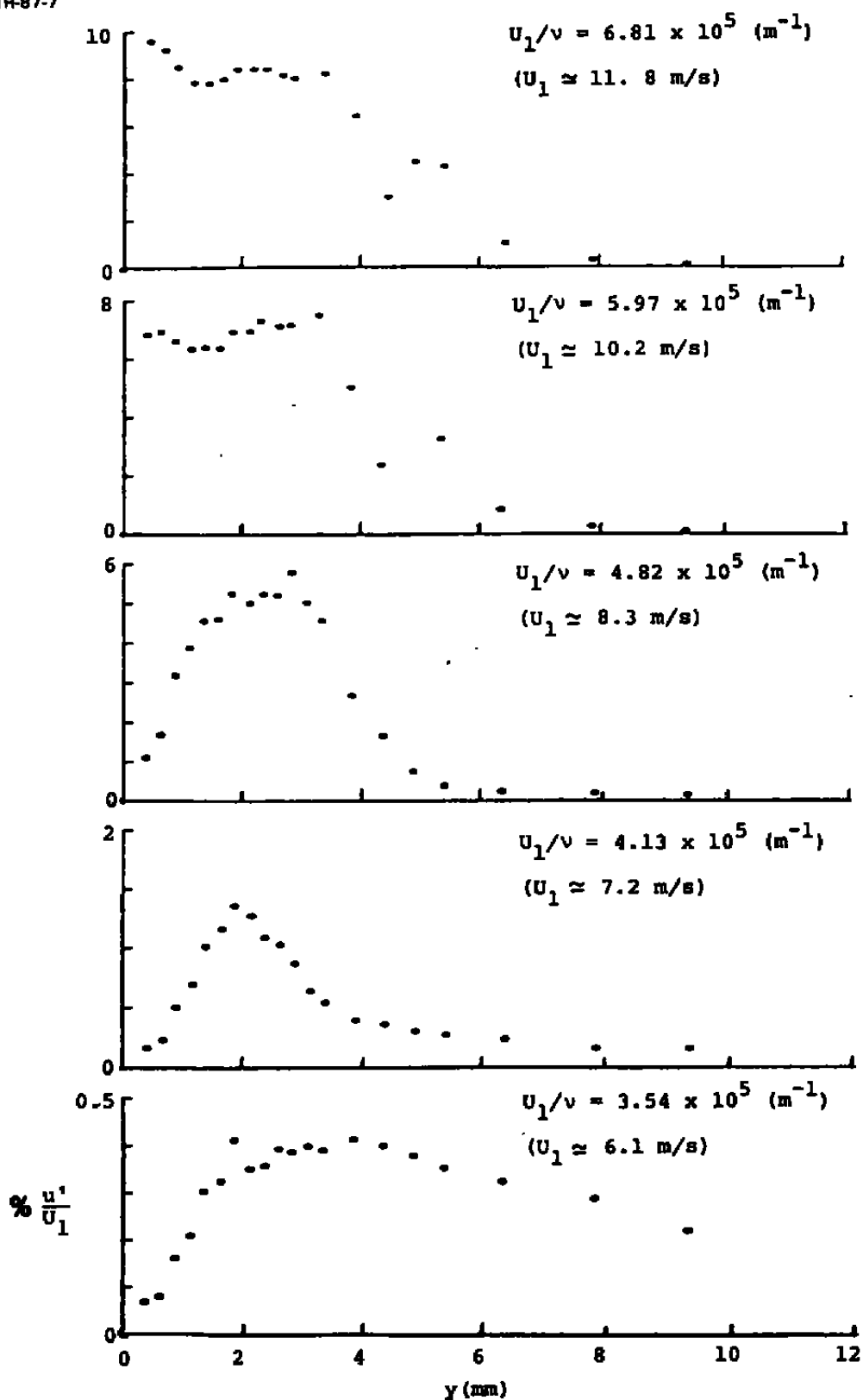


a. $\bar{x} = 1.27 \text{ cm}$

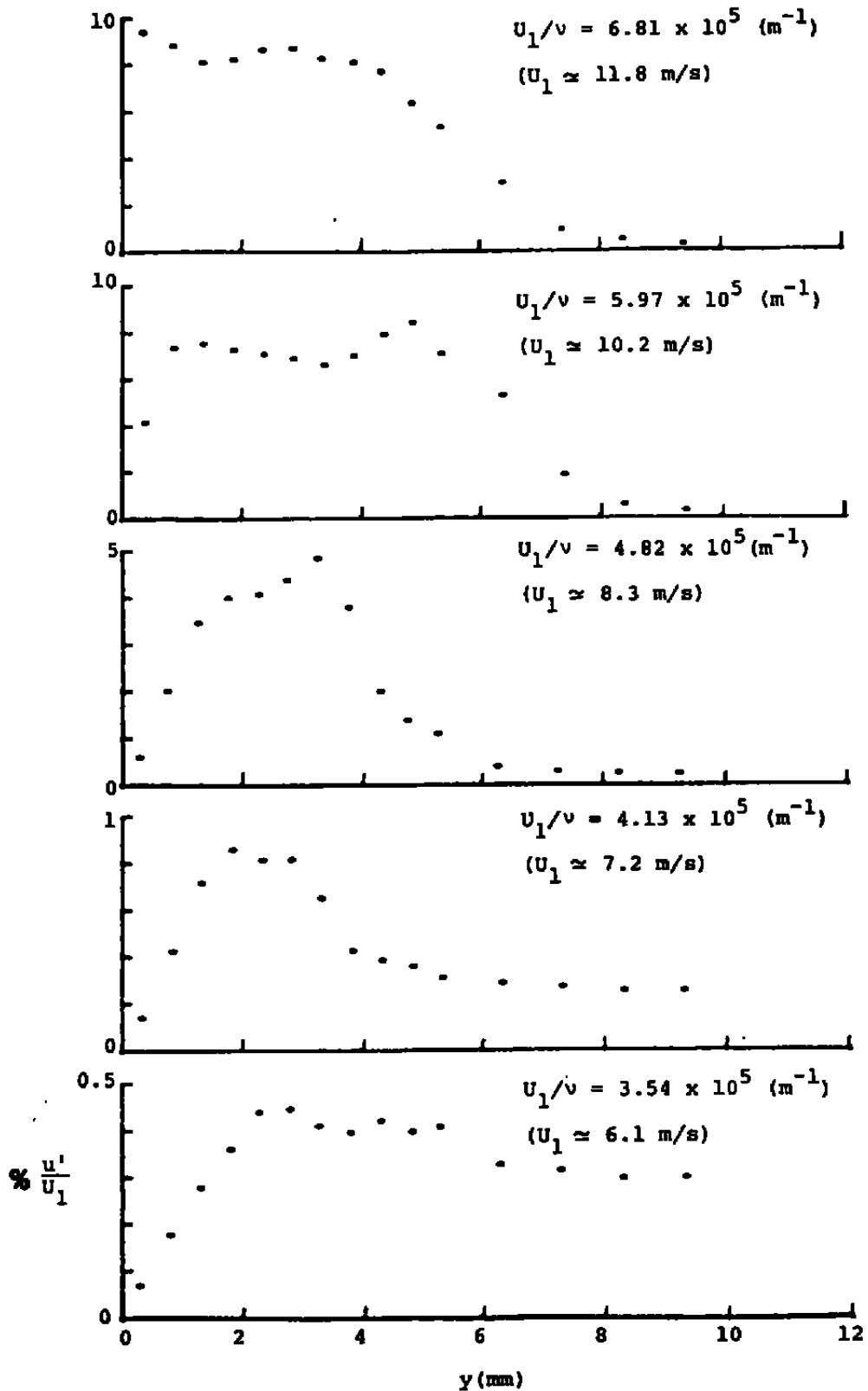
Figure 42. Intensity of u -fluctuation for varying unit Reynolds number; $k = 1.7 \text{ mm}$, $x_k = 91.4 \text{ cm}$, $\bar{z} = 0.0 \text{ cm}$.



b. $\bar{x} = 2.54 \text{ cm}$
Figure 42. Continued.

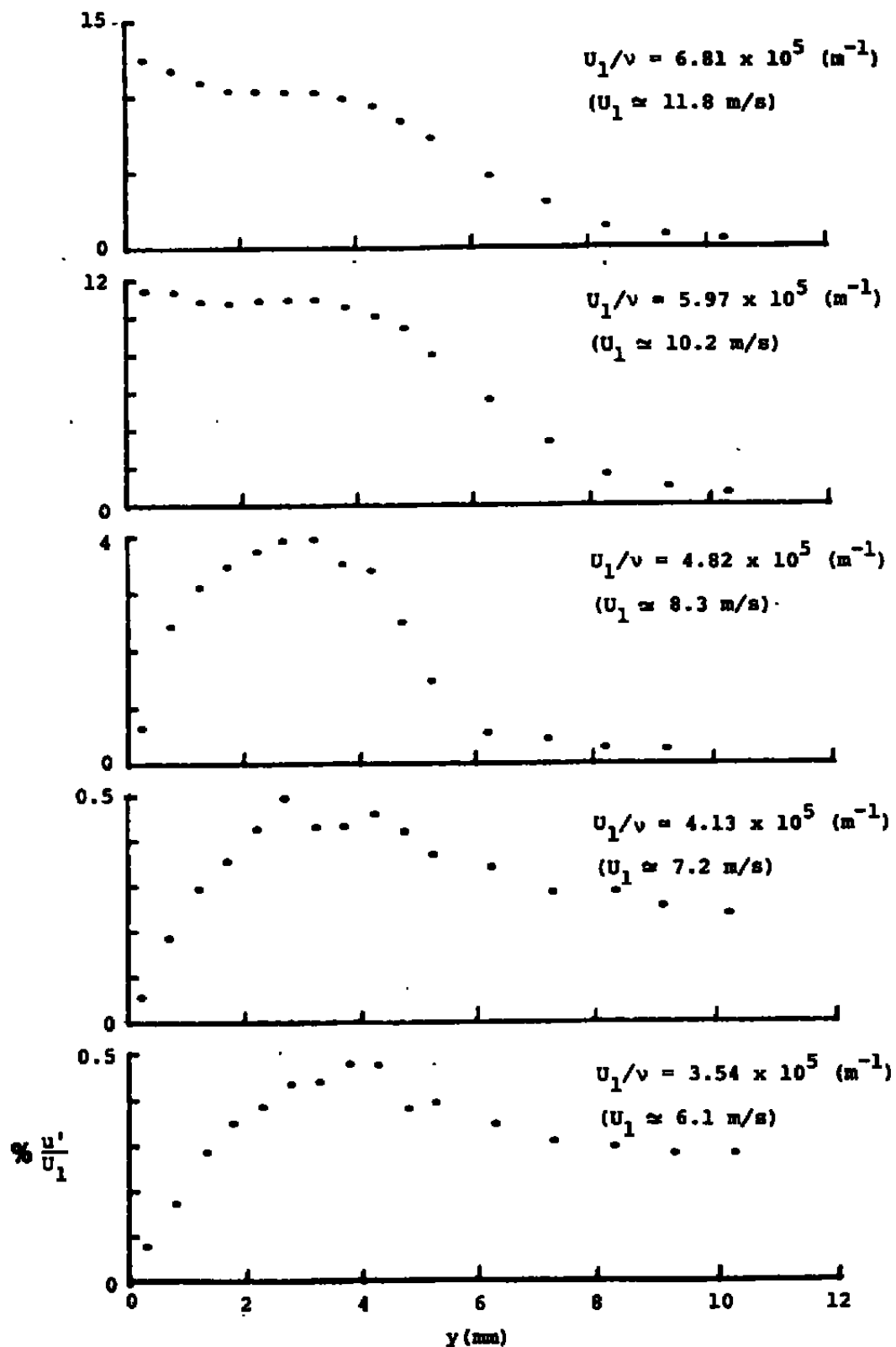


c. $\bar{x} = 5.08 \text{ cm}$
 Figure 42. Continued.

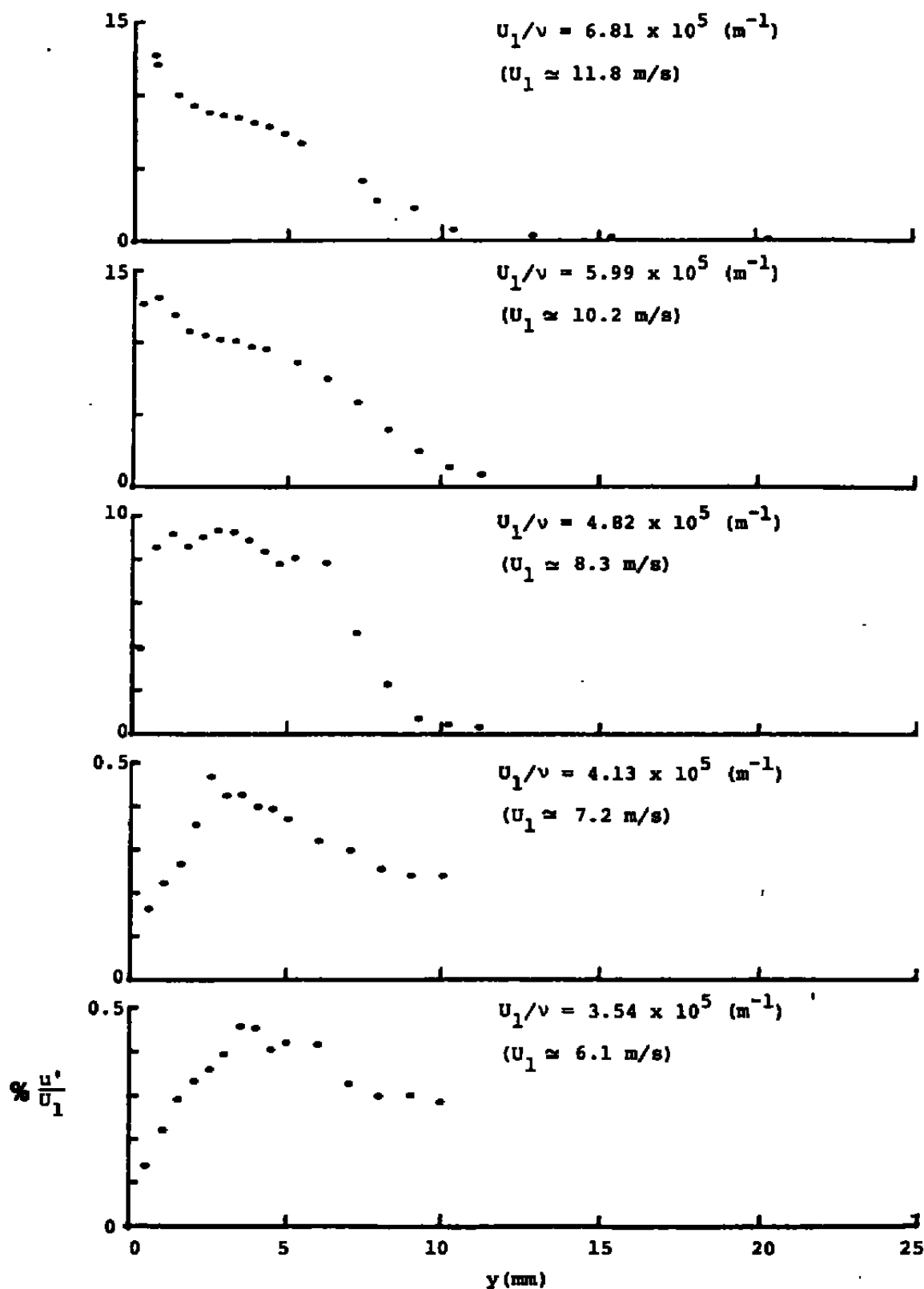


d. $\bar{x} = 7.62 \text{ cm}$

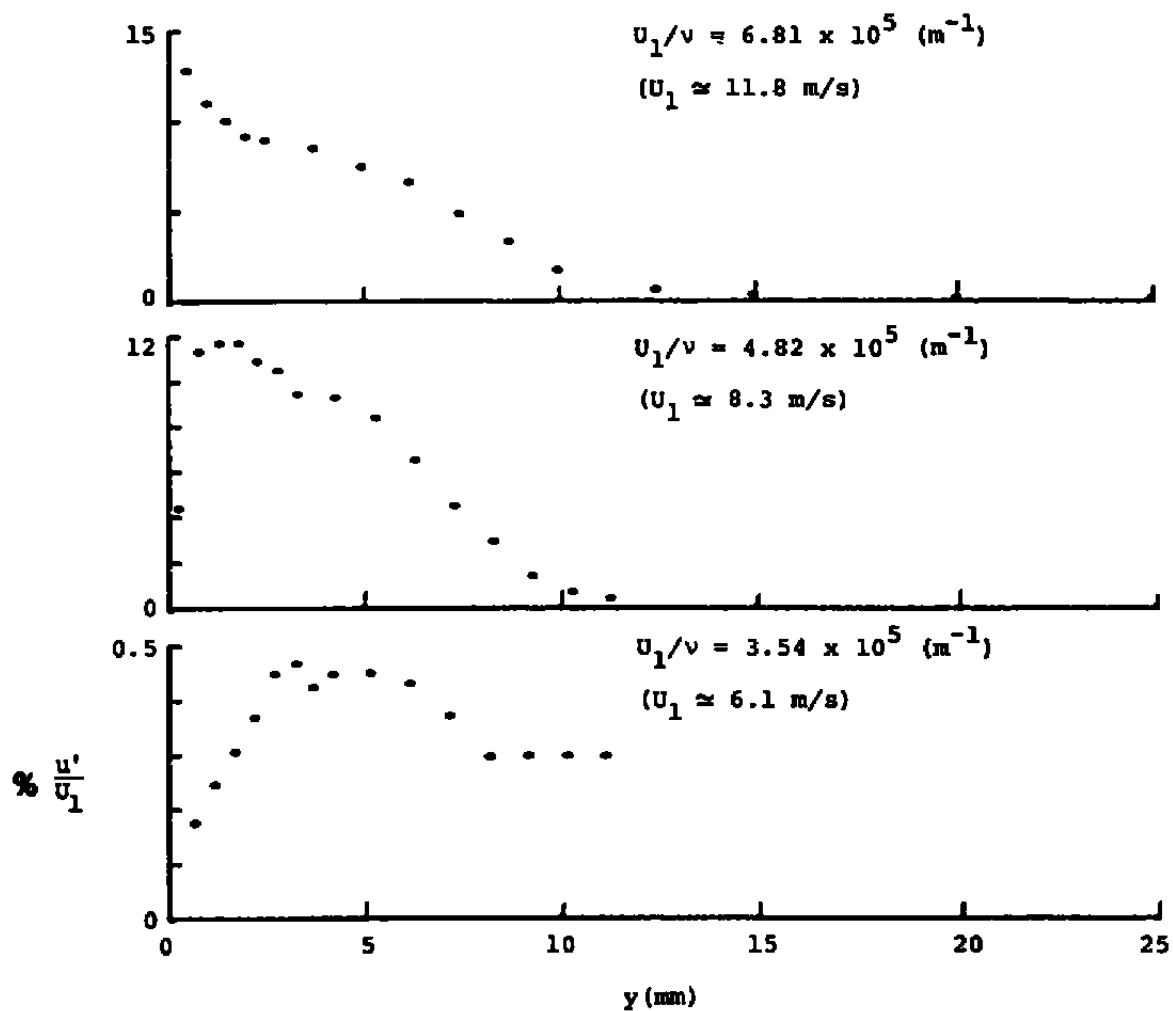
Figure 42. Continued.



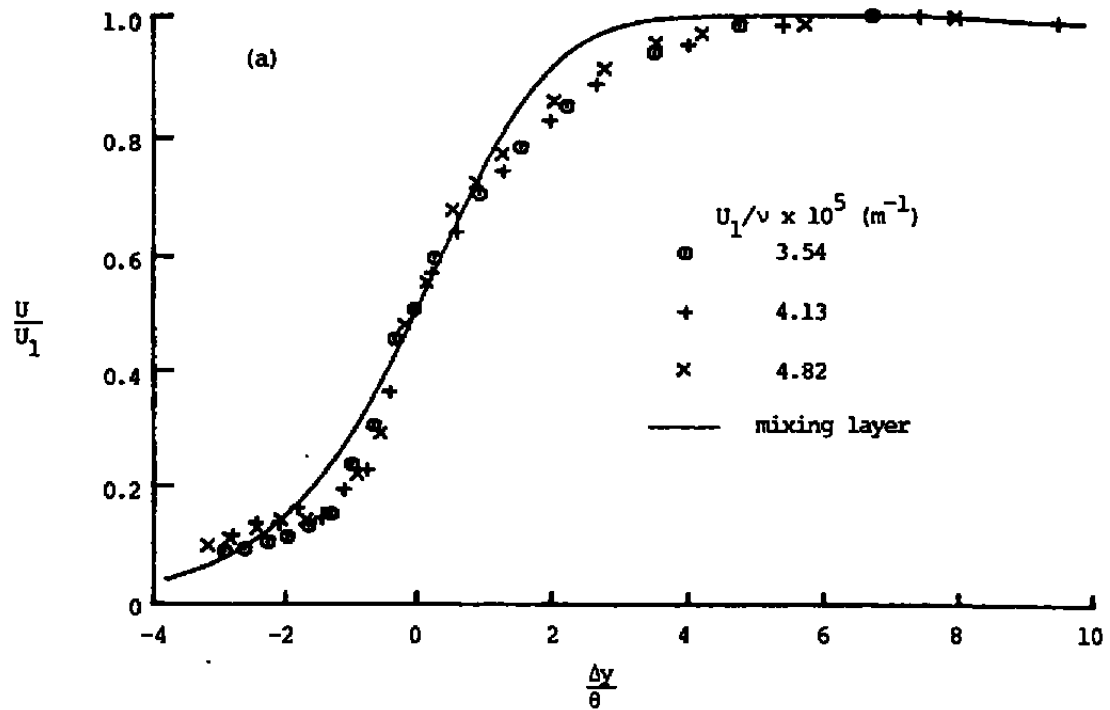
e. $\bar{x} = 12.7 \text{ cm}$
 Figure 42. Continued.



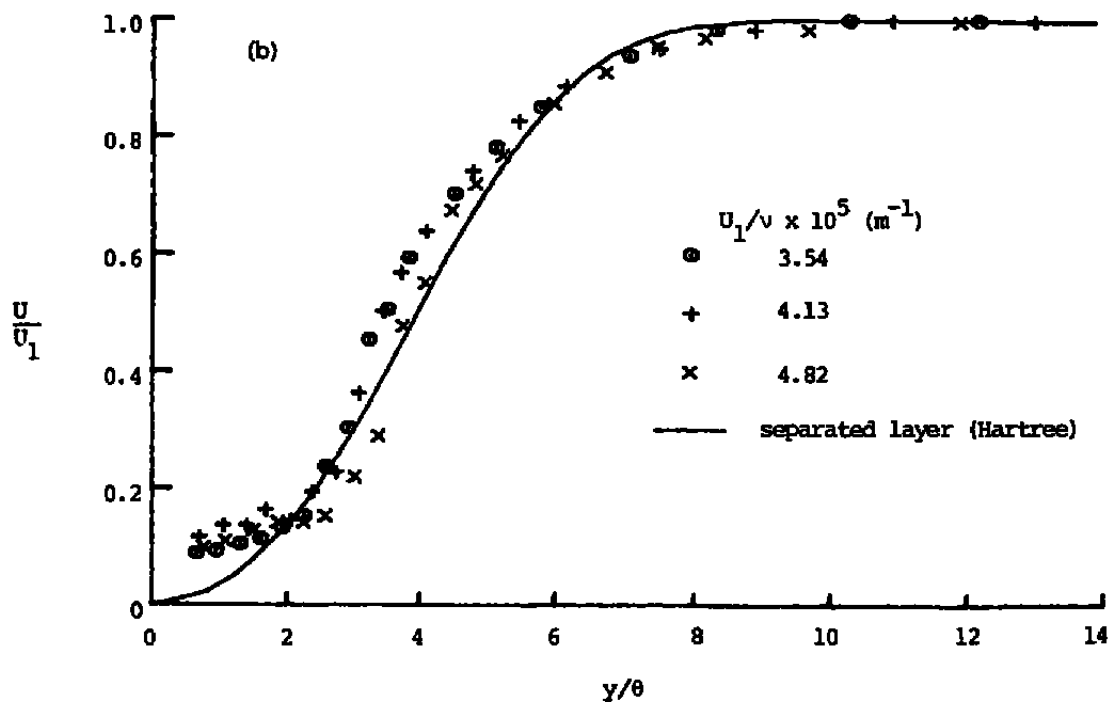
$f. \bar{x} = 20.3 \text{ cm}$
 Figure 42. Continued.



g. $\bar{x} = 30.5 \text{ cm}$
 Figure 42. Concluded.



a. Mixing layer



b. Separated boundary layer

Figure 43. Comparison of mean-velocity profiles at 1.27 cm downstream of a hemispherical roughness element with the mean-velocity profiles; $k = 1.7 \text{ mm}$, $x_k = 91.4 \text{ cm}$, $\bar{z} = 0.0 \text{ cm}$.

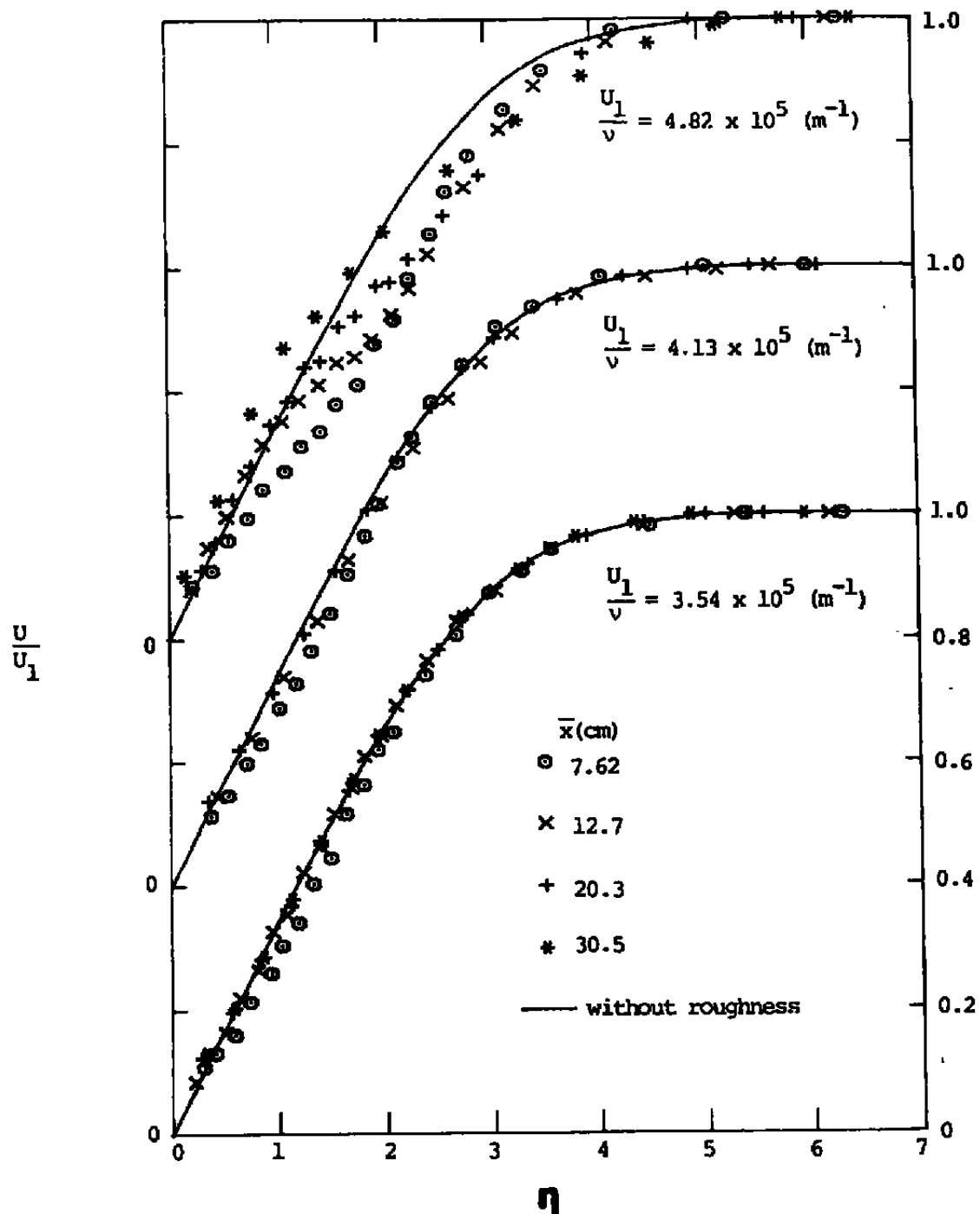


Figure 44. Comparison of mean-velocity profiles downstream of a hemispherical roughness element with the mean-velocity profile without roughness; $k = 1.7 \text{ mm}$, $x_k = 91.4 \text{ cm}$, $\bar{z} = 0.0 \text{ cm}$.

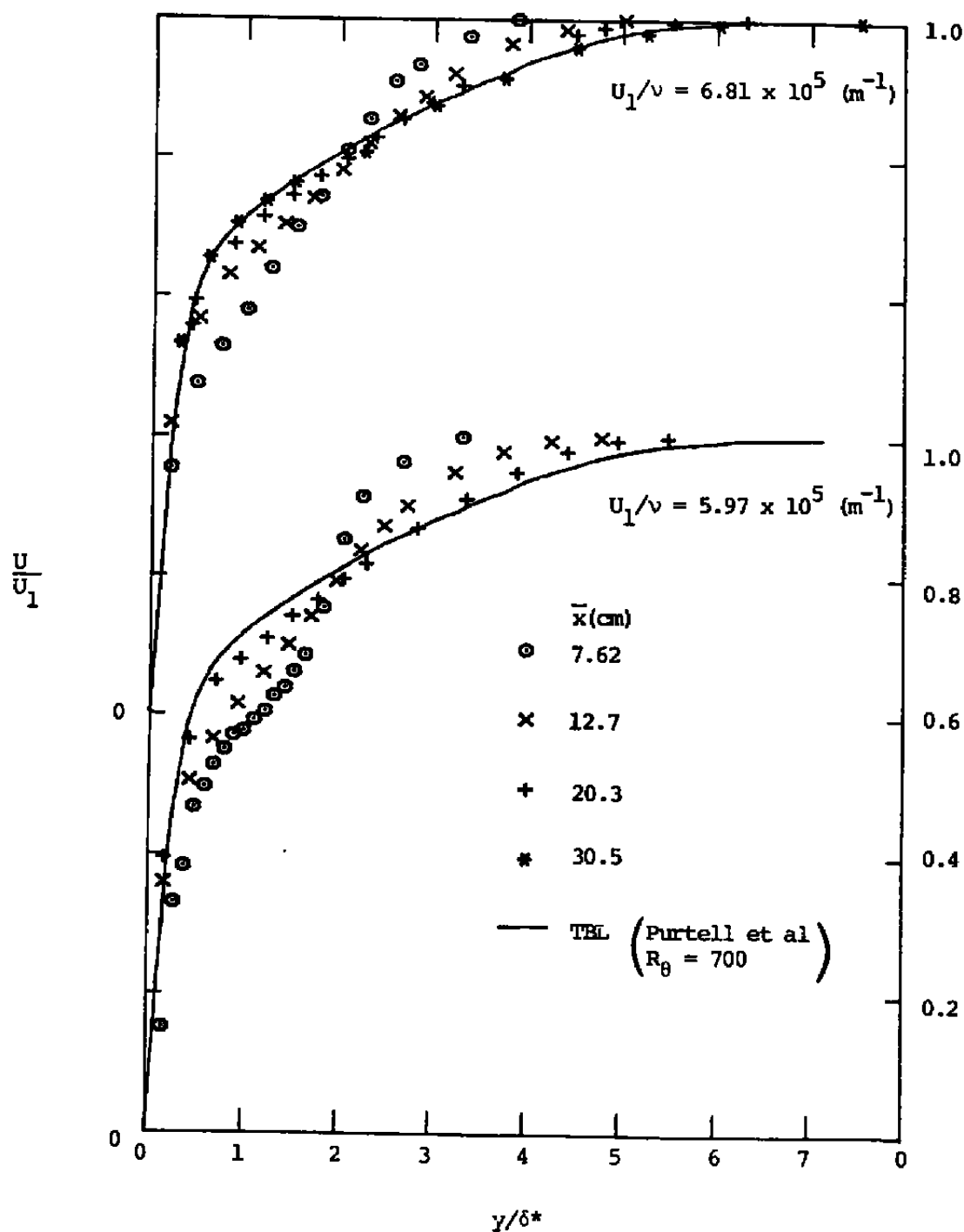


Figure 45. Comparison of mean-velocity profiles downstream of a hemispherical roughness element with the mean-velocity profile for a "fully-developed" turbulent boundary layer; $k = 1.7 \text{ mm}$, $x_k = 91.4 \text{ cm}$, $\bar{z} = 0.0 \text{ cm}$.

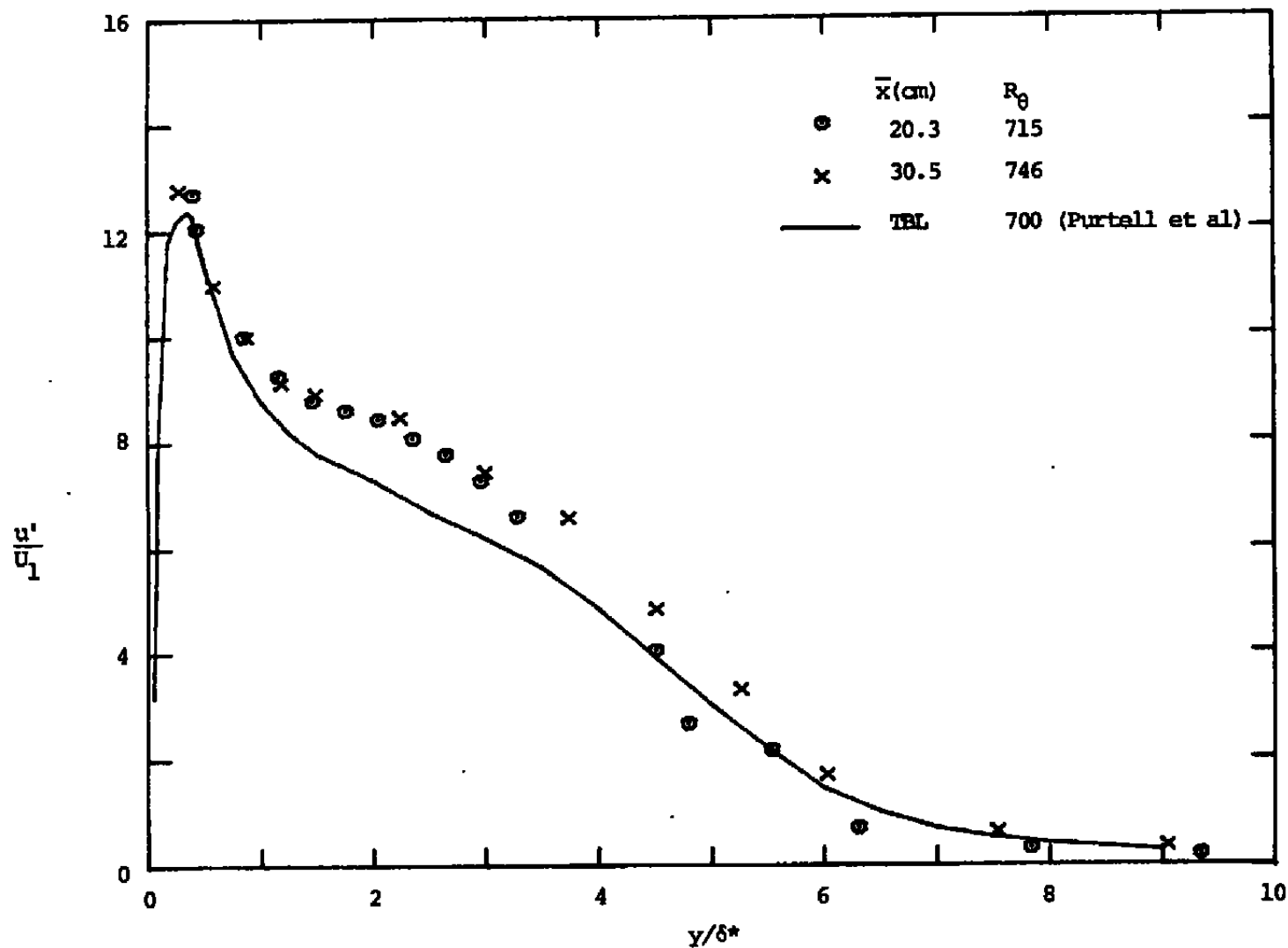


Figure 46. Comparison of intensity of u-fluctuation downstream of a hemispherical roughness element with the intensity of u-fluctuation for a "fully-developed" turbulent boundary layer; $k = 1.7 \text{ mm}$, $x_k = 91.4 \text{ cm}$, $z = 0.0 \text{ cm}$, $U_1/\nu = 6.81 \times 10^5 (\text{m}^{-1})$.